Co-Production of Electricity and Hydrogen Using a Novel Iron-based Catalyst

Final Technical Report

Reporting Period:
April 1, 2006 to September 30, 2011

By

Ahmad Hilaly, Adam Georgas, Jose Leboreiro, Salil Arora, Megann Head, Jason Trembly, Brian Turk, and Raghubir Gupta

DOE Cooperative Agreement No. DE-FC26-06NT42758

Submitted by:

RTI International
P.O. 12194
Research Triangle Park, NC 27709-2194

February 2013

Disclaimer

This report was prepared as an account of work sponsored by an agency of the United States Government. Neither the United States Government nor any agency thereof, nor any of their employees, makes any warranty, express or implied, or assumes any legal liability or responsibility for the accuracy, completeness, or usefulness of any information, apparatus, product, or process disclosed, or represents that its use would not infringe privately owned rights. Reference herein to any specific commercial product, process, or service by trade name, trademark, manufacturer, or otherwise does not necessarily constitute or imply its endorsement, recommendation, or favoring by the United State Government or any agency thereof. The views and opinions of authors expressed therein do not necessarily state or reflect those of the United States Government or any agency thereof.

Acknowledgements

This project was sponsored by the National Energy Technology Laboratory (NETL) of the U.S. Department of Energy (DOE) under Contract No. DE-FC26-06NT42758. This financial assistance from DOE/NETL is gratefully acknowledged. In addition, the major cost-sharing for this project was provided by Archer Daniel Midland (ADM), BOC, Süd-Chemie (SCI), and RTI. Recognition of contributing individuals from these organizations is provided below.

DOE/NETL: John Stipanovich.

BOC: A.K.S. Murthy, S. Tamhanker, and Segundoo Park.

Süd-Chemie: Troy Walsh, Tom Pusty, and Jeff Braden.

RTI: Engineering and Analytical Support: Gary Howe, Justin Farmer, Josh Hlebak, Mathew Van Holle, Timothy Bellamy, Pradeep Sharma, Santosh Gangwal, Dharmesh Kumar, Carrie Richardson Fry, and Wesley Yellin. Technical Support: Ernie Johnson and Martin Lee. Financial Support: Crystal Wilding. Administrative Support: Deanna Penick.

Table of Contents

Chapter **Page**

Disclaimer i

Acknowledgements ii

Table of Contents iii

List of Tables v

List of Figures vi

Abstract viii

Executive Summary ES-1

1. Introduction 1-1
   - 1.1 Background 1-1
   - 1.2 Advanced IGCC Technologies 1-2
   - 1.3 Proposed Technology 1-2
   - 1.4 Prior Art 1-5
     - 1.4.1 Cyclic Fixed- and Fluidized-Bed Reactor Processes 1-5
     - 1.4.2 Dual Fluidized Bed Reactor Research 1-5
     - 1.4.3 Recent High-Temperature SIP Research 1-6
     - 1.4.4 Recent Catalyst Research for SIP at Lower Temperature 1-6
     - 1.4.5 Recent Process Research for SIP 1-7

2. Catalyst Development 2-1
   - 2.1 Objectives 2-1
   - 2.2 Catalyst Synthesis 2-1
   - 2.3 Catalyst Screening 2-2
     - 2.3.1 Lab-scale Reactor System 2-2
     - 2.3.2 Selection of Catalyst Support 2-5
     - 2.3.3 Determination of Catalyst Iron Loading 2-6
     - 2.3.4 Promoter Loading and Selection 2-9
     - 2.3.5 Long Term Testing 2-12
     - 2.3.6 Effect of Reduction Cycle Length on Catalyst Hydrogen Productivity 2-14
     - 2.3.7 Effect of Syngas Composition on Hydrogen Productivity 2-15
     - 2.3.8 Hydrogen Product Purity 2-17
     - 2.3.9 Catalyst Stability Testing 2-18
   - 2.4 Catalyst Scale Up 2-19

3. Prototype Reactor System 3-1
3.1 Objectives 3-1
3.2 SIP Reactor Design 3-1
3.2.1 Cold Flow Testing 3-10
3.2.2 Process Safety Review 3-13
3.2.3 PSRS Fabrication and Installation 3-13

4. PSRS Testing Results 4-1

5. Techno-economic Analysis 5-1
5.1 Overall Process Description 5-1
5.1.1 Block Flow Diagram 5-1
5.2 Process Modeling Details 5-6
5.2.1 Gasification 5-6
5.2.2 Coal Pre-Feed Treatment 5-6
5.2.3 Air Separation Unit (ASU) 5-6
5.2.4 Gasifier Unit 5-6
5.2.5 High Temperature Desulfurization Cleanup 5-7
5.2.6 Boiler Feed Water Unit 5-8
5.2.7 SIP Reaction 5-8
5.2.8 Power Generation 5-10
5.2.9 CO_2 Capture 5-11
5.2.10 Pressure Swing Adsorption 5-11
5.3 Performance and Economic Comparison 5-11
5.3.1 Operating Costs 5-12

6. Biomass Transportation Model 6-1
6.1 Biomass Selection 6-1
6.2 Biomass Production, Transportation, and Storage Costs 6-1
6.3 Evaluation of Biomass Cost on Plant Size 6-4
6.4 Practicality Analysis 6-4

7. Life Cycle Analysis 7-1
7.1 Introduction 7-1
7.2 Goal of the LCA Study 7-1
7.3 Scope of the LCA Study 7-2
7.3.1 System Boundary 7-2
7.3.2 Functional Unit 7-2
7.3.3 Data Sources, Quality Requirements, and Key Assumptions 7-2
7.4 Life Cycle Inventory Analysis 7-3

8. Conclusions 8-1

References R-1

List of Tables

Number **Page**

2-1 Iron-based Supported Catalysts Synthesized by Precipitation. 2-5
2-2 Physical Properties Results for Catalyst Formulations with Different Iron Loadings 2-7
2-3 Synthesized Catalyst Compositions with Promotors and Supports 2-9
2-4 Physical Properties of the Best Performing Catalyst 2-11
2-5 Simulated Coal Syngas Compositions Investigated....2-15
2-6 CO Concentrations in Hydrogen Products....2-18
2-7 Summary of Characterization Results for Catalysts-50 and -51 2-18
2-8 Best Performing Catalyst Formulations and Properties. 2-19
2-9 Summary of Characterization Results for Laboratory and Commercial Catalysts 2-21

4-1 Syngas Compositions used during Parametric Testing in PSRP 4-1

5-1 Major Streams Associated with the Proposed Process for the Production of Hydrogen from the SIP Technology 5-3
5-2 Major Streams Associated with the Proposed Process to Produce Hydrogen Using Pressure Swing Adsorption....5-5
5-3 Coal Properties....5-6
5-4 Capital Cost Summary for the Proposed Process to Produce Hydrogen from the SIP Technology....5-12
5-5 Capital Cost Summary for the Base Case Scenario to Produce Hydrogen Using Pressure Swing Adsorption....5-12
5-6 Summary of the Unit Costs Used in this Study....5-13
5-7 Operating Cost Summary for the Proposed Process to Produce Hydrogen from the SIP Technology....5-13
5-8 Operating Cost Summary for the Base Case Process to Produce Hydrogen Pressure Swing Adsorption 5-13

7-1 Input and Output Data for the Base Case LCA of Hydrogen and Electricity Co-production 7-5
7-2 Input and Output Data for the Alternative Case LCA of Hydrogen and Electricity Co-production 7-6
7-3 Life Cycle GHG Emissions for the Base Case LCA of Hydrogen and Electricity Co-production 7-7
7-4 Individual Product Revenue for the Alternative LCA Case....7-7
7-5 Life Cycle GHG Emissions for the Alternative Case LCA of Hydrogen and Electricity Co-production....7-8

List of Figures

Number		Page
1-1	Co-production of electricity and hydrogen using the steam-iron process.	1-3
1-2	Gibb's free energy of the main SIP reactions.	1-3
1-3	Enthalpy of the SIP reduction and oxidation reactions.	1-4
1-4	Gibb's free energy of potential iron-carbon side reaction.	1-5
2-1	Steps involved in co-precipitation and spray drying of iron- based catalysts.	2-2
2-2	Laboratory-scale fluid-bed catalyst test facility.	2-3
2-3	Fluid-bed reactor.	2-4
2-4	H_2-TPR profiles of Fe-based supported catalysts.	2-6
2-5	Typical hydrogen curve during oxidation cycle. Area under curve is calculated using Simpson's rule to determine the hydrogen productivity of the catalyst.	2-8
2-6	Performance of catalysts with varying Fe_2O_3 loadings.	2-8
2-7	Performance of catalysts with varying promoter(s) and promoter loadings.	2-10
2-8	Performance of the best promoted catalyst catalysts and a non-promoted catalyst.	2-10
2-9	TPR profiles of the best performing catalysts.	2-11
2-10	XRD profiles of best performing catalysts before and after operation in the SIP.	2-12
2-11	Long-term performance test of selected catalysts.	2-13
2-12	Long term performance for Catalyst-11.	2-14
2-13	Hydrogen productivity of Catalyst-9 using different reduction times.	2-15
2-14	Hydrogen productivity of Catalyst-9 with various gas compositions.	2-16
2-15	CO concentration profiles in hydrogen product stream.	2-17
2-16	Performance of Catalyst-50 and -51 during 30 cycle redox testing.	2-19
2-17	Laboratory and commercially prepared Iron-based catalysts Hydrogen production performance.	2-20
2-18	TPR results with H_2 for laboratory and commercially prepared catalyst.	2-21
3-1	Dual circulating fluidized-bed reactor.	3-2
3-2a	PSRS PID-Sheet 1.	3-3
3-2b	PSRS PID-Sheet 2.	3-4
3-2c	PSRS PID-Sheet 3.	3-5
3-2d	PSRS PID-Sheet 4.	3-6
3-2e	PSRS PID-Sheet 5.	3-7
3-2f	PSRS PID-Sheet 6.	3-8
3-2g	PSRS PID-Sheet 7.	3-9
3-3	PSRS 3D layout.	3-10
3-4	Dual circulating fluidized-bed reactor a) cold flow model and b) schematic.	3-11
3-5	Effect of standpipe aeration on system pressure.	3-12
3-6	DCFBR solids circulation rate over extended operation.	3-133

3-7 PSRS unit during check out activities at vendor's fabrication facility. 3-14
3-8 PSRS unit installation. (a) Raising of the test unit's upper half. (b) Completion of test unit installation 3-14
3-9 Commissioned PSRS unit 3-15

4-1 Results from parametric testing of syngas composition in the reducer reactor.....4-2
4-2 Results from parametric testing of syngas composition in the oxidizer reactor. 4-2
4-3 Results from parametric testing of temperature in the reducer reactor. 4-3
4-4 Results from parametric testing of temperature in the oxidizer reactor. 4-3
4-5 Results from parametric testing of pressure in the reducer reactor. 4-4
4-6 Results from parametric testing of pressure in the oxidizer reactor. 4-4
4-7 Results from testing with syngas containing H_2S in the reducer reactor. 4-5
4-8 Results from testing with syngas containing H_2S in the oxidizer reactor. 4-6
4-9 Reaction rates for the water-gas-shift and reduction reaction in the reducer and steam oxidation in the oxidizer. 4-7

5-1 Block flow diagram of proposed process for production of hydrogen from the SIP technology. 5-2
5-2 Block flow diagram of reference process for production of hydrogen from pressure swing adsorption of syngas produced from a gasifier unit. 5-2
5-3 Experimental run in bench top fluidized bed reactor at 300 psig with 15 cc of catalyst with 34.1% iron content; syngas composition and gas flow rate as a function of time. 5-10

6-1 Schematic diagram of transportation model; where Rc is the collection radius, Ac is the collection area, and dt,i is the road distance from farm i to the plant. 6-2
6-2 Collection radius as a function of hydrogen production for the SIP process using corn stover as a feedstock. 6-3
6-3 Breakdown of production cost per lb of hydrogen as a function of plant capacity for the SIP process using corn stover as a feedstock; total production cost, cost of delivered corn stover, capital depreciation, and other costs (which include maintenance, taxes and insurance, and labor). 6-4

7-1 Block flow diagram and system boundary for hydrogen and electricity co-production using Coal PSA process. 7-9
7-2 Block flow diagram and system boundary for hydrogen and electricity co-production using Coal SIP process. 7-10
7-3 Block flow diagram and system boundary for hydrogen and electricity co-production using natural gas PSA process. 7-11
7-4 Life cycle GHG emissions for the base case LCA of hydrogen and electricity co-production. 7-12
7-5 Life cycle GHG emissions for the alternative case LCA of hydrogen and electricity co-production. 7-13

Abstract

The primary objective of this project was to develop a hydrogen production technology for gasification applications based on a circulating fluid-bed reactor and an attrition resistant iron catalyst. The work towards achieving this objective consisted of three key activities:

- Development of an iron-based catalyst suitable for a circulating fluid-bed reactor
- Design, construction, and operation of a bench-scale circulating fluid-bed reactor system for hydrogen production
- Techno-economic analysis of the steam-iron and the pressure swing adsorption hydrogen production processes.

This report describes the work completed in each of these activities during this project.

The catalyst development and testing program prepared and iron-based catalysts using different support and promoters to identify catalysts that had sufficient activity for cyclic reduction with syngas and steam oxidation and attrition resistance to enable use in a circulating fluid-bed reactor system. The best performing catalyst from this catalyst development program was produced by a commercial catalyst toll manufacturer to support the bench-scale testing activities.

The reactor testing systems used during material development evaluated catalysts in a single fluid-bed reactor by cycling between reduction with syngas and oxidation with steam. The prototype SIP reactor system (PSRS) consisted of two circulating fluid-bed reactors with the iron catalyst being transferred between the two reactors. This design enabled demonstration of the technical feasibility of the combination of the circulating fluid-bed reactor system and the iron-based catalyst for commercial hydrogen production. The specific activities associated with this bench-scale circulating fluid-bed reactor systems that were completed in this project included design, construction, commissioning, and operation.

The experimental portion of this project focused on technical demonstration of the performance of an iron-based catalyst and a circulating fluid-bed reactor system for hydrogen production. Although a technology can be technically feasible, successful commercial deployment also requires that a technology offer an economic advantage over existing commercial technologies. To effective estimate the economics of this steam-iron process, a techno-economic analysis of this steam iron process and a commercial pressure swing adsorption process were completed. The results from this analysis described in this report show the economic potential of the steam iron process for integration with a gasification plant for coproduction of hydrogen and electricity.

Executive Summary

The objective of this project was to develop a gasification-based technology for the coproduction of hydrogen and electricity. The primary focus of the research on this project has been developing a hydrogen production process based on a circulating fluid-bed reactor and an attrition resistant iron catalyst with stable activity for cyclic reduction and oxidation

The key technical challenge for previous attempts to develop this process was a rapid decline in activity that made catalyst replacement costs too large even when using a mined iron ore. The key cause cited for this deactivation was excessive sintering of the active iron sites due to the very high operating temperatures and repetitive cycling between reduced and oxidized states. Our approach opted to reduce the operating temperature by using carbon monoxide (CO) as a reductant rather than hydrogen (H_2). This approach had the advantage of more favorable thermodynamics and an operating temperature in to 400 to 600°C range versus 800 to 1,000°C.

Our initial research efforts began with catalysts development. Our catalyst development efforts used parametric testing of supports, iron concentration, and individual as well as combinations of promoter materials to rapidly and effectively screen different catalyst formulations. Through these efforts, we were able to successfully develop several catalyst formulations that could be reduced at 400 to 600°C with syngas primarily using the CO as the reductant. Because our intended application also involved a circulating fluid-bed reactor, we made sure these catalyst formulations also had the physical and mechanical strength as demonstrated by their attrition resistance and suitability for circulating fluid-bed reactors.

Although achieving our goal with a catalyst prepared at small scale in a laboratory was an impressive result, we continued our catalyst development efforts working with Clariant (formerly Sud Chemie, Inc.) to scale up production in commercial equipment to demonstrate potential commercial production of our iron-based catalyst. Through this effort, we found that effectively controlling the oxidation state through the production process was critical to optimizing the activity of the final catalyst product. In the end Clariant was able to deliver a 100 lb batch of our best iron-based catalyst that was subsequently testing in our Prototype Steam Iron Reactor System (PSRS).

In addition to enabling optimization of our catalyst formulation, the screening tests we completed also provided important information about operating constraints for the process. One of these was that there was an optimal reduction window. If the catalyst was allowed to reduce for too long, the long term activity for cyclic reduction and oxidation declined. By limiting reduction time, the catalyst was able to achieve higher and more stable long term cyclic activity for reduction and oxidation.

Screening our best catalyst formulations with different syngas compositions was able to demonstrate the preference of our catalyst for CO-rich syngas, but it also demonstrated high purity hydrogen production with air-blown syngas compositions. This is an important finding because conventional technologies for hydrogen production from syngas like pressure swing adsorption and membranes are impractical for air-blown syngas. The large nitrogen concentration in air-blown syngas significantly increases the processing complexity to produce a high purity hydrogen product with these conventional technologies.

The reactor testing system used during catalyst development evaluated catalysts in a single fluid-bed reactor by cycling between reduction with syngas and oxidation with steam. Because this provides only

limited information about our circulating fluid-bed reactor process, we designed, constructed and operated the PSRS, which consisted of two circulating fluid-bed reactors, to demonstrate the technical feasibility of the combination of the circulating fluid-bed reactor system and the iron-based catalyst for commercial hydrogen production.

Through a series of parametric tests conducted in the PSRS, we were able to shown effective hydrogen production with syngas produced by all current commercial gasifier design. The optimal performance was with syngas from a dry-fed oxygen-blown gasifier, because of its high CO concentration and low steam concentration. These parametric tests also confirmed the applicability of this process for hydrogen production with syngas from air-blown gasifiers. From 400 to 500°C, no difference in reduction reaction rate was observed, but a significant increase in steam oxidation was observed at 500°C. Pressure also seemed to improve both reduction and steam oxidation reaction rates. Testing with a syngas containing 100 ppmv of H_2S showed that no decline in reduction, water-gas-shift, or steam oxidation reaction rate was observed.

With this successful demonstration of the technical feasibility of our hydrogen production technology demonstrated, our efforts turned to evaluation of the process economics of the process. To effective estimate the economics of this steam-iron process (SIP), a techno-economic analysis of this SIP and a commercial pressure swing adsorption (PSA) process were completed. The results from this analysis show a significant capital cost reduction of our steam-iron process compared to the pressure swing adsorption process. Because of the potential of this process for air-blown gasifiers, which is the preferred gasifier type for biomass, we investigated application of the steam iron process with biomass gasification and found that the optimum plant size for a biomass facility for corn stover in the Midwest produced 300 ton/day of hydrogen at a cost of $1.02 per lb.

Finally, we did some life cycle analysis (LCA) on our SIP compared to the PSA process and conventional steam methane reforming (SMR) process for hydrogen production. The LCA results demonstrate a greenhouse gas (GHG) emission reduction of 307% for SIP and 280% for the PSA process compared to conventional SMR technology.

1. Introduction

1.1 Background

About 50 million metric tons of hydrogen are produced globally every year. The uses of hydrogen are expanding and represent a $135 billion per year industry. New environmental regulations and growing demands in food and fuel sector will lead to significant increase of hydrogen consumption in the near future.

Hydrogen is used extensively in oil refineries. One of hydrogen's primary uses in refineries is hydrotreating to remove sulfur, nitrogen, and aromatics producing cleaner burning fuels which result in lower NO_x and SO_x emissions. Various reactions take place during hydrotreatment, such as, desulfurization, denitrogenation, deoxygenation, dehalogenation, and hydrogenation. Consumption of hydrogen depends on the concentration of sulfur, nitrogen and oxygen in the oil and the degree of removal. Typical consumption of hydrogen in hydrotreatment operations is 70 scf/bbl (standard cubic feet per barrel) of oil per percent sulfur removed, 320 scf/bbl of oil per percent nitrogen removed, and 180 scf/bbl of oil per percent oxygen removed. In modern hydrotreatment operations, total hydrogen consumption is about 200-800 scf/bbl of oil. Recent legislation has reduced the required concentrations of sulfur and nitrogen in transportation fuels to reduce current NO_x and SO_x emissions, which has increased the hydrogen required for hydrotreating.

In refineries, cracking operations are widely utilized to upgrade heavy fractions from crude oil distillation to produce more gasoline, kerosene and diesel, which are higher value products. Hydrocracking simultaneously combines cracking and hydrogenation reactions. Hydrocracking enables refiners to improve gasoline yield and better balance the product slate consisting of gasoline and distillate. Hydrogen consumption typically in hydrocracking is about 1000-1500 scf/bbl.

Large amounts of hydrogen are also consumed in ammonia production, which is used widely in fertilizer production and other chemical applications around the world. In order to keep pace with the expanding global population, fertilizer consumption is rising rapidly and consequently hydrogen consumption.

There are many uses of hydrogen in the food industry. Vegetable oils are hydrogenated to produce margarine and shortening. Sorbitol is a useful sugar alcohol which is produced by hydrogenation of glucose. Hydrogen is also used in metal refining and electronics manufacturing. However, the total consumption of hydrogen in the food industry and other industrial applications is small compared to petroleum and chemicals sectors.

This projected growth in global hydrogen demand will fuel the construction of new hydrogen generation facilities. Currently, the primary technology being used for hydrogen production is steam methane reforming (SMR) which is a mature technology and uses natural gas as a starting material. Because the product for SMR is hydrogen, all the carbon in the natural gas is emitted as CO_2. SMR also operates at very high temperatures for hydrogen production and is an endothermic process. The energy necessary to support this process is provided through combustion of natural gas. The net result is that SMR has a relatively large CO_2 footprint.

Gasification-based technology, such as integrated gasification combined cycle (IGCC), is the only environmental friendly technology that provides the flexibility to co-produce H_2, substitute natural gas (SNG), premium hydrocarbon liquids including transportation fuels, and electric power in desired

combinations from coal and other carbonaceous feed-stocks. Gasification technologies also offer the potential to capture CO_2 and significantly reduce the CO_2 footprint associated with production of these products. Our nation has vast reserves of low-cost coal available for gasification. Furthermore, recent techno-economic evaluations have shown that at natural gas costs of to \$4.50–\$4.75 per million BTU, hydrogen from coal gasification can compete with hydrogen from natural gas (Doctor et al., 2001; Longanbach et al., 2002; Gray and Tomlinson, 2002).

1.2 Advanced IGCC Technologies

These techno-economic evaluations show that advanced gasification technologies novel technologies can reduce the cost of hydrogen even more, particularly when the plant co-produces hydrogen and electricity. DOE and its stakeholders have been aggressively pushing developing advanced IGCC systems through demonstration projects for solids feeding systems, novel gasifier designs, warm syngas clean up technologies, and CO_2 capture that should be completed within the next few years.

Even with these advanced gasification technologies, hydrogen production via gasification will require the use of conventional downstream processing to produce hydrogen. Examples of these conventional commercial technologies include water gas shift (high temperature/sour gas and low temperature shift processes) and hydrogen separation (pressure swing adsorption (PSA) or membranes) equipment. PSA can produce both high pressure and high purity hydrogen directly, whereas membranes systems typically produce low pressure hydrogen that must be compressed for most commercial hydrogen uses. This makes PSA the preferred hydrogen separation technology in commercial coal-to-hydrogen production.

1.3 Proposed Technology

As shown in Figure 1-1, we propose to couple a steam-iron process (SIP) for hydrogen production with advanced gasification technologies. The commercial embodiment of SIP consists of coupled transport reactors circulating a novel, attrition-resistant iron-based catalyst between a reducer and an oxidizer. In the first reactor, syngas will be used to reduce the iron-based catalyst. The product syngas from this reduction process would still contain sufficient fuel value to be used for combustion in a gas turbine. In the second reactor, steam would be used to generate a hydrogen product. Hydrogen is the prime product from the oxidation reactions, which consist of

$$3FeO + H_2O \rightarrow Fe_3O_4 + H_2$$
$$3Fe + 4H_2O \rightarrow Fe_3O_4 + 4H_2$$

As a consequence, this process should enable production of a very high pressure and purity hydrogen from syngas in single process.

To overcome many of the problems, which have plagued previous attempts to develop the SIP, RTI has developed develop a SIP which operates at much lower temperatures. Lower operating temperatures significantly reduce sintering of iron-based catalysts developed. Figure 1-2 presents the thermodynamics of the main reactions for SIP. Although Fe_2O_3 (hematite) might be present in a starting iron-oxide catalyst, it is easily reduced to Fe_3O_4 (magnetite). However, steam cannot easily oxidize Fe or FeO back to Fe_2O_3 (hematite) due to a very large positive free energy change (Roine, 2002). Therefore, the reduction of hematite is not considered one of the key reduction reactions for SIP.

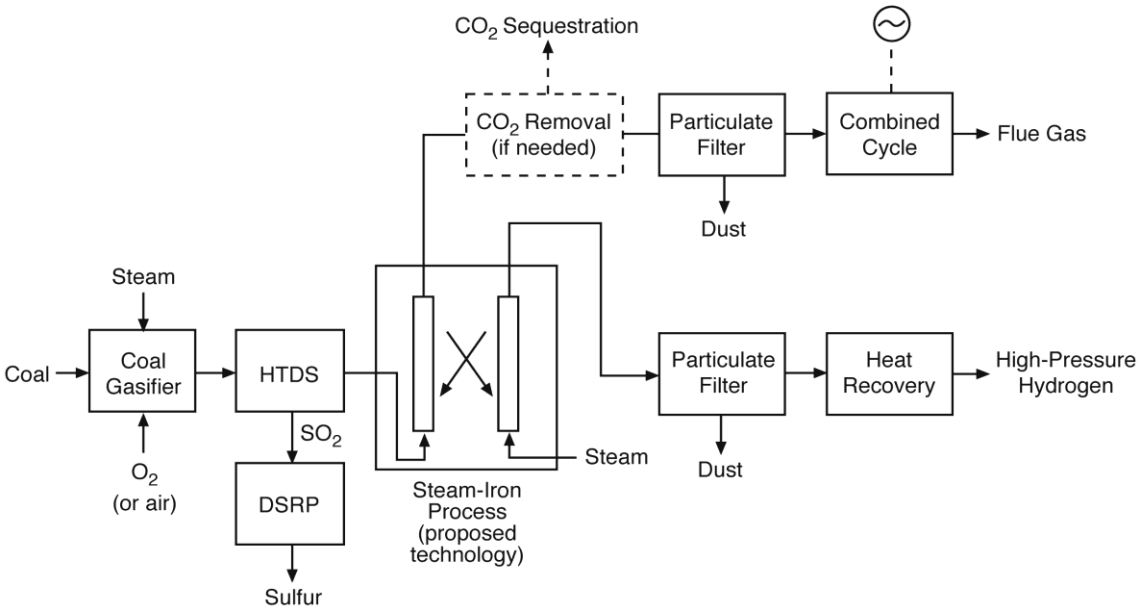

Figure 1-1. Co-production of electricity and hydrogen using the steam-iron process.

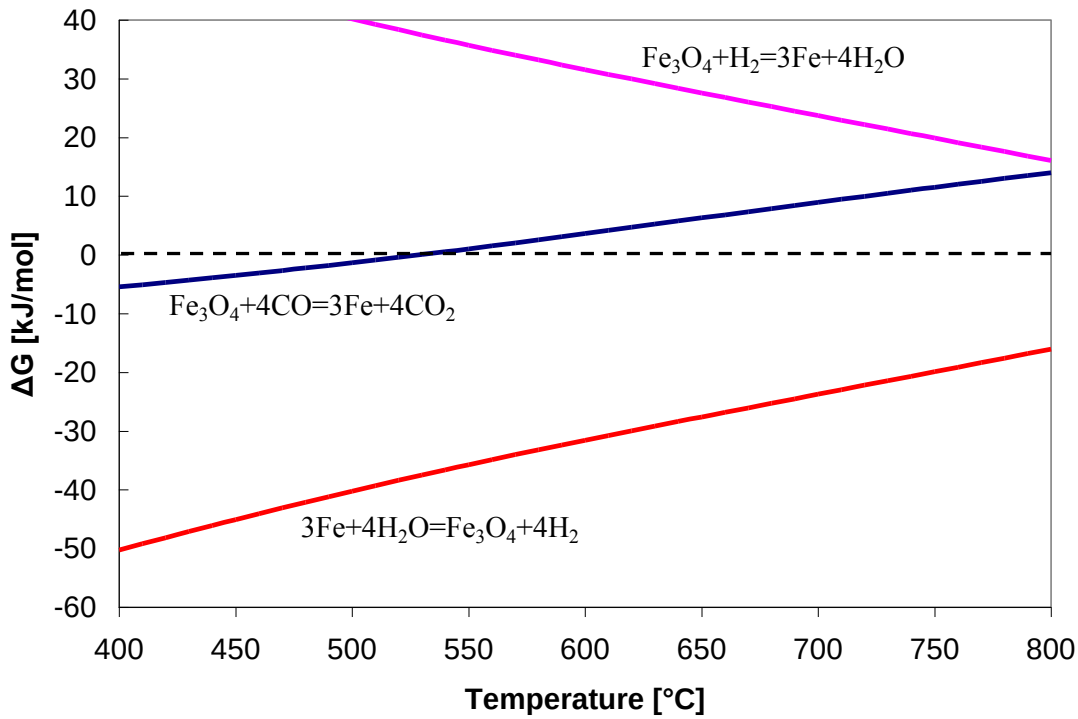

Figure 1-2. Gibb's free energy of the main SIP reactions.

Examining the thermodynamic data in Figure 1-2, the reduction of magnetite with CO as opposed to hydrogen becomes thermodynamically favorable at temperatures below 550°C. Because one of the key technical challenges for previous applications of this technology was deactivation of the iron-based

catalyst due to sintering, the reduced operating temperature for CO reduction should significantly reduce sintering issues. Another advantage of using CO for reduction is this reduction effectively converts the CO into CO_2 reducing or eliminating the need for water gas shift reactors to enable CO_2 capture and reduce CO_2 emissions from the combined cycle.

One of the unique features of SIP, particularly with the use of CO as a reductant, is that both reactions are exothermic as seen in Figure 1-3. No additional energy is required to sustain these reactions. In fact, the transport reactor design might enable effective recover of this heat improving the overall thermal efficiency of the process.

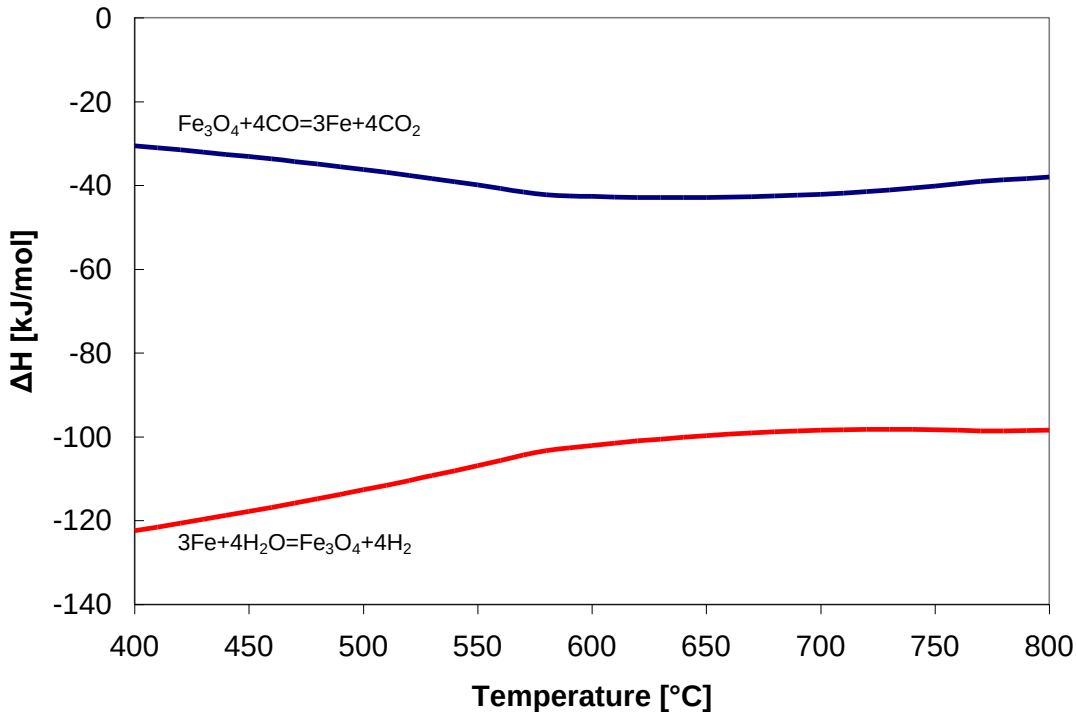

Figure 1-3. Enthalpy of the SIP reduction and oxidation reactions.

One technical challenge with the reduction process was to avoid allowing the reduction to proceed until iron carbides are formed. Allowing deeper reduction increases the potential for catalyst poisoning via formation of secondary iron phases. Formation of iron carbides would be particularly detrimental because the operating conditions would favor the slow conversion of the iron in the iron catalyst into Fe_3C. This can be seen in Figure 1-4, where the reaction for Fe_3C is thermodynamically favorable at the lower temperatures being targeted for CO reduction, but the oxidation reaction for Fe_3C only becomes thermodynamically favorable at temperatures above 700°C.

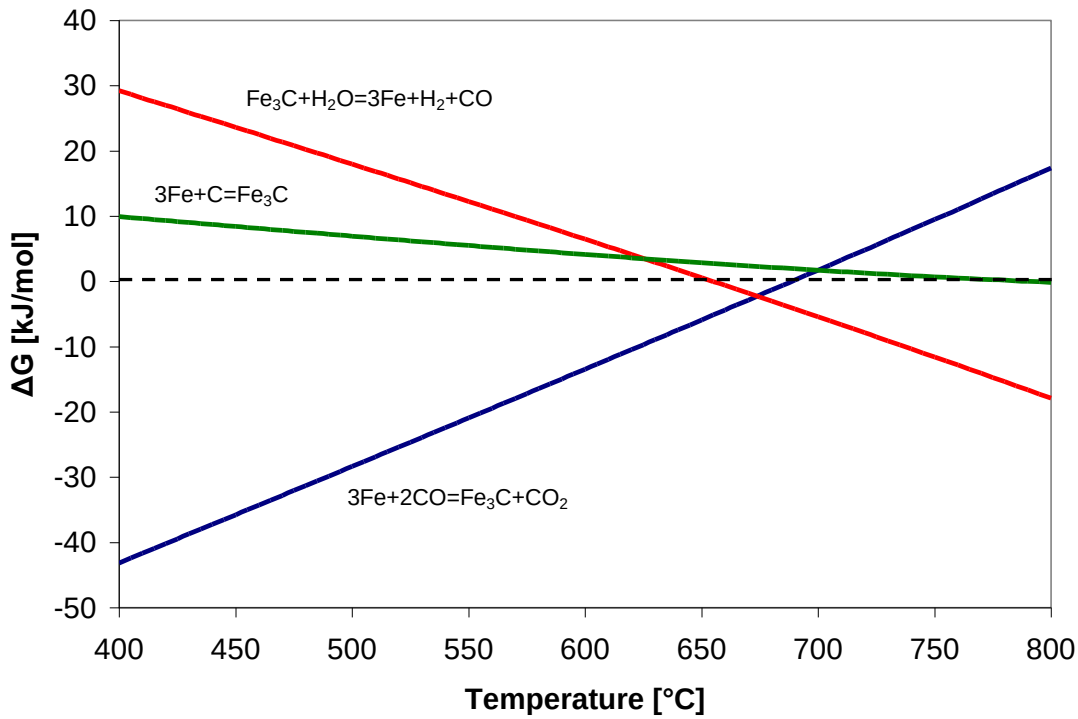

Figure 1-4. Gibb's free energy of potential iron-carbon side reaction.

1.4 Prior Art

1.4.1 Cyclic Fixed- and Fluidized-Bed Reactor Processes

SIP has been known for a century and was, from 1900 to 1930, an important commercial route for making H_2 (Messerchmidt, 1911). However, the process was abandoned as it was not suited for large-scale operation due to the cyclic, fixed-bed, atmospheric pressure reactor. In the late 1950's, U.S. Bureau of Mines conducted extensive research on SIP using a single 2.0inch diameter 10 to 20 feet high fluidized-bed reactor that was cyclically used for both reduction and oxidation (Gasior, et al., 1961). A simulated syngas typical of an air-blown gasifier was used for reduction, and steam and/or CO_2 was used for oxidation, at temperatures ranging from 600 to 900°C and pressures up to 200 psig. Both a synthetic magnetite (containing 4.62 wt% MgO and 0.61 wt% K_2O) and a naturally occurring magnetite containing 0.08% K_2O were used as the iron catalysts. They concluded that about 530 lbs of 35% reduced solid is required to produce 1,000 scf of H_2. They also showed that the synthetic magnetite was more reactive than the natural magnetite and the presence of K_2O in the synthetic magnetite hindered carbon formation. They further concluded that SIP utilizing fluidized beds merits serious consideration when the use of coal for hydrogen production becomes economically feasible.

1.4.2 Dual Fluidized Bed Reactor Research

In 1961, the Institute of Gas Technology (IGT) began development of the steam iron process using separate fluidized beds for the oxidizer and reducer (Elliott, 1981). In the early 1970s, IGT envisioned a process using two fluidized-bed reducers stacked on top of two fluidized-bed oxidizers with gravity flow of the iron ore from the reducers to the oxidizers. From the bottom of the oxidizer, the solids were then lifted back to the reducer. They began commissioning a 1.1 million scf/day hydrogen pilot plant in 1976. However, it appears that the project ended with several problems unresolved. These were: 1) low

reactivity of the natural ore used required large amounts of iron to be circulated, 2) rapid loss of activity, 3) high attrition resulting in dust build up and 4) poor transport of solids.

Casper (1978) provides a conceptual design of the steam-iron process for co-producing 250 billion BTU/day H_2 and 967 MW power from gasification of 32,000 tons/day of a Montana sub-bituminous coal containing 22 wt% moisture. He lists the advantages of the steam-iron process as follows:

- Production of high purity hydrogen
- No need for an oxygen plant because air is used in the plant
- No need for CO shift
- Production of large amount of by-product power.

The plant efficiency, based on the enthalpy of the coal, was given as 59% with 45% converted to hydrogen and 14% converted to power.

1.4.3 Recent High-Temperature SIP Research

Recently, interest in SIP has been revived, particularly in Europe and Japan, due to its potential ability to produce very high purity hydrogen with less than 10 ppm CO (Ariadna, 2005). Hacker et al. (2000) reports experimental results for sponge iron pellet reduction using biomass syngas and re-oxidation using steam at 750°–900°C as follows:

- pellets with the lowest iron content had the highest mechanical and cyclic stability
- purity of produced H_2 was CO < 8 ppm, HCl < 4 ppm and H_2S < 1 ppm

Hacker (2003) is developing a novel process for stationary hydrogen production using the reformer sponge iron cycle (RESC). To enhance the overall efficiency, this process combines SIP with a methane or liquid hydrocarbon reformer, where the reformer is operated using the CO_2 and H_2O stream from the reducer of SIP.

Alchemix Corporation in the United States is attempting to develop the steam-iron process under conditions of molten iron (Kindig et al., 2003; Kindig and Weyand, 2004; Kindig et al., 2004). They claim that their "Hydro-Max" process can produce hydrogen very cheaply compared to steam-methane reforming. Alchemix needs to overcome a number of development hurdles before their process can be scaled up. The severity of the process may preclude high pressure operation.

1.4.4 Recent Catalyst Research for SIP at Lower Temperature

The motivation to move to lower temperature for SIP is due to severe sintering the iron catalysts experiences at high temperatures. Sintering is a phenomenon of ongoing micro-and nanostructural rearrangements resulting in a progressive decline in active reaction surface area. Pizak and colleagues (1996) have investigated the effect of a number of metallic and metal oxide dopants (promoters) to iron oxide on the steam-iron process cycle stability and reactivity at 300-600°C. These authors conclude that all elements more noble than iron, especially Cu and Ni accelerate the sintering of the iron, where as non-reducible oxides, especially alumina, chromia, calcium oxide and magnesium oxide inhibit the sintering. There was no catalytic effect of any of the metals (Pt, Pd, Ru, Cu and Ag) on the steam oxidation step. In contrast, due to hydrogen spill over, the reduction step was catalyzed. The oxide dopants (Al_2O_3, CaO, CrOx, MnOx, and MgO) retarded the reduction step. These authors conclude that a very large and stabilized surface area that can be provided by a highly dispersed nano-particle catalyst is needed for the steam iron process to proceed at temperatures below 300°C.

Research being conducted at the Tokyo Institute of Technology (TIT) has focused on developing iron-based catalysts for storage of hydrogen for proton exchange membrane (PEM) fuel cells. TIT has concentrated on modifying iron oxide-based catalysts to improve iron's cycling stability and activity towards hydrogen production. TIT has reported the development of iron-based catalysts with the following promoters Al, Sc, Ti, V, Cr, Y, Zr, Mo, Ce, Mn, Co, Ni, Cu, Zn, Ga, Nb, W, Re, Ru, Rh, Pd, Ag, Ir, and Pt (Otsuka et al., 1983; Otsuka et al., 2003; Takanaka et al., 2004; Takenaka et al., 2005). Otsuka (2004) reported that oxides of Al, Sc, Ti, V, Cr, Y, Mo and Ce stabilized the deactivation of iron oxide catalysts for redox cycling production of hydrogen. Similarly, the group reported the addition of Ni, Cu, Rh to the iron oxides improved the hydrogen productivity of the storage catalysts. However the group used hydrogen and methane as the reduction media in their studies over a temperature range of 300-475°C instead of coal-derived syngas.

Similar work at the Technical University of Graz investigated the use of sponge iron ore and simulated iron ore catalysts in the SIP for production of hydrogen (Hacker et al., 2000, Thaler et al., 2006). Thaler (2006) investigated the addition Si, Ca, and Al oxides to iron oxide to improve the hydrogen production activity of the catalyst. The results showed that Si and Al were able to act as stabilizers but Ca increased the sintering of the catalyst. As in previous studies, the authors used hydrogen as the reduction agent over a temperature range of 700-900°C. Several other researchers have also investigated the addition of promoters to iron oxide catalysts to enhance its stability and hydrogen productivity. Shimokawabe et al. (1979) showed that doping iron oxides with other metals (Cu, Mn, Co and Ni) reduced the iron oxide reduction temperature and increased hydrogen production yields. Urasaki (2005) investigated the influence of Pd and Zr on the redox properties of iron oxide and showed both promoters increased the activity of the iron oxides for hydrogen production (Urasaki et al., 2005). Pena et al. (2006) investigated the co-promotion of Ni and Cu on iron oxides and showed the dual combination increased hydrogen productivity (Pena et al., 2006). Akiyama (2004) investigated the potential use of Fe_3C as a hydrogen production catalyst for redox cycling processes at 300°C. Although that catalyst was shown to be capable of producing hydrogen, its productivity was found to be lower than other catalysts (Akiyama et al., 2004).

1.4.5 Recent Process Research for SIP

Hydrogen present in syngas also participates in reduction of iron oxide. Unlike CO reduction, the reaction is endothermic and there must be energy transfer between the reduction and oxidation steps. This consideration lead Seiler and Emig (1999) to examine periodic flow reversal using packed beds of Fe_3O_4 for SIP. They observed that iron cycled between a mixture of Fe and FeO and FeO and Fe_3O_4. There was also a gradual loss of capacity and production rate.

Packed beds were also considered by Bop Ju et al. (2006) in an as yet unpublished study. These Canadian investigators examined the effect of CO to H ratio on reduction of pelleted Fe_3O_4 between 500 and 600°C. They observed rapid reduction regardless of gas composition up to about 50 % of the possible conversion to the metal. Carbide formation or carbon deposition then set in. The rate of these processes depended strongly on gas composition. Either process led to the presence of CO in the H_2 product. Duration of the reduction step is thus crucial for hydrogen purity. Furthermore, they found that pure CO gave rapid reduction.

Limited cyclic studies undertaken by Bop Ju et al. with a fixed reduction duration of 10 minutes showed that there was a loss of H_2 production capacity in the first two cycles, but thereafter production stabilized provided a predominately hydrogen syngas was used for reduction. CO content of the hydrogen product was well under 1 % by volume. However, when the syngas contained more than 40 % CO, the packed bed plugged after just 5 cycles.

2. Catalyst Development

2.1 Objectives

The key element for the success of our hydrogen production process is the iron-based catalyst. Based on the prior art, our novel catalyst needed to possess the following characteristics:

- High reduction and oxidation activity.
- Minimal activity and selectivity for side reactions like water gas shift (WGS), carbide or methane formation and CO disproportionation.
- High Fe dispersion.
- High porosity to increase available/accessibility to Fe dispersion.
- Strong and stable catalyst structure/support to inhibit core shrinkage and sintering.
- Stable reduction and oxidation activity in spite of repeated cycling between and oxidized and reduced state.

With these characteristics, the catalyst will have the necessary physical and chemical properties to achieve optimal performance in our process. However, process economic and proposed transport reactor design imposed additional constraints. These constraints include:

- Suitable hydrodynamic properties like shape, particle size distribution, and density.
- High attrition resistance to minimize catalyst losses resulting from solids circulation.
- Reliable and low cost commercial production process.

Drawing upon RTI's previous catalyst/sorbent experience, co-precipitation and spray drying would support effective catalyst development at laboratory-scale of catalyst formulations possessing these characteristics. Furthermore, commercial production of many different materials relies on application of these techniques at commercial scale. RTI's catalyst/sorbent development experience has also demonstrated that production of catalysts/sorbents can readily and rapidly be scaled up for commercial production based on a laboratory-scale formulation and preparation procedure. The following sections contain details on RTI's laboratory-scale co-precipitation and spray drying approach for preparing the iron-based catalysts.

2.2 Catalyst Synthesis

The general flow sheet for laboratory-scale catalyst production is shown in Figure 2-1. For the catalysts prepared in this project, the co-precipitation of the metal salt solution was accomplished with ammonium hydroxide as the base at a pH of about 6. The washing and filtration process were repeated until the pH of the filtrate solution was neutral. During the reslurry process, the pH of the slurry was adjusted to achieve specific pH and viscosity values before spray drying. For some catalyst formulations prepared, promoters were also added during the reslurry process. Spray drying was performed with a gas inlet temperature of 315ºC and an outlet temperature of 110ºC. The fine and coarse catalysts were dried, calcined, and sieved to capture the desired particle ranges for analysis and testing.

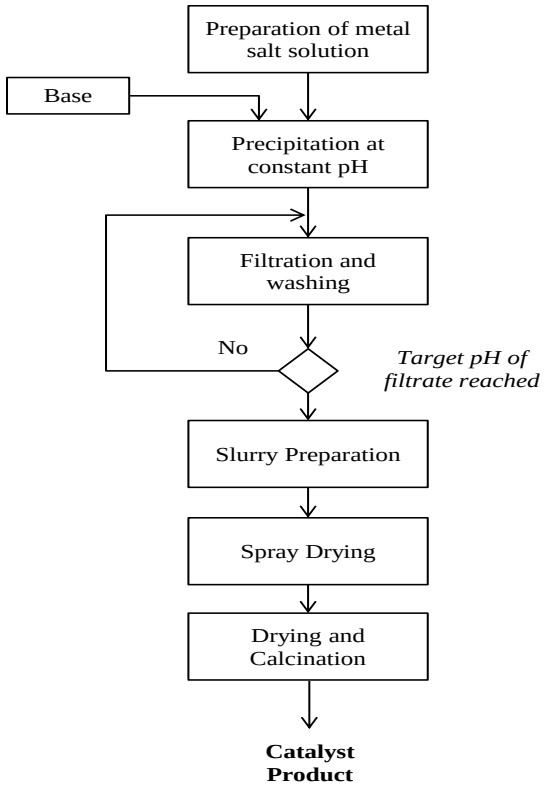

Figure 2-1. Steps involved in co-precipitation and spray drying of iron- based catalysts.

2.3 Catalyst Screening

In order to develop a catalyst with the desired characteristics mentioned previously, the composition and ingredients in the metal salt solution as well as promoters added during the reslurry process were varied in a systematic manner to generate different catalyst formulations. These catalyst formulations were analyzed and tested to establish their ability to meet all of the desired characteristics previously mentioned. Standard physical characterization techniques that were used included BET surface area, x-ray diffraction (XRD), temperature programmed reduction (TPR), and attrition resistance. For attrition resistance, the ASTM 5757 methodology was used.

2.3.1 Lab-scale Reactor System

The catalytic performance of the catalyst formulations was evaluated in a lab-scale reactor system. The lab-scale reactor system was designed and built specifically for testing the cyclic reduction and oxidation of iron-based catalysts. The lab-scale reactor was designed for operation at 300 psig and temperatures up to 600°C. Figure 2-2 presents a simplified process flow diagram of the lab-scale reactor system. The entire lab-scale system can be divided into four subsystems:

1. Gas delivery,
2. Reactor,
3. Product gas processing system,
4. Data acquisition and process control.

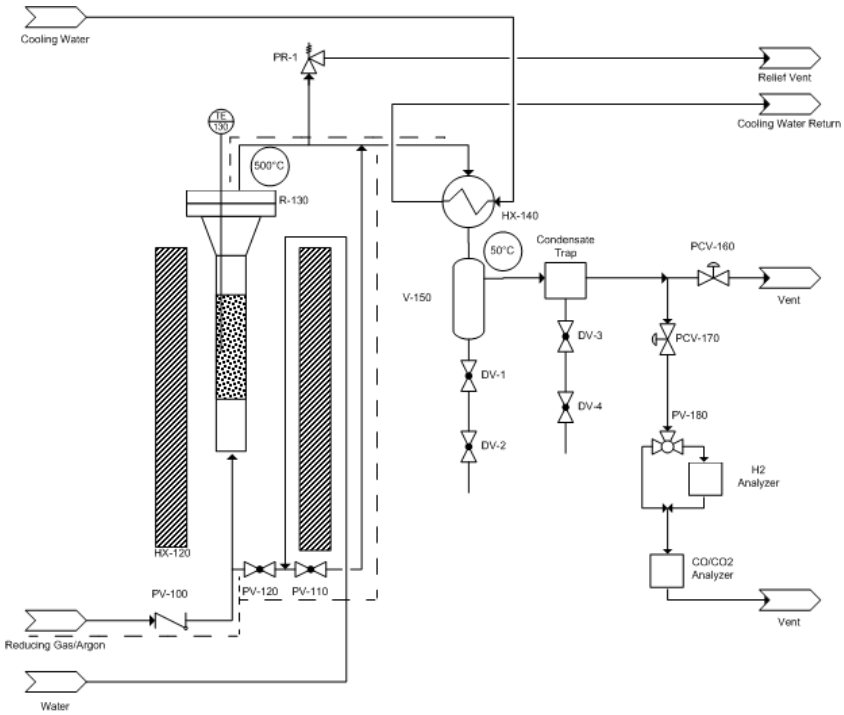

Figure 2-2. Laboratory-scale fluid-bed catalyst test facility.

Gas Delivery System

The gas delivery system was designed to be capable of generating simulated syngas mixtures representative of all commercial gasifier designs from a mixture of CO, H_2, CO_2, Ar, and H_2S. The flow rate of this gas mixture gas was controlled with a mass flow controller (MFC). Steam flow to the reactor for both the syngas and oxidation of the reduced iron catalyst was generated by vaporization of DI water. The required flow rate of DI water was pumped through a heated coil within the reactor furnace to vaporize the water, the resulting steam was introduced into the reactant feed mixture at the inlet for the reactor. To avoid condensation of the steam, both the inlet and outlet gas lines were heat traced and maintained at a temperature 50°F above the dew point of the gas. Argon was used as a purge gas during reactor heat up, shut down and transitioning between oxidation and reduction cycles.

Reactor

To support testing in a fluidized-bed of catalyst, the reactor was designed as an upflow reactor. The lower section of the reactor consisted of ¾ inch Schedule 80 pipe with a sintered metal frit located approximately 5 inches above the reactor inlet. These reactor dimensions and the sintered metal frit created a pocket which held a 15 cm^3 fluidized bed of catalyst particles in the 50 to 150 μm range. At the top of the reactor, the diameter was gradually increased to 1.5 inches to slow the gas velocity down and enable the catalyst particles to settle and fallback into the reactor. This reactor vessel was surrounded by a 3-zone furnace. Figure 2-3 provides a schematic of the reactor with dimensions.

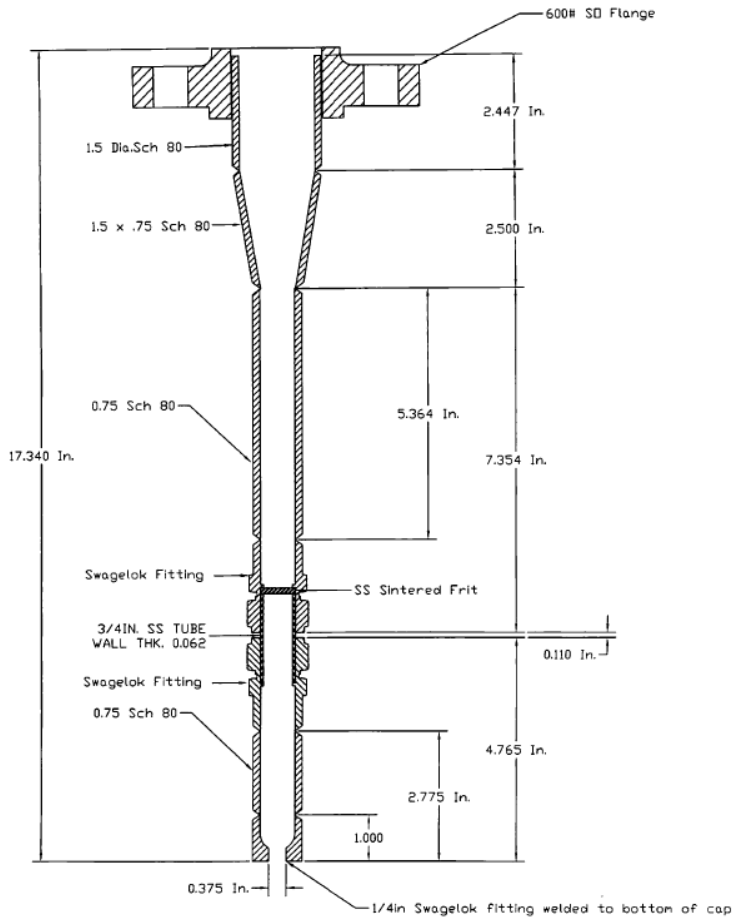

Figure 2-3. Fluid-bed reactor.

Product Gas Processing System

The product gas from the reactor was cooled using a heat exchanger (HX-140), shown in Figure 2-2. This was a 12 inch double-pipe heat exchanger in which laboratory cooling water was used to cool the product gas. Any condensate was separated from the product gas in a knockout pot. System pressure was maintained by a back pressure control valve (PCV-160). A second pressure regulating valve (PCV-170) was used to separate a slipstream of dry syngas for analysis. The gas from the reduction and oxidation cycle were analyzed with an H_2 Scan Model 700 hydrogen analyzer and a Horiba VA-300 gas analyzer for CO/CO_2 analysis. Although these instruments are continuous analyzers, the composition of the gas stream was only recorded every 15seconds by the data acquisition program.

Data Acquisition and Process Control

Key process parameters for this lab-scale reactor system included temperature, pressure and reactor inlet flow rate. Three distinct temperatures were monitored and recorded. These temperatures were the inlet and outlet gas temperatures and the temperature in the catalyst bed just above the sintered metal frit. The MFC controlling the flow react of the gas mixture was used to monitor and record gas inlet flow rate. Pressure control was provided by a back-pressure regulator. The pressure indicator used for the pressure control loop was also recorded as the system pressure. The composition of the product gas was monitored

using the two continuous gas analyzers discussed in the previous section. The date acquisition recorded the temperatures, pressure, flow rate and gas compositions at 15 second intervals. The data acquisition system was also equipped with an alarm system, which was set to alarm at specified high and low limits for each important process variable.

Standard Test Procedure

A typical experimental run consisted of the performing the following steps until a total of 10 reduction and oxidation cycles had been performed.

1. A known mass of 15cm^3 in the particle size range of 50 to 150μm was charged to the reactor.
2. The reactor was pressurized to 300 psig and heated to 500°C under an argon flow.
3. Steam, at the appropriate concentration, was added to the argon feed 5 minutes prior to the addition of the syngas.
4. The syngas mixture of interest flowed through the reactor together with steam for 0.5-2.0 minutes to reduce the catalyst.
5. Following this reduction cycle, the steam flow was stopped leaving an argon flow to purge the system of any remaining syngas. This purge was continued until the CO concentration in the effluent was below 100 ppmv.
6. After completing the syngas purge, a 1.9 slpm stream composed of 47 vol% steam with the balance nitrogen flowed through the reactor to oxidize the reduced catalyst. The steam flow continued until the hydrogen concentration in the stream dropped below 0.27 vol%, which was the lower detectable limit of the hydrogen analyzer.
7. After hydrogen production ceased, the reactor was again purged with argon for 5 minutes.
8. Steps 3-7 are repeated until the run was halted.
9. The spent catalyst sample was removed from the reactor system and captured using a vacuum system

2.3.2 Selection of Catalyst Support

Because the primary desired reaction activity for this iron-based catalyst is stable transitioning between an oxidized to reduced state, a key criteria for selection of a support material was promoting this transition. To evaluate the effect of support materials, a series of catalyst samples were prepared with different potential supports. The different supports and iron loadings on these samples are shown in Table 2-1. The results from temperature programed reduction (TPR) for these samples and bulk iron oxide with hydrogen are provided in Figure 2-4.

Table 2-1. Iron-based Supported Catalysts Synthesized by Precipitation.

Support	Fe2O3 Loading [wt%]
Transition Al_2O_3	30
Precipitated Al_2O_3	80
Transition Al_2O_3	40
USY Zeolite	40

The profile of bulk Fe_2O_3 exhibits a sharp and but less intense peak near 250°C and a broad and intense peak near 500°C. These peaks are attributed to the reduction of Fe_2O_3 to Fe_3O_4 and Fe_3O_4 to metallic Fe, respectively. The supported catalysts also exhibit similar low temperature and high temperature peaks. However, the peaks are shifted by 100 to 150°C higher compared to those of the bulk Fe_2O_3, probably due to the nano size Fe_2O_3 particles dispersed on the supports.

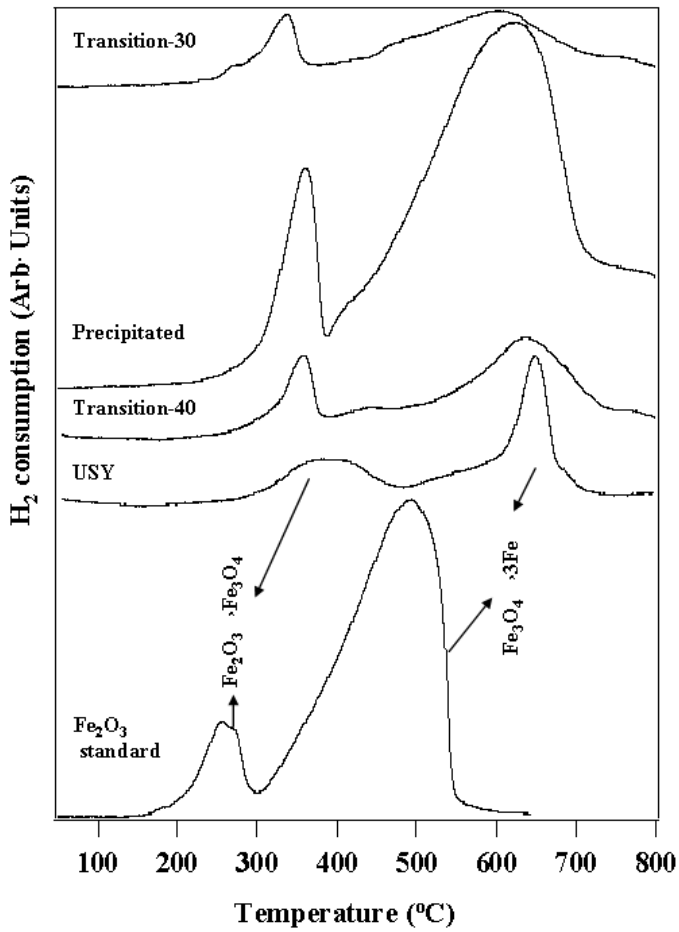

Figure 2-4. H_2-TPR profiles of Fe-based supported catalysts.

The unique result is that the transition of these two reduction peaks for supported materials were essentially of the same magnitude for all catalyst supports tested. Based on this observation, a support structure was chosen based on RTI's previous experience of support materials requiring long term stability in oxidizing and reducing environments and that is suitable for spray drying and yields particles with high attrition resistance. This support is $ZnAl_2O_4$-Al_2O_3, which has been will be used as the support of choice in this project since the support has proven to be very successful in demonstration testing of RTI's High Temperature Desulfurization System (HTDS) technology in which over 3,000 hours of stable operation in a transport reactor were completed. This choice was made to accelerate catalyst development by using a support that could readily be adapted for this application through RTI's previous experience with minimal development efforts.

2.3.3 Determination of Catalyst Iron Loading

A set of three catalyst samples were prepared with different iron loadings. Table 2-2 shows the specific iron loading for each sample along with attrition resistance and surface area results obtained for these samples.

Table 2-2. Physical Properties Results for Catalyst Formulations with Different Iron Loadings

Catalyst	Iron content [wt%]	Attrition ratio[1]	Surface Area [m^2/g]	
			Fresh	Spent[2]
Catalyst-1	34% Fe_2O_3	0.14	36.6	23.4
Catalyst-2	40% Fe_2O_3	0.11	72.0	29.1
Catalyst-3	70% Fe_2O_3	1.75	33.9	20.1

[1] Attrition ratio is defined as the ratio of the attrition loss for catalyst sample to that of a Grace FCC catalyst (16.8%)

[2] Spent catalyst represents the values for the catalyst after 10 cycles of redox cycling

The specific redox testing for these catalyst samples consisted of:

- Reduction
  - Reducing gas: 37.4 vol% CO, 28.0 vol% H_2, 11.2 vol% CO_2, 14.8 vol% steam, 10.3 vol% Ar and 50 ppmv H_2S (simulated syngas)
  - Flow rate: 3.1 slpm
  - Duration: 120 seconds
- Oxidation
  - Oxidizing gas: 47.9 vol% steam in argon
  - Flow rate: 1.9 slpm
  - Duration: Until the hydrogen concentration fell below 0.27 vol% (lower detection limit of the hydrogen sensor)

Both the reduction and oxidation cycles were operated at 500°C and 300 psig. A total of about 10 reduction and oxidation cycles were completed for each catalyst.

A typical hydrogen profile from an oxidation cycle is presented in Figure 2-5. The hydrogen produced during the oxidation cycle was calculated by using the Simpson's rule which approximates the area under a curve using parabolic arcs rather than straight line segments (trapezoidal rule). The hydrogen amounts were used to calculate hydrogen production for the catalysts. The hydrogen production for each catalyst during the 10 cycle redox testing is shown in Figure 2-6.

Figure 2.6 indicates that as iron loading of the catalyst increases hydrogen production for the catalyst increases. The challenge is that the other required physical property, attrition resistance (see Table 2-2), also significantly decreases at the highest iron loadings. The reduction in attrition resistance at higher iron loadings is not unexpected as iron oxides are softer materials than the Al_2O_3-$ZnAl_2O_4$ support. Surface area loss from redox cycling of the catalysts ranged from 36.1% (Catalyst-1) to 59.6% (Catalyst-2). This is attributed to sintering as well as attrition.

It is apparent that the iron content of the catalyst significantly affects both the physical and chemical properties of the catalyst. As the iron content of the catalyst increases, so does the hydrogen production. The mechanical strength of the catalyst remained quite strong provided that the Fe_2O_3 content of the catalyst remained below 50 wt%. Attrition resistance is just as crucial as chemical activity for catalyst used in fluidized-bed reactors. To balance the chemical and mechanical properties of the catalyst, a Fe_2O_3 composition of approximately 48.0 wt% was chosen for further catalyst development. Although the selection of a lower iron content adversely impacts the hydrogen production of the catalyst, the potential to significantly improve this hydrogen production with promoters may more than make up for hydrogen

production that would be possible at a higher iron loading and still maintain the superior attrition resistance achieved with the lower iron loadings. These promoters are also expected to improve catalyst stability.

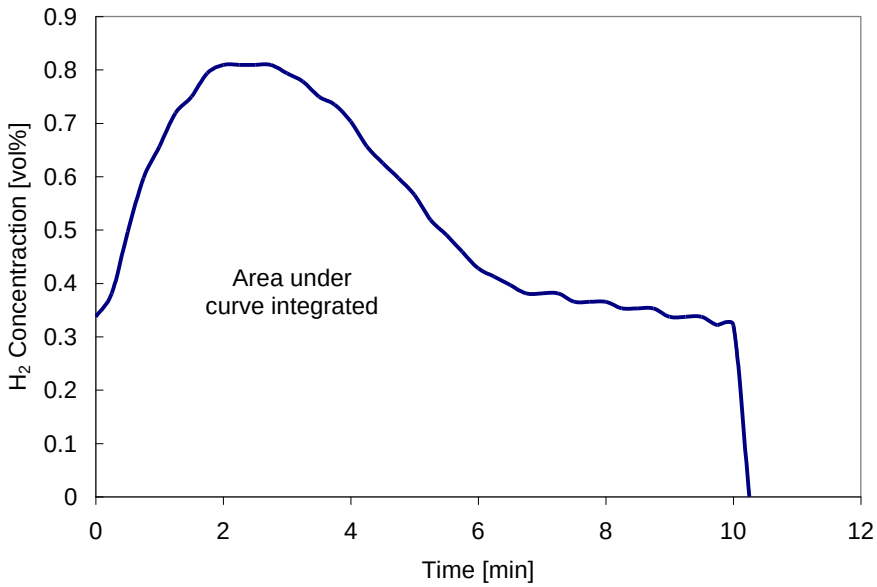

Figure 2-5. Typical hydrogen curve during oxidation cycle. Area under curve is calculated using Simpson's rule to determine the hydrogen productivity of the catalyst.

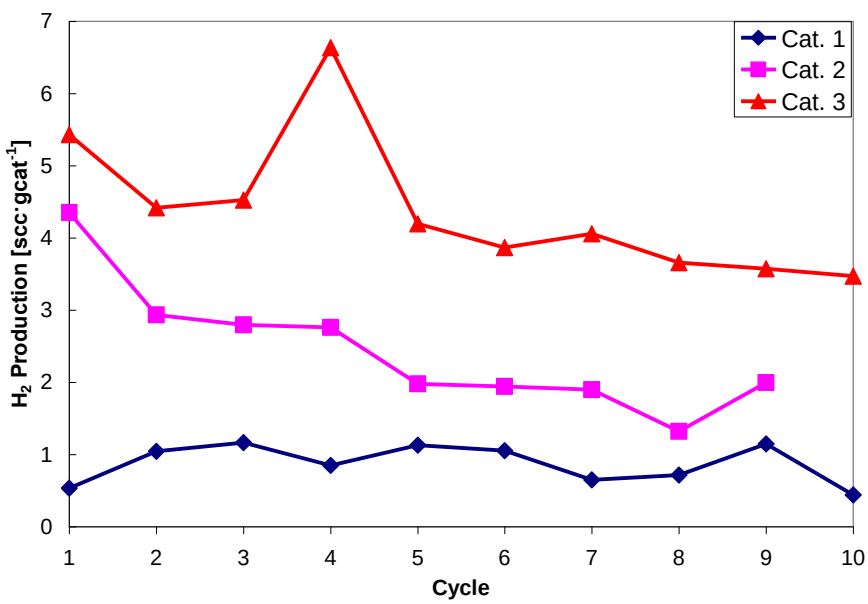

Figure 2-6. Performance of catalysts with varying Fe_2O_3 loadings.

2.3.4 Promoter Loading and Selection

The catalysts listed in Table 2-3 were prepared and tested using the standard testing procedure described in Section 2.3.1 to investigate the effects of CuO, K_2O, K_2CO_3, Cs_2CO_3, VO_x and CeO_2 as promoters. Most tests were carried out to complete 10 redox cycles. Surface area of fresh and spent catalysts and the attrition index of each catalyst were also measured. TPR profiles for each catalyst were collected to determine the effect of the promoter on catalyst reducibility. The hydrogen production observed with the standard testing procedure is given in Figure 2-7. The results from Catalyst-9, -14, -15, -16 are not shown in Figure 2-7, because little to no hydrogen product was detected during oxidation.

Table 2-3. Synthesized Catalyst Compositions with Promotors and Supports

Catalyst	Promoter	Iron Loading [wt%]	Support
Catalyst-4	CuO	40	$ZnAl_2O_4 + Al_2O_3$
Catalyst-5	TiO_2	40	$ZnAl_2O_4 + Al_2O_3$
Catalyst-6	K_2O and CuO	83	SiO_2
Catalyst-7	K_2CO_3 and CuO	40	$ZnAl_2O_4 + Al_2O_3$
Catalyst-8	K_2CO_3	38.5	$ZnAl_2O_4 + Al_2O_3$
Catalyst-9		40	FCC catalyst
Catalyst-10	K_2CO_3	28.0	$ZnAl_2O_4 + Al_2O_3$
Catalyst-11	K_2CO_3	47.6	$ZnAl_2O_4 + Al_2O_3$
Catalyst-12	K_2CO_3	56.5	$ZnAl_2O_4 + Al_2O_3$
Catalyst-13	K_2CO_3 and CuO	47.6	$ZnAl_2O_4 + Al_2O_3$
Catalyst-14	K_2CO_3	47.6	$ZnAl_2O_4 + Al_2O_3$
Catalyst-15	K_2CO_3	38.5	$ZnAl_2O_4 + Al_2O_3$
Catalyst-16	K_2CO_3 and CuO	47.6	$ZnAl_2O_4 + Al_2O_3$
Catalyst-17	Cs_2CO_3 and CuO	47.6	$ZnAl_2O_4 + Al_2O_3$
Catalyst-18	K_2CO_3 and VO_x	47.6	$ZnAl_2O_4 + Al_2O_3$
Catalyst-19	K_2CO_3 and CuO	47.60	$ZnAl_2O_4 + Al_2O_3$
Catalyst-20	K_2CO_3, CuO, and CeO_2	47.6	$ZnAl_2O_4 + Al_2O_3$
Catalyst-21	K_2CO_3 and CeO_2	47.6	$ZnAl_2O_4 + Al_2O_3$
Catalyst-22	Cs_2CO_3 and CuO	47.6	$ZnAl_2O_4 + Al_2O_3$

The addition of promoters clearly has an impact on hydrogen productivity based on the results in Figure 2-7. As one of the objectives of this product is to maximize hydrogen, the four best performing catalysts were selected. Hydrogen production for these catalysts is shown in Figure 2-8 with an unpromoted catalyst sample (Catalyst-2) as a reference. Table 2-4 provides the surface area before and after testing and attrition resistance for the four best performing catalysts and the base catalyst (Catalyst 2).

Figure 2-8 clearly shows the improvement in hydrogen production associated with the addition of promoters in the best performing catalysts. The promoters showing the largest influence on the performance of the catalysts were CuO, K_2CO_3, CeO_2 and Cs_2CO_3.

Figure 2-9 presents the TPR profiles of these best performing catalysts. The reduction profiles in Figure 2-9 show that the addition of promoters results in large decrease in the reduction temperature. This temperature reduction decrease is observed both for the reduction of Fe_2O_3 to Fe_3O_4 and Fe_3O_4 to Fe. Comparison of the hydrogen productivity in Figure 2-9 and reduction temperatures in Figure 2-9 shows a correlation between hydrogen production and reduction temperature. Higher hydrogen productions are observed for catalysts with lower reduction temperatures. The most successful promoter for this was CuO.

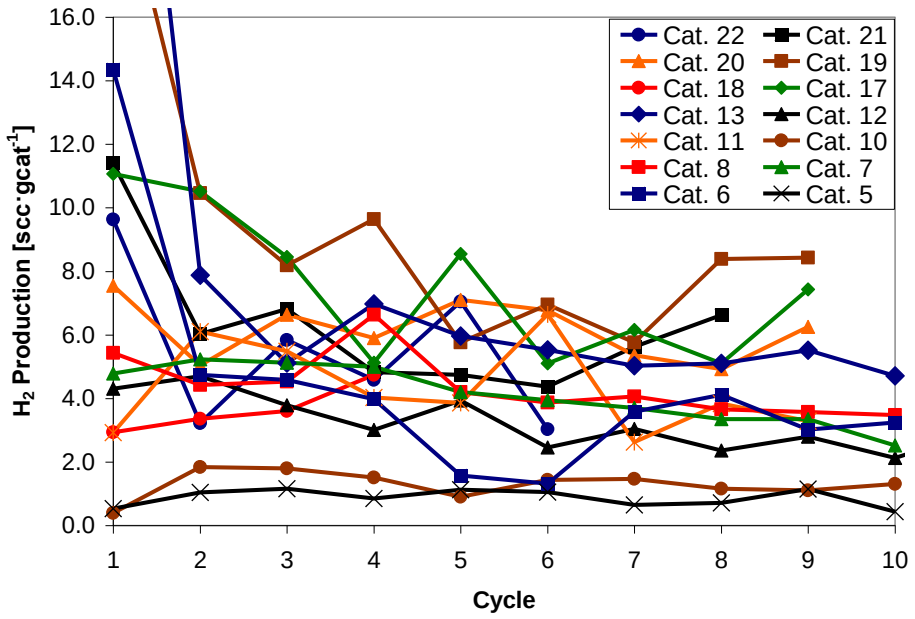

Figure 2-7. Performance of catalysts with varying promoter(s) and promoter loadings.

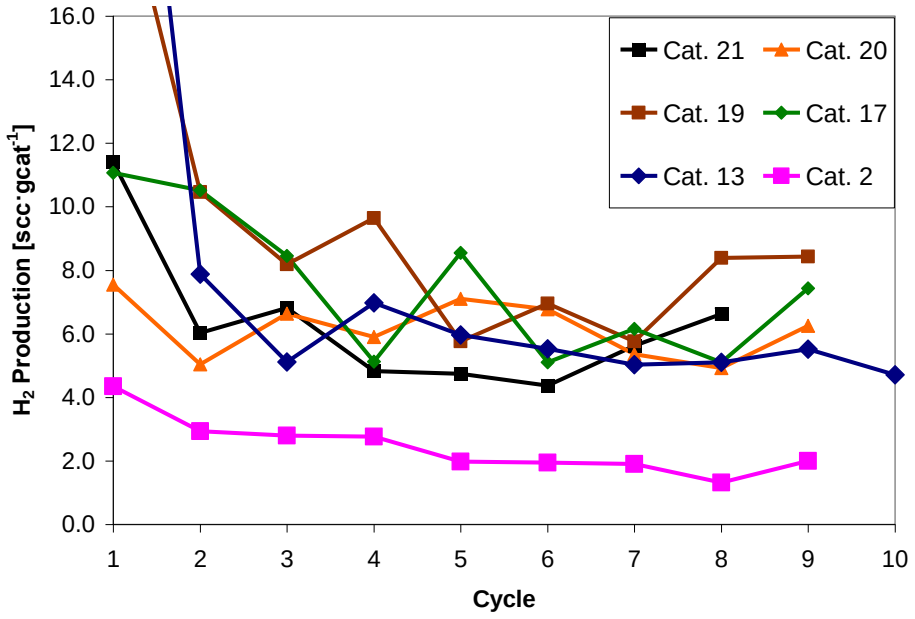

Figure 2-8. Performance of the best promoted catalyst catalysts and a non-promoted catalyst.

Table 2-4. Physical Properties of the Best Performing Catalyst

Catalyst	Attrition Ratio[1]	BET Surface Area[$m^2 \cdot g^{-1}$]	
		Fresh	Spent
Catalyst-13	0.68	62.7	50.9
Catalyst-17	0.10	73.2	63.6
Catalyst-19	0.21	67.1	55.3
Catalyst-20	0.10	76.6	64.6
Catalyst-21	0.88	79.42	67.8

[1] Attrition ratio is defined as the ratio of the attrition loss for catalyst sample to that of a Grace FCC catalyst (16.8%)

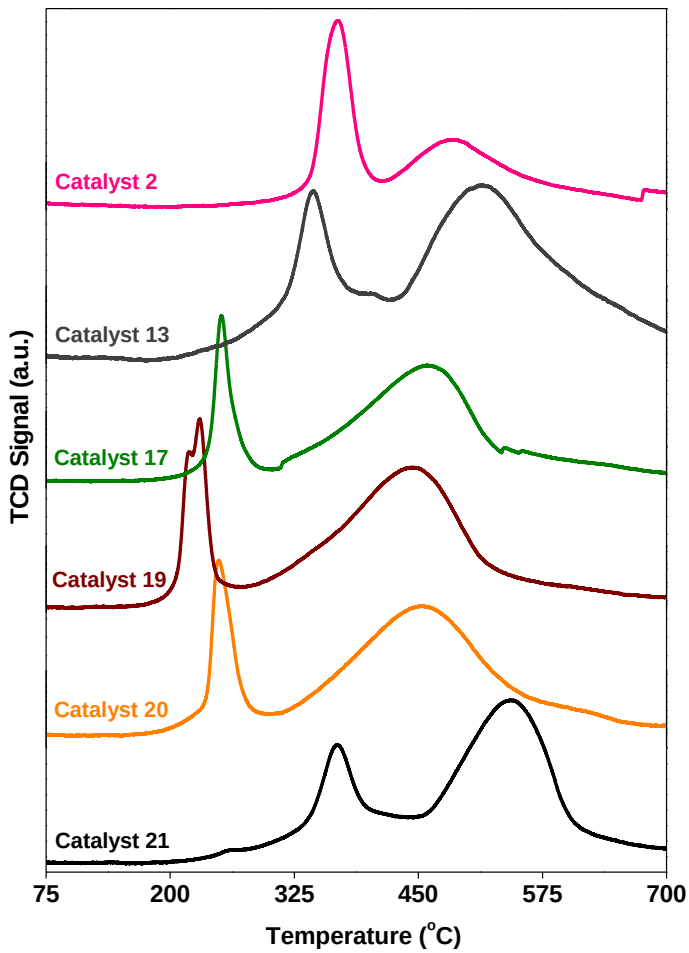

Figure 2-9. TPR profiles of the best performing catalysts.

Figure 2-10 shows the XRD profiles for these best performing catalysts before and after testing. The XRD profiles for the spent catalysts show that the oxidation with steam stops almost exclusively at Fe_3O_4. This result demonstrates that the oxidation potential for oxidation of Fe_3O_4 to Fe_2O_3 ($P_{O_2} \geq 6.5 \cdot 10^{-18}$) is not

achieved using steam as an oxidant. This observation agrees with data collected by Bop Ju et al. (2006) and Seiler and Emig (1999).

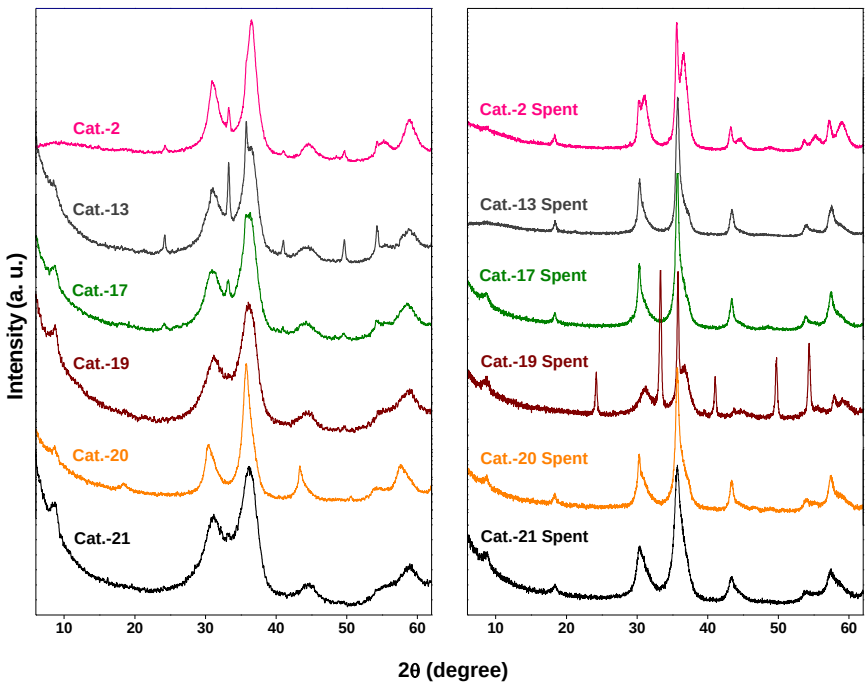

Figure 2-10. XRD profiles of best performing catalysts before and after operation in the SIP.

2.3.5 Long Term Testing

Another important criterion for catalyst development was stable reduction and oxidation activity in spite of repeated cycling between an oxidized and reduced state. To evaluate the stability for repeated cycling between reduction and oxidation, the standard test procedure was repeated to achieve a total of 50 cycles. Figure 2-11 shows the hydrogen production values for four catalyst samples during these 50 cycle tests. For Catalyst-2, -7 and -11, the reduction period during each cycle was maintained at 120 seconds. For Catalyst-19, a shorter reduction period of 30 seconds was used for each reducing cycle. The large oscillations in hydrogen production shown in Figure 2-11 are believed to be caused by a leaking steam bypass valve (PV-110), effectively reducing the steam content of the syngas and increasing the hydrogen production.

The universal trend observed in these hydrogen production profiles for all four catalysts in Figure 2-11 is a gradual decline in hydrogen production with increasing redox cycling. Closer examination of these profiles shows that the most significant decline occurs during the first 10 cycles. During cycles 20 through 40, the decline in hydrogen production is much slower and more consistent from cycle to cycle. During the last 10 cycles, the hydrogen production is essentially constant.

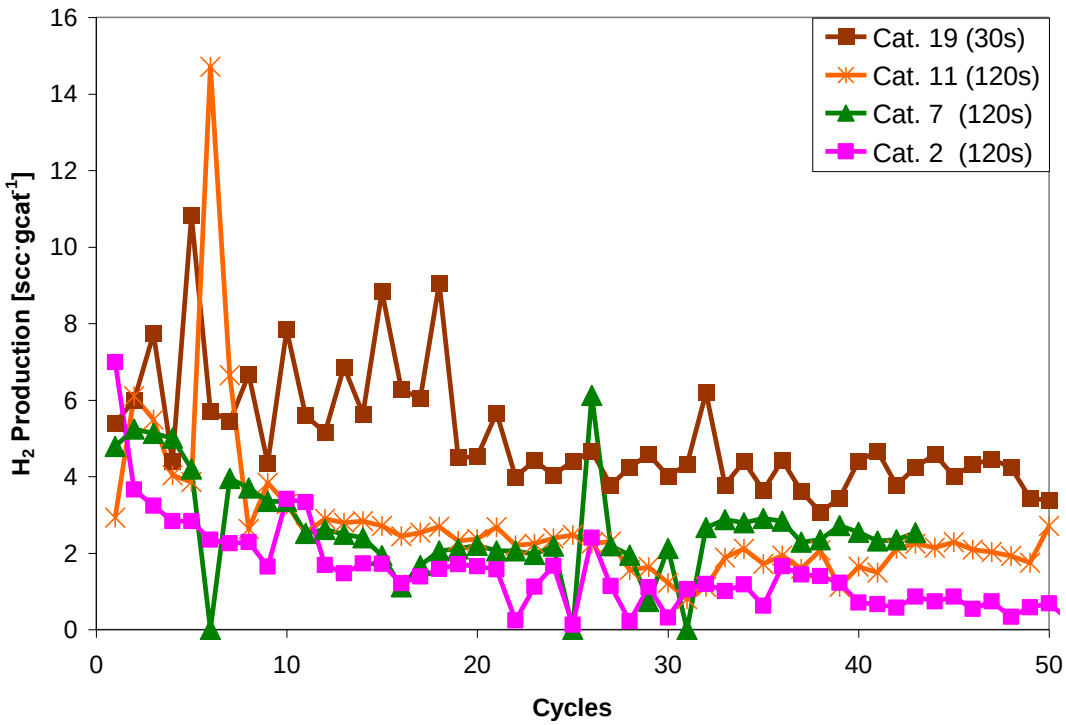

Figure 2-11. Long-term performance test of selected catalysts.

Comparison of the decline in stability between the different reduction time that was used for Catalyst 19 versus Catalyst-2, -7 and -11 indicates that a longer reduction time results in a larger and faster decline in hydrogen productivity. During a longer reduction, more reduction of the iron oxide to metallic iron is expected. Metallic iron is known to be more susceptible to sintering and carbide formation (or carbon deposition) that are causes of loss of activity (or poisoning), which will result in hydrogen production losses. Recent unpublished work of Bop Ju et al. (2006) confirms that the reduction state of the iron is linked with the stability for redox cycling. As these results show that optimizing the reduction time could have a large benefit for catalyst stability, the effects of reduction time on catalyst performance were evaluated. The results from parametric testing of reduction time are described in Section 2.3.6.

To evaluate if the decline in hydrogen production observed during 50 cycles represented a reasonable estimate of long term stable activity, the testing for Catalyst-11 was continued for an additional 50 cycles. The results from this test, shown in Figure 2-12, show that the hydrogen production for cycles 60 to 100 is very consistent. Although this stable hydrogen production is only approximately 50% of its initial value, it is very stable, which was one of the objectives of this catalyst development effort.

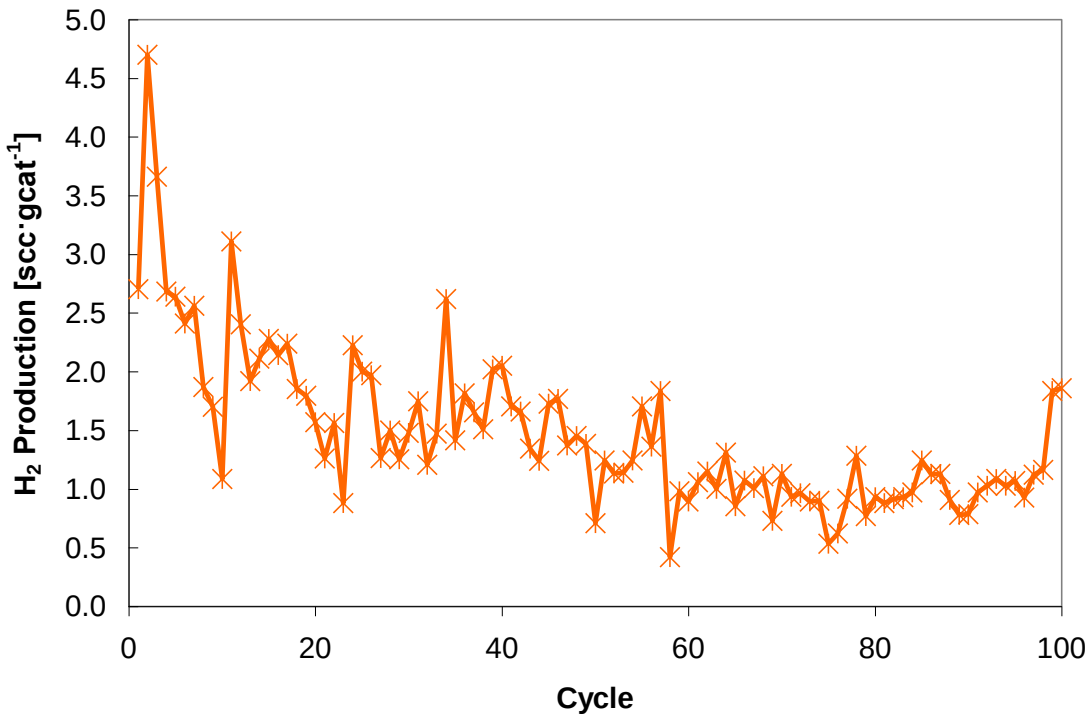

Figure 2-12. Long term performance for Catalyst-11.

2.3.6 Effect of Reduction Cycle Length on Catalyst Hydrogen Productivity

Based on the differences in hydrogen productivity associated with differences in reduction time observed during testing for long term catalyst stability, a series of tests were conducted at different reduction times from 120 seconds down to 20 seconds. The results for this 10 cycle test with different reduction times with Catalyst-9 are shown in Figure 2-13.

The key feature of Figure 2-13 is hydrogen production goes up as the reduction time is reduced from 120 seconds to about 30 seconds. The results between hydrogen production with 20 and 30 second reductions are similar enough to suggest that no further benefit can be achieved for reduction times below 30 seconds.

The explanation of these results is based on the fact that the most easily accessible iron crystallites are rapidly reduced upon exposure to syngas. For longer reduction periods, more reduced states of iron are formed with metallic iron becoming the predominant iron species. Metallic iron results in less hydrogen production during oxidation with steam. At longer reduction times, the decline in the hydrogen production can be observed to become significantly more severe. This is probably because the metallic iron tends to experience more sintering and carbide formation which reduces the active iron sites available for hydrogen production.

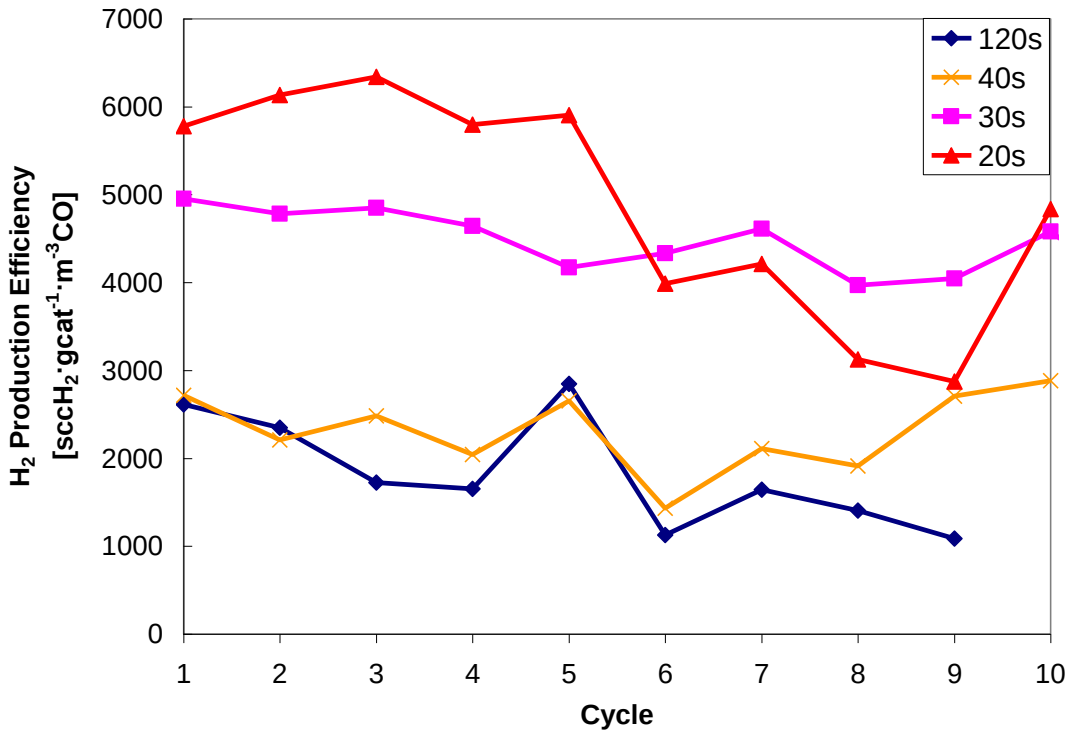

Figure 2-13. Hydrogen productivity of Catalyst-9 using different reduction times.

2.3.7 Effect of Syngas Composition on Hydrogen Productivity

As the performance of the iron-based catalyst was affected by the extent of reduction, the potential impact of the composition of the syngas especially the reducing species was investigated for potential effects on hydrogen production. A set of three syngas compositions were chosen based on the three most representative coal gasification technologies: slurry-fed and O_2-blown (Gas A), dry-fed and O_2-blown (Gas B), and air-blown (Gas C). The compositions for the simulated syngas mixtures are listed in Table 2-5.

Table 2-5. Simulated Coal Syngas Compositions Investigated

Component	Gas A [vol%]	Gas B [vol%]	Gas C [vol%]
CO	37.4	59.7	21.7
H_2	28.0	33.3	11.2
CO_2	11.2	0.0	0.0
H_2O	14.8	2.0	4.8
CH_4	0.0	0.0	2.3
Ar	10.3	0.0	0.0
N_2	0.0	4.9	60.0
H_2S	50 ppm	50 ppm	50 ppm
Reducing Power*	2.5	46.5	6.9

* Reducing Power = $([CO]+[H_2])/([CO_2]+[H_2O])$

The testing with the different syngas mixtures was carried out according to the standard test procedure described in Section 2.3 with a reduction time of 120 seconds. The catalyst used for these tests was Catalyst-9. Hydrogen production profiles for these tests are shown in Figure 2-14.

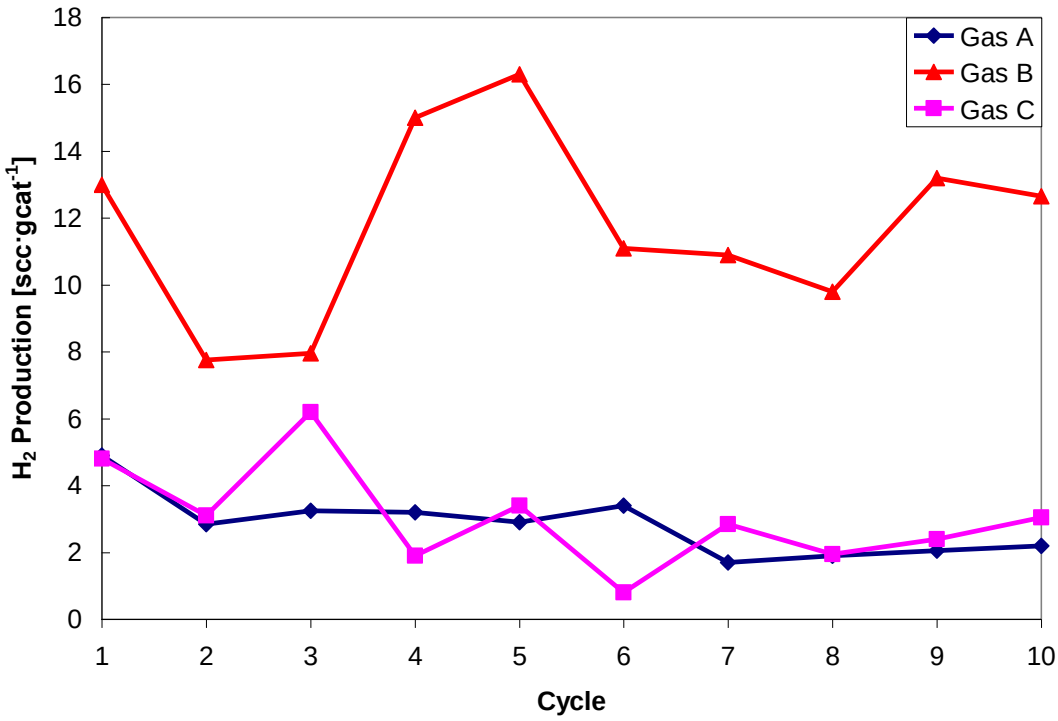

Figure 2-14. Hydrogen productivity of Catalyst-9 with various gas compositions.

In Figure 2-14, the hydrogen production for Gas B is significantly greater than either Gas A or Gas C. Because Gas B has a significantly greater amount of reducing species (H_2 and CO) to oxidizing species (H_2O and CO_2) or reducing power than Gas A and C, the differences in hydrogen production could easily be effect of the reducing power. However, the fact that Gas C has about twice the reducing power as Gas A and yet the hydrogen production for Gas A and C are approximately identical indicates that reducing power is only part of the difference. Gas C in addition to having a greater reducing power than Gas A also has a very large quantity of inert nitrogen. This large nitrogen composition does not affect the gas' reducing power, but does reduce the amount of reducing gas fed into the reactor. When both the reducing power and amount of reducing gas being introduced into the reactor are considered to be factors affecting hydrogen production, Gas A and C should have similar hydrogen production as observed.

A very unique feature of this test that is not immediately evident is that equipment, operating procedures and hydrogen product quality for all three syngas mixtures were essentially identical. This is important because conventional commercial hydrogen production from syngas, which relies on pressure swing adsorption (PSA) or selective membranes could definitively not use the same equipment, operating conditions or generate the same quality hydrogen product from all three syngas mixtures. For Gas C, PSA and selective membranes might not be able to produce high purity H_2 in a cost effective manner. This ability of RTI's steam iron process makes it uniquely suited for hydrogen production from air blown gasifiers.

2.3.8 Hydrogen Product Purity

Although hydrogen purity was not one of the goals of the catalyst development program, it has an extremely important impact on the value and potential applications of the hydrogen product. Furthermore, the primary contaminants that would be present in the hydrogen product are CO and CO_2, which could be generated from carbide formation on the catalyst. Therefore, the CO and CO_2 concentrations in the hydrogen product were measured during a 100 cycle test with Catalyst-9. No CO_2 was observed in the syngas and the CO profiles for key cycles are shown in Figure 2-15.

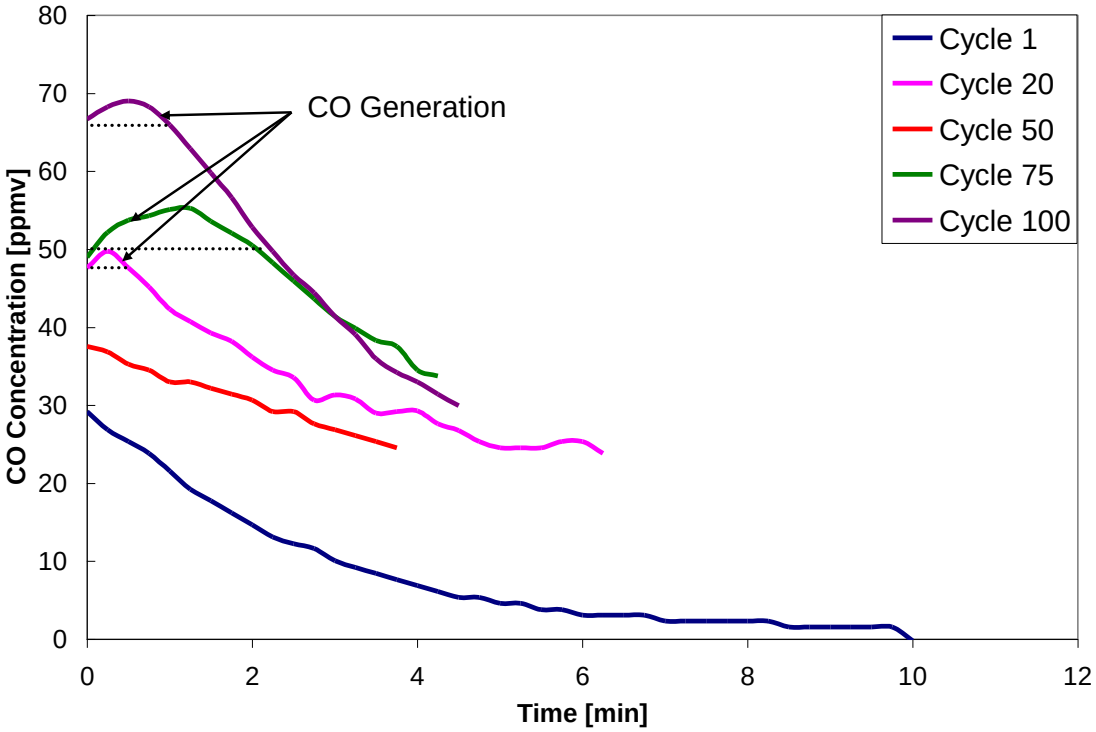

Figure 2-15. CO concentration profiles in hydrogen product stream.

Figure 2-15 shows that CO is present in the hydrogen product stream. However, since the reduction and oxidation cycles are carried out in the same reactor, it is very probably that a majority of this CO is residual CO from the reduction step in the cycle. The fact that the CO concentration rapidly drops off to very low concentrations supports this hypothesis. After 2 min of H_2 production, the CO content is less than 50 ppm regardless of cycle number. By 5 min., it drops to about 30 ppm. Unfortunately, the highest production of CO during hydrogen production is also at the beginning of the hydrogen production process.

Because the purging of CO from the system represents a decrease in CO concentration and any CO production would represent an increase in CO concentration, any CO production at the beginning of the hydrogen production would result in a local maximum in CO concentration. Using the area under the curve for these local maximum, estimates of the CO produced during the hydrogen production process were calculated. The estimated CO produced, the total hydrogen produced and the resultant CO concentration for Cycles 20, 75, and 100 are provided in Table 2-6.

Table 2-6. CO Concentrations in Hydrogen Products

Cycle	H_2 Generated [scc]	CO Generated [scc]	CO Concentration [ppmv]
20	34.0	3.0E-05	1
75	19.7	5.0E-05	3
100	40.7	3.0E-05	1

Table 2-6 shows the purity of the hydrogen product from the SIP is quite high, and would be suitable for proton exchange membrane (PEM) fuel cells which require hydrogen with CO concentrations below 10 ppmv. Because these results were obtained with a reduction time of 120 seconds where more metallic iron is produced and carbide formation more likely, the results that would be obtained with lower reduction times, which maximize hydrogen production, should be even lower.

2.3.9 Catalyst Stability Testing

Towards the end of the catalyst development effort for this project, a new promoter that could improve catalyst stability was identified through several recent journal publications. Two catalysts were prepared with about 8 wt% (Catalyst-50) and 4 wt% (Catalyst-51) of this new promoter. Characterization testing for these catalyst samples included TPR with hydrogen, BET surface area and attrition resistance. A summary of these characterization results is provided in Table 2.7. There are no significant differences in the characterization results in Table 2-7 and 2.4 indicating that the additional of this new promoter has not significantly changed these primary characterization values.

Table 2-7. Summary of Characterization Results for Catalysts-50 and -51

Catalyst	SA_{BET}	Attrition Ratio[1]	TPR Reduction Temperature[2]
	(m^2/g)		(°C)
50	53.6	0.2	235
51	61.0	0.2	255

[1] Attrition ratio is defined as the ratio of the attrition loss for catalyst sample to that of a Grace FCC catalyst (16.8%)

[2] Reduction temperature refers to the peak temperature for the Fe_2O_3 to Fe_3O_4 transition

The next step for evaluating these catalyst samples was testing in the lab-scale reactor system using the standard testing procedure described in Section 2.3. Because optimal stability performance has been demonstrated for a reduction time ≤ 30 seconds, a 30 second reduction time was used in all 30 redox cycles completed in this test. The hydrogen production profiles generated from this test are provided in Figure 2-16.

Figure 2-16 shows that Catalysts 50 and 51 have very similar hydrogen production. The variance associated with the previous best performing catalysts was 1.4-1.7 scc/g_{cat} whereas the variance for Catalysts 50 and 51 was 0.7 and 0.6 scc/g_{cat} respectively. These results demonstrate that the addition of the new promoter has increased the stability of catalyst performance.

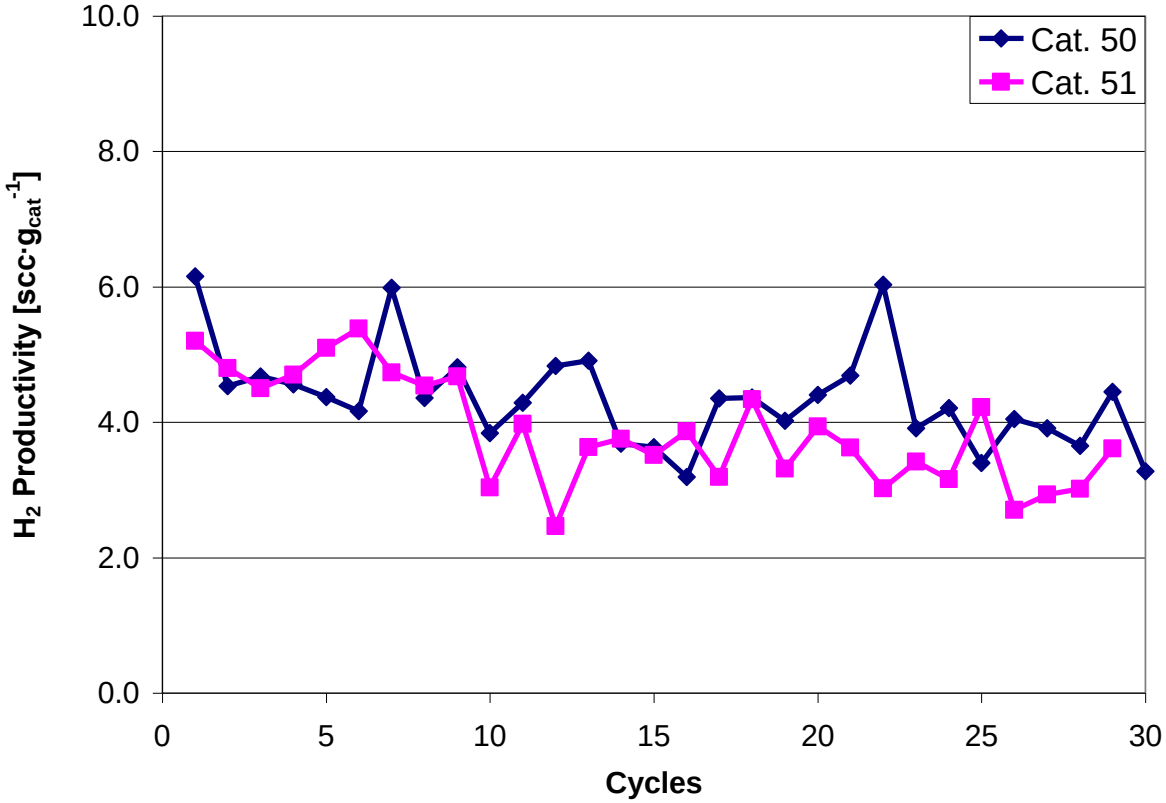

Figure 2-16. Performance of Catalyst-50 and -51 during 30 cycle redox testing.

2.4 Catalyst Scale Up

The performance of all the catalyst samples prepared during the catalyst development effort was reviewed and the four most promising catalyst formulations are selected for evaluation for scale-up. The specific properties of these four catalysts are summarized in Table 2-8.

Table 2-8. Best Performing Catalyst Formulations and Properties.

Catalyst	Average 10 Cycle Performance ($sccH_2/g_{cat}$)*	SA_{Fresh} (m^2/g_{cat})	SA_{Spent} (m^2/g_{cat})
A	7.6±1.7	76.6	64.6
B	5.2±0.6	65.3	58.7
C	6.2±1.7	67.1	55.3
D	6.2±1.5	62.7	50.9

*Syngas Composition: 37.4% CO, 28.0% H_2, 11.2% CO_2, 14.8% H_2O and 10.3% N_2

RTI worked with Süd-Chemie Inc. (SCI) to develop a strategy for scale up the most promising iron-based catalyst for this project. This jointly developed strategy consisted of:

- RTI and SCI reviewing original preparation procedures for Catalyst-A with the goal of scaling production up to commercial scale
- RTI preparing a series of catalysts to evaluate process modifications that enable improved production at the commercial scale
- SCI preparing a 25 lb trial batch of catalyst
- RTI testing this trial batch to confirm similar primary properties and performance of this trial batch to the catalyst prepared in RTI's laboratory
- Repeating the last two steps until the trial batch did have similar primary properties and performance to RTI's laboratory prepared catalyst.

For the first trial batch, the physical properties of the trial catalyst were similar to those RTI prepared. However, as shown in Figure 2-17, the hydrogen production performance of the trial batch was significantly less that RTI's catalyst. Specific analysis were performed including x-ray diffraction, temperature programmed reduction, BET surface area, and ICP analysis to assist in identifying a solution. These analyses identified a secondary iron phase in SCI's large batch that was not found in the laboratory catalyst. This secondary iron phase is assumed responsible for the poor H_2 productivity of SCI's trial batch of catalyst.

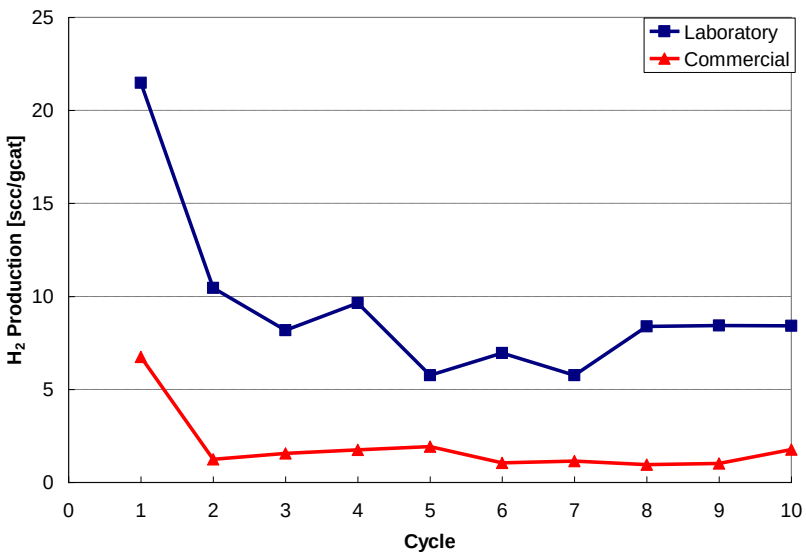

Figure 2-17. Laboratory and commercially prepared Iron-based catalysts Hydrogen production performance.

To investigate factors and conditions that result in the formation of this secondary iron phase, RTI prepared several batches of iron oxide material using modified synthesis procedures at different precursor concentrations, temperatures, and slurring techniques. Based on the results from these modified synthesis tests, RTI and SCI believe the factors resulting in the formation of the secondary iron phase has been identified. Furthermore, RTI and SCI have identified several material synthesis strategies that will prevent the formation of this secondary iron phase during catalyst synthesis.

These strategies for the commercial preparation procedure were implemented with the production of a second trial batch. A comparison to the physical properties of this new trail and catalyst prepared by RTI are provided in Table 2-9 and Figure 2-18. These results demonstrated the commercial production of a catalyst with identical properties to the catalysts prepared by RTI has been achieved. With this

confirmation, preparations were complete to prepare a large 100 lb batch of the catalyst for testing in the bench-scale prototype unit.

Table 2-9. Summary of Characterization Results for Laboratory and Commercial Catalysts

Material	Surface Area [m^2/g]	Attrition Ratio[1]
RTI	55.8	0.2
Commercial	53.3	0.3

[1] Attrition ratio is defined as the ratio of the attrition loss for catalyst sample to that of a Grace FCC catalyst (16.8%).

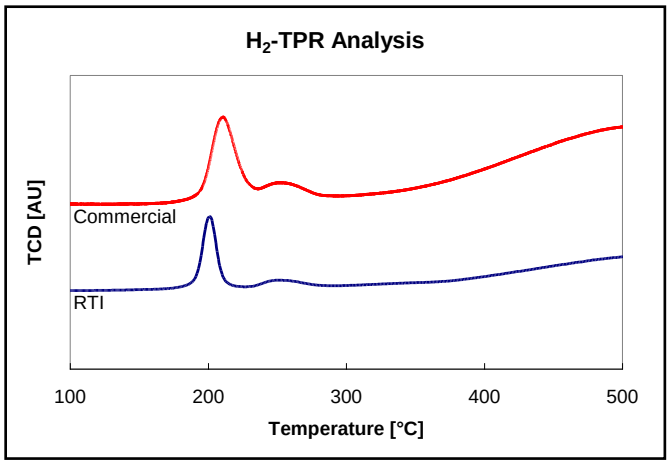

Figure 2-18. TPR results with H_2 for laboratory and commercially prepared catalyst.

3. Prototype Reactor System

3.1 Objectives

The objective of the reactor design and fabrication efforts was to develop a reactor system to safely demonstrate and validate continuous operation at prototype-scale and obtain operational information necessary to complete a detailed techno-economic assessment. This chapter details development of the prototype SIP reactor system (PSRS) from concept through commissioning.

3.2 SIP Reactor Design

The PSRS was designed to demonstrate key features of RTI's SIP and establish a window of suitable operating conditions for the process at commercial-scale. Features to be demonstrated by the PSRS include

- Operational reliability of the proposed process
- Long-term chemical and mechanical stability of the iron oxide-based material
- Production of high-purity, high-pressure H_2 product

RTI's SIP process, shown in Figure 3-1, uses a transport reactor as the reducer and a bubbling fluidized-bed as the oxidizer with an attrition-resistant iron oxide-based catalyst circulated between the reactors. A preliminary design for a 650 SCFH (50 kW_{Th}) prototype dual circulating fluidized-bed reactor system, was developed based on iron redox kinetics and reactor hydrodynamics using process information obtained from catalyst test results during catalyst development. To compensate for kinetic rate differences between the reduction and oxidation reactions two fluidized regimes were chosen. A transport reactor consisting of a mixing zone and riser was selected for the reducer to provide a high solids-to-gas ratio ensuring good heat and mass transfer, while limiting contact time to prevent complete reduction of the iron oxide catalyst and coke formation. Due to the slower kinetics associated with the oxidation reaction, a bubbling fluidized-bed reactor design was chosen to provide the iron oxide-based material sufficient mixing and contact time with steam to oxidize the catalyst and produce H_2.

Sizing and design of the PSRS was completed accounting for sizing constraints imposed by the high-bay facility in which the PSRS system would be operated. The high-bay facility sizing constraints included a ceiling height of 15-ft 6-in and a limited foot print area of 5-ft by 10-ft. Accounting for design and sizing requirements a dual circulating fluidized-bed reactor (DCFBR) design, shown in Figure 3-1, was developed. Additional design attributes which were taken into account include the cyclone, loop seal, J-leg and pressure taps. The cyclone for separating reduced iron oxide material from the reducer effluent was sized based upon standard design criteria for collecting up to 99 percent of the iron oxide material from 60-120 µm in diameter [1]. The loop seal, typically used in solids circulating systems, was incorporated into the design to prevent reactor gas crossover. A non-mechanical valve was selected to control solids flow from the oxidizer to the reducer due to its simplicity and ability to control solids flow rate via aeration gas. An approximated J-valve design was chosen over L- and Y-valve designs since the J-valve design provides a better gas seal. Pressure taps were positioned throughout the solids circulation loop to monitor operating conditions. Differential pressure transmitters were used to monitor essential operating parameters such as reactor solids density, solids flow rate, and differential pressure between the reactors. The DCFBR design was also optimized to maximize solids circulation rate through a series of cold flow trials. Details of the cold flow trials are provided in a section below.

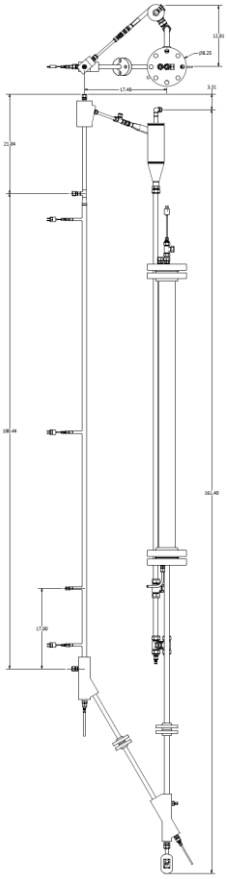

Figure 3-1. Dual circulating fluidized-bed reactor.

With the DCFBR design as a basis for the reactors, a detailed design package was developed for the remaining support systems for the complete PSRS. Key portions of the complete PSRS design included gas flow and pressure control, condensate collection, effluent analysis, and data acquisition/process control in addition to the DCFBR. The detailed design package includes piping and instrumentation diagrams (PIDs), bill of materials, process equipment specifications, process equipment layout, control input/output lists, control philosophy and utility requirements. PIDs and a 3D model for the PSRS are shown in Figure 3-2a-g and Figure 3-3, respectively

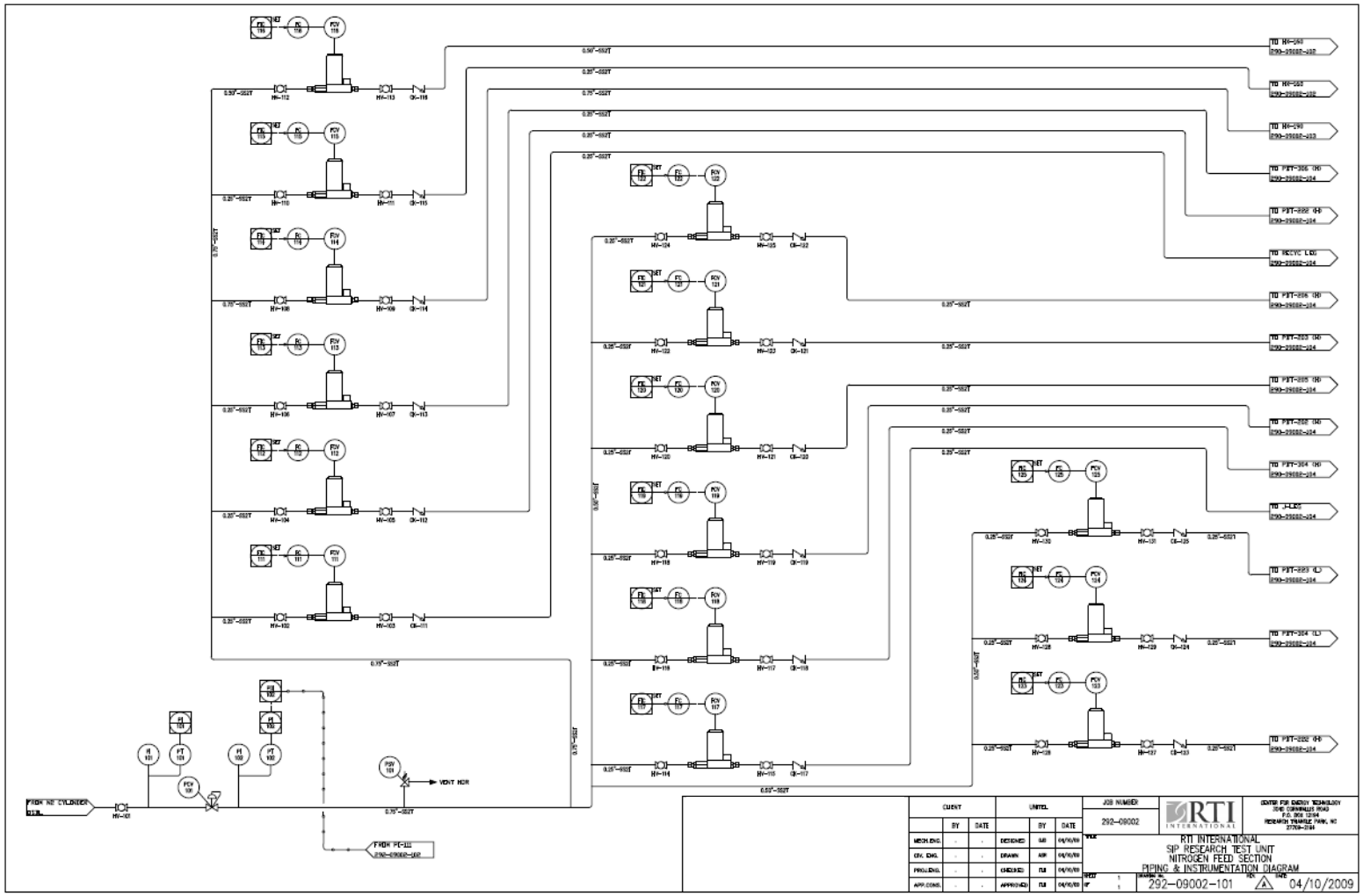

Figure 3-2a. PSRS PID-Sheet 1.

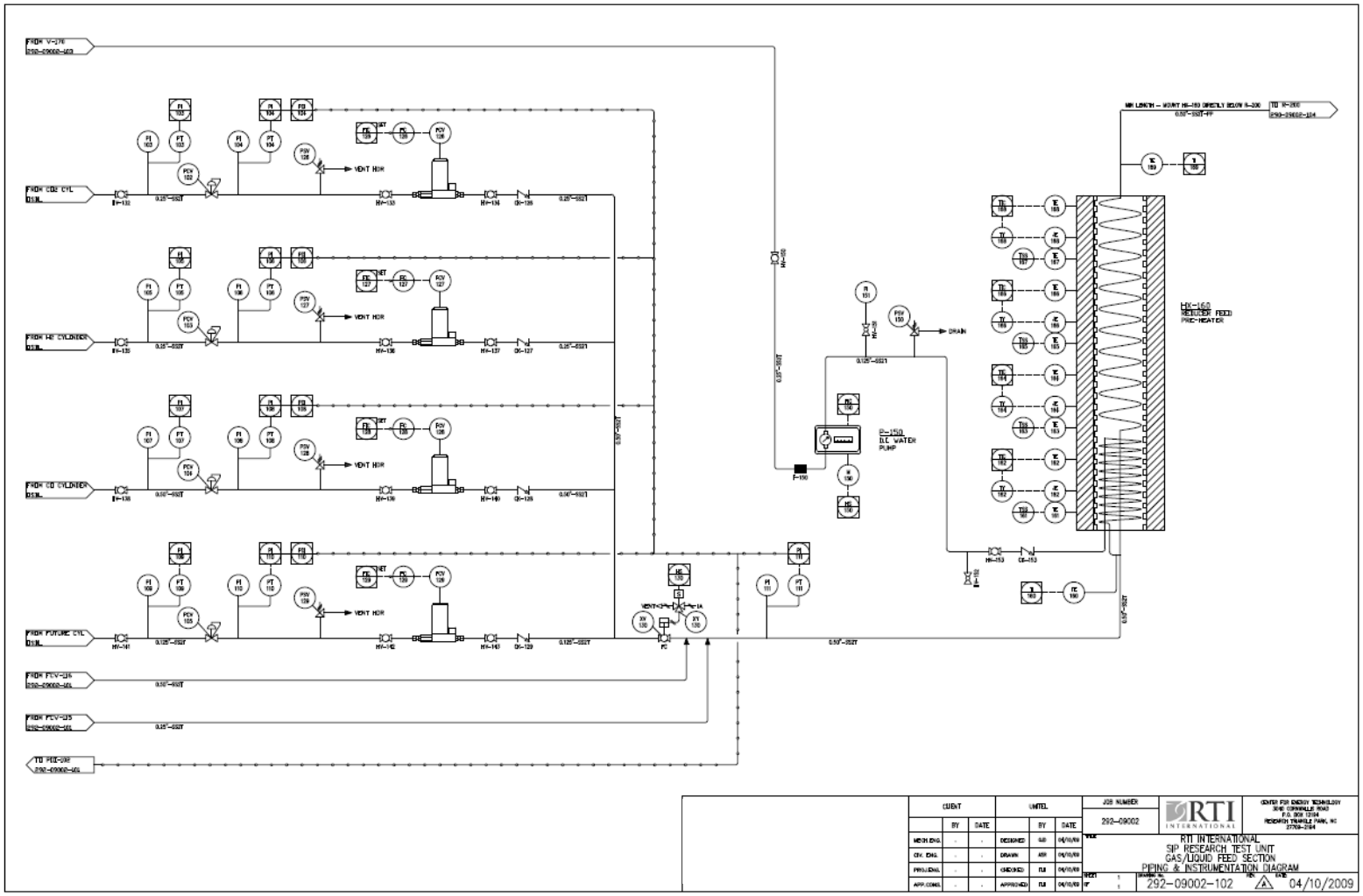

Figure 3-2b. PSRS PID-Sheet 2.

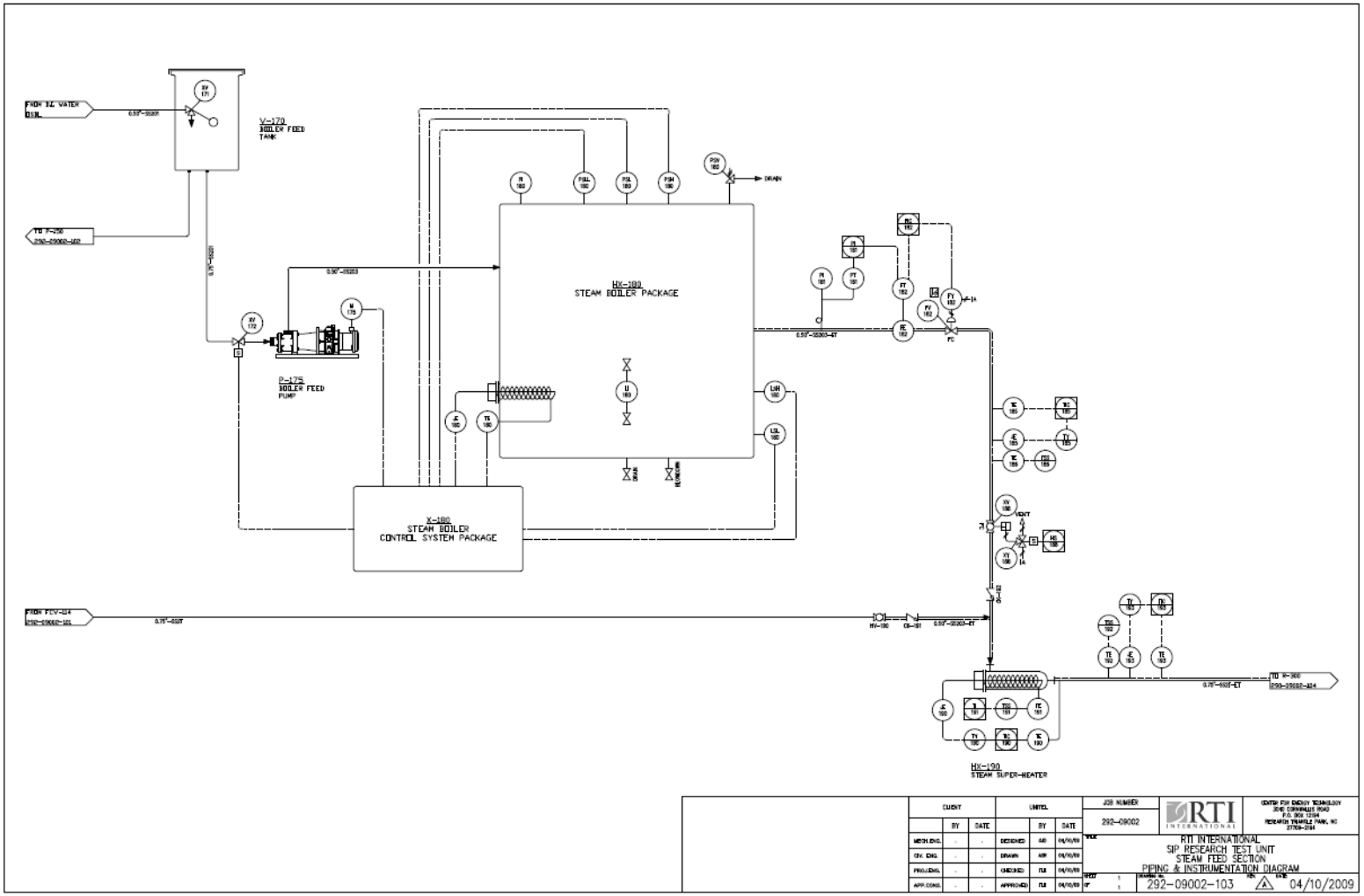

Figure 3-2c. PSRS PID-Sheet 3.

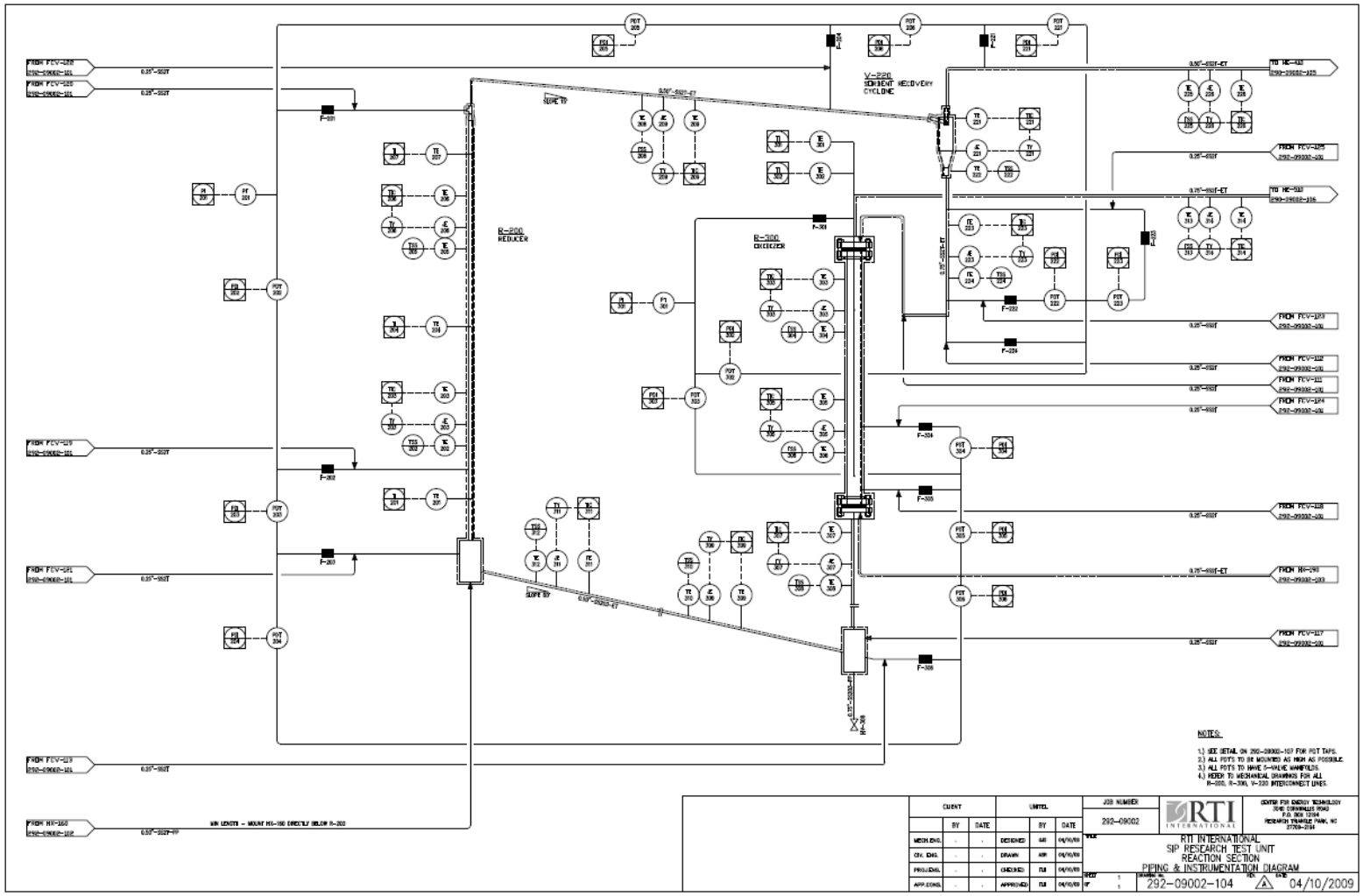

Figure 3-2d. PSRS PID-Sheet 4.

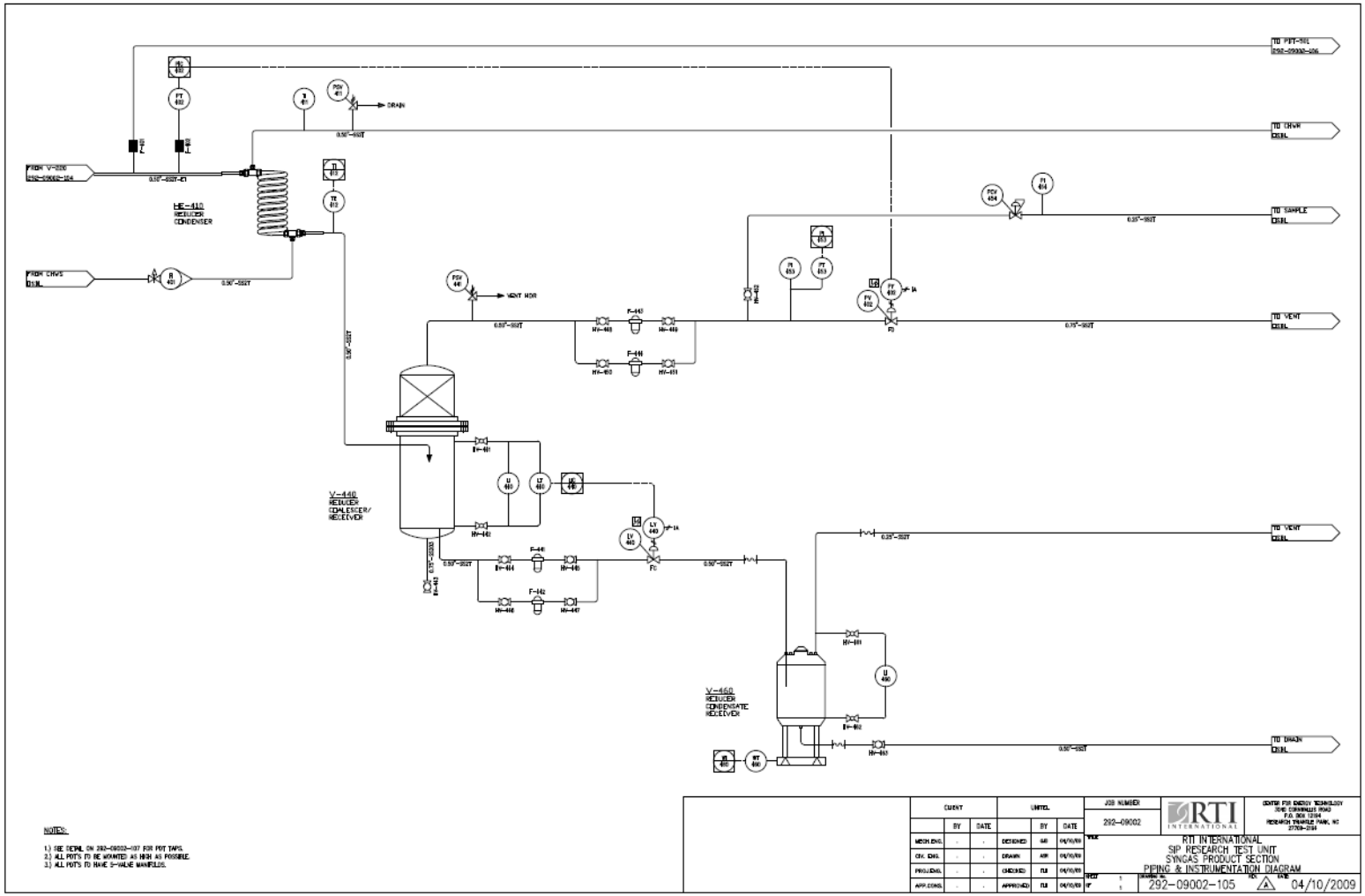

Figure 3-2e. PSRS PID-Sheet 5.

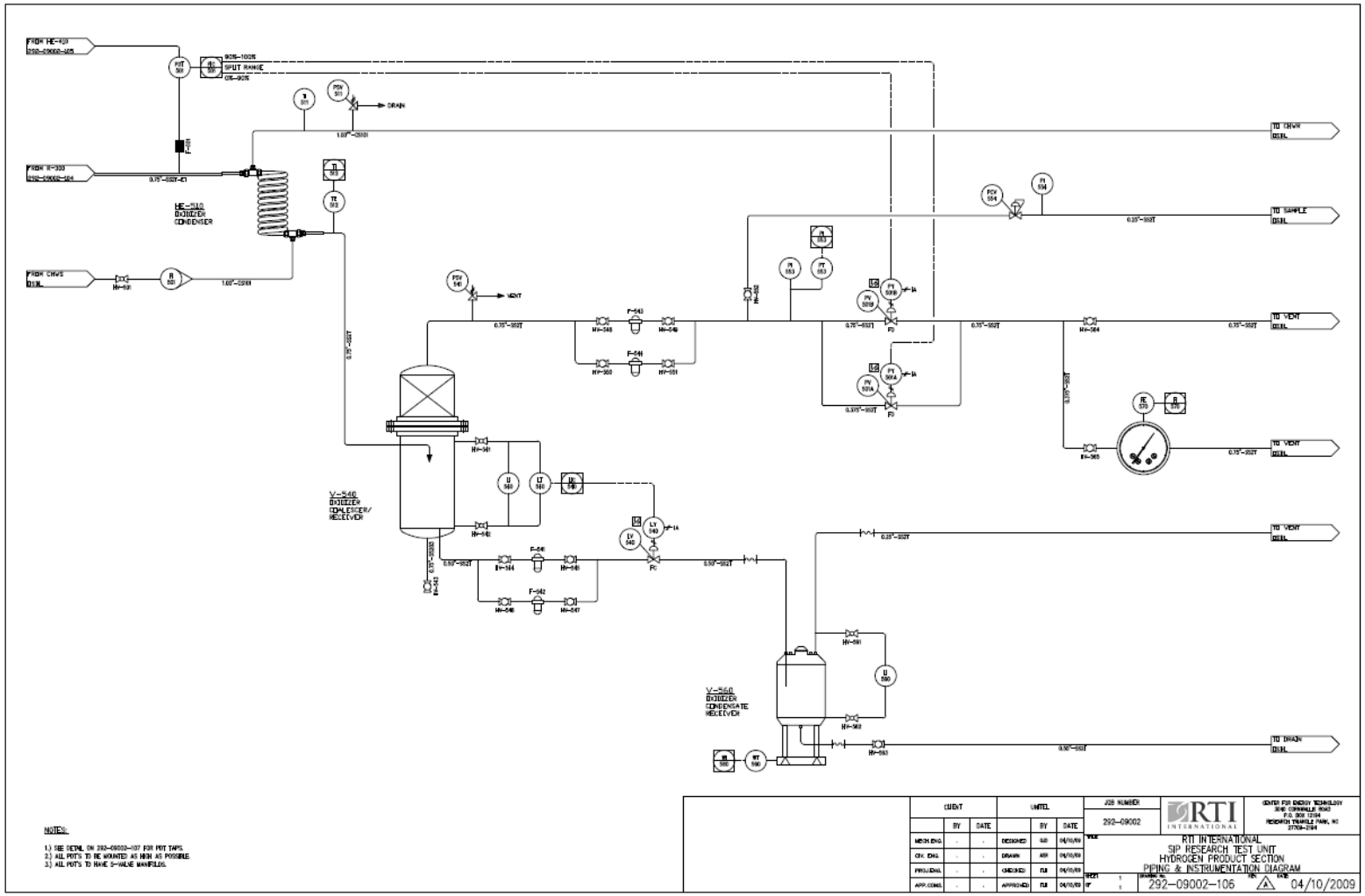

Figure 3-2f. PSRS PID-Sheet 6.

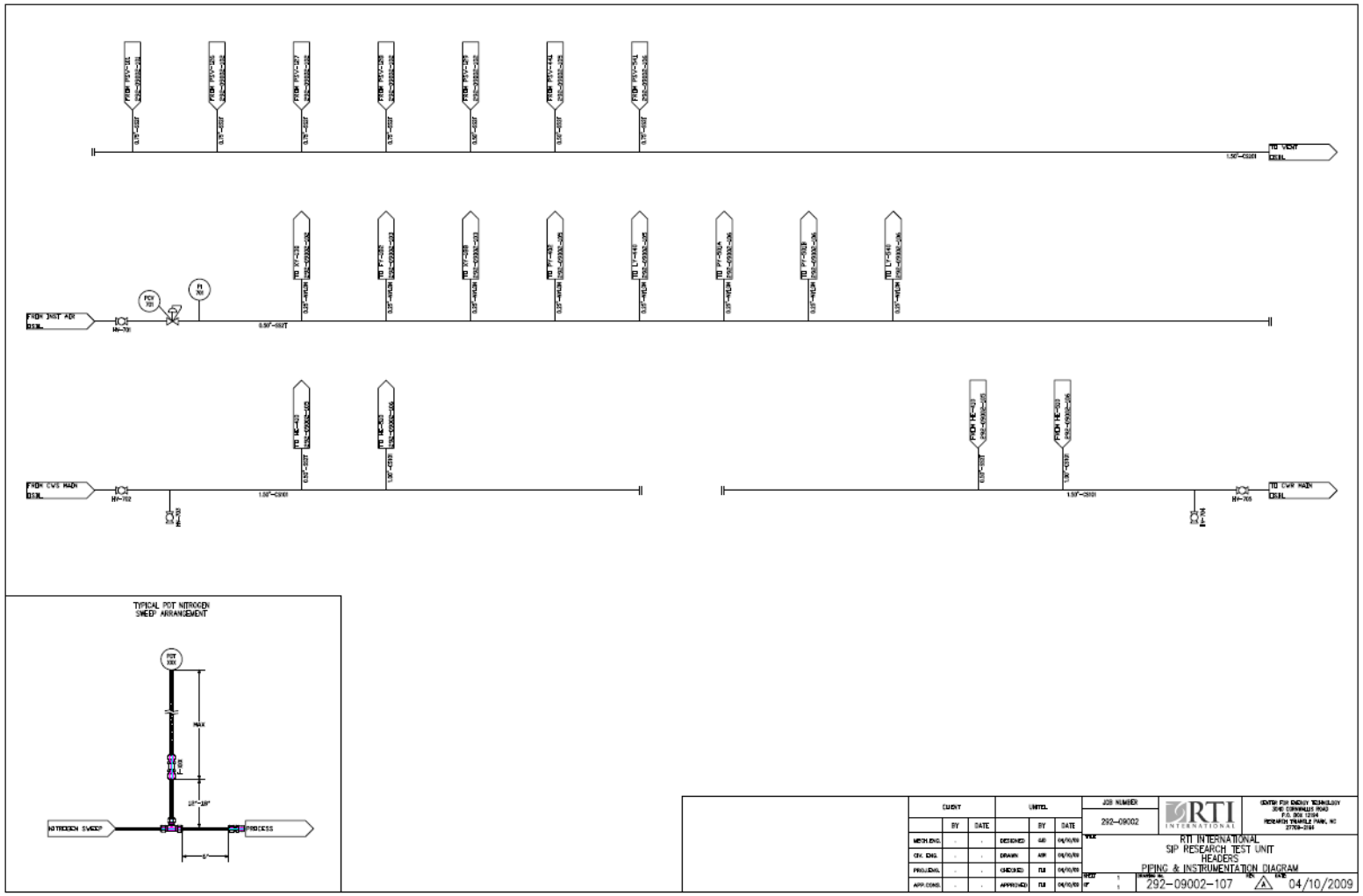

Figure 3-2g. PSRS PID-Sheet 7.

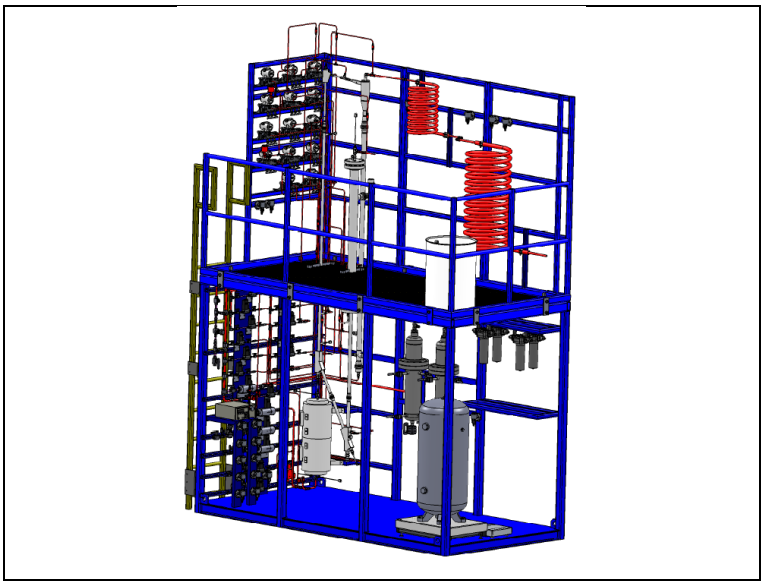

Figure 3-3. PSRS 3D layout.

3.2.1 Cold Flow Testing

An actual scale cold-flow model of the DCFBR, shown in Figure 3-4, was constructed to validate the reactor design specifications for the prototype, identify any potential improvements, and develop operating strategies for the PSRS. This strategy was selected to accelerate the prototype design and process development since the cold-flow unit required minimal capital investment and allowed for rapid validation of the prototype design and process operation strategies.

A fluidizable material possessing similar density and particle size was used in the cold-flow unit. Parametric testing was completed to validate key prototype design issues (maximizing reducer bed density and solids circulation rate) and develop system operating experience.

The cold flow unit was used to investigate several parameters to develop operating strategies for the PSRS including loop seal and J-valve diameters, superficial and aeration velocities, and operational stability. The cold flow unit allowed for rapid optimization of the J-valve and loop seal diameters as preliminary design diameters were determined to limit solids flow. To improve solids circulation the J-valve diameter was increased from ½-inch to ¾-inch schedule 40 pipe and the J-valve pickup block was bored out to decrease pressure loss between the oxidizer and reducer. As a result of the J-valve changes, increased solids throughput was observed through the reducer. With increased solids flow through the reducer, the loop seal diameter was increased from ¾-inch to 1¼ schedule 40 pipe to ensure optimum solids circulation through the DCFBR by making sure that solids circulation rates through the loop seal and J-valve were compatible. After optimizing the J-valve and loop seal diameters, a series of cold flow circulation trials were completed to establish and effective operating window for the system. Results from parametric testing of standpipe aeration are shown in Figure 3-5. Higher standpipe aeration was shown to increase standpipe pressure and the bed density in the reducer to a maximum value. However, when standpipe aeration increased sufficiently that the bubble size was equivalent to the standpipe diameter, standpipe pressure and bed density in the reducer decreased eventually resulting in disruption of solids flow through the standpipe. Using information obtained from the cold flow unit, a set of operational parameters were developed which would allow for stable operation of the DCFBR. Further testing with the unit, shown in Figure 3-6, showed the optimized DCFBR possessed a dynamic operating window and was capable of stable solids circulation.

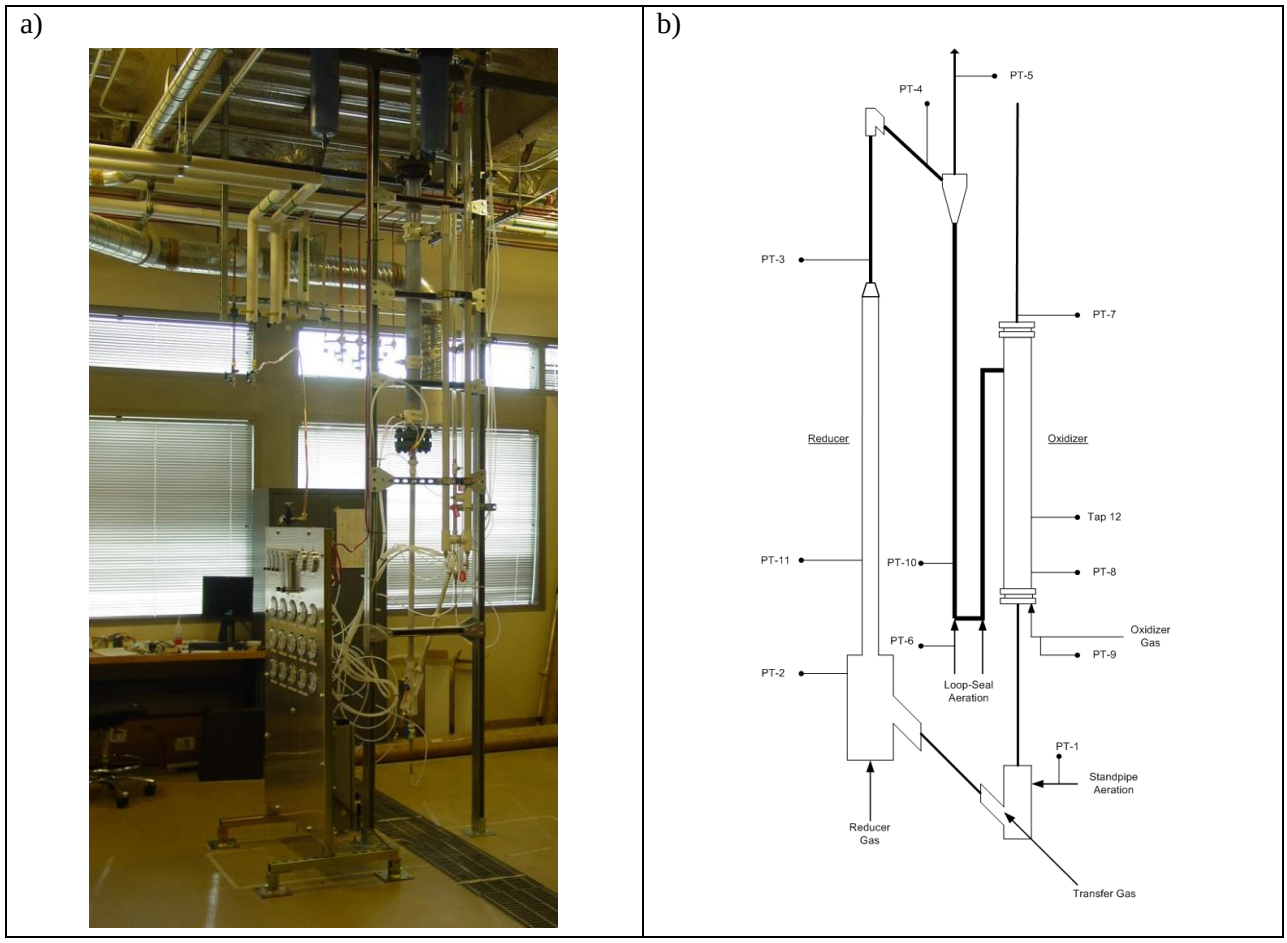

Figure 3-4. Dual circulating fluidized-bed reactor a) cold flow model and b) schematic.

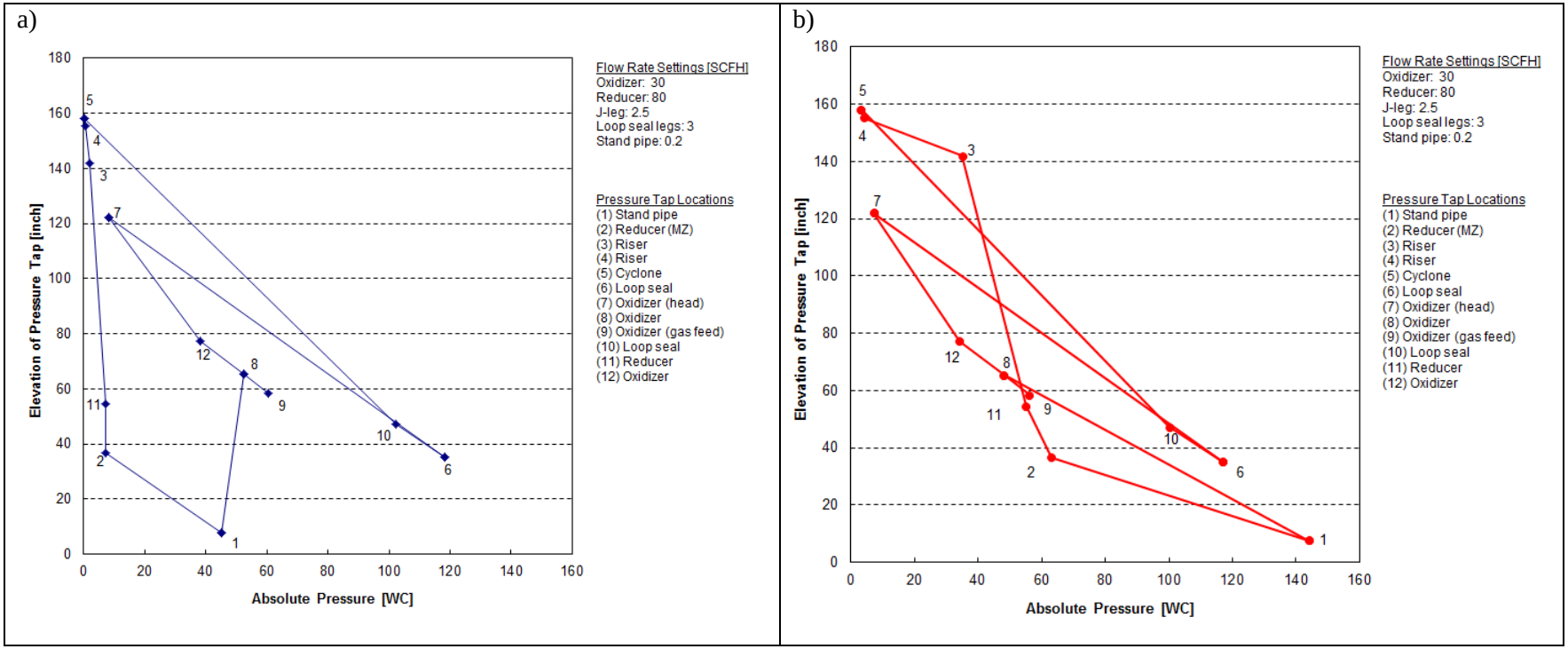

Figure 3-5. Effect of standpipe aeration on system pressure.

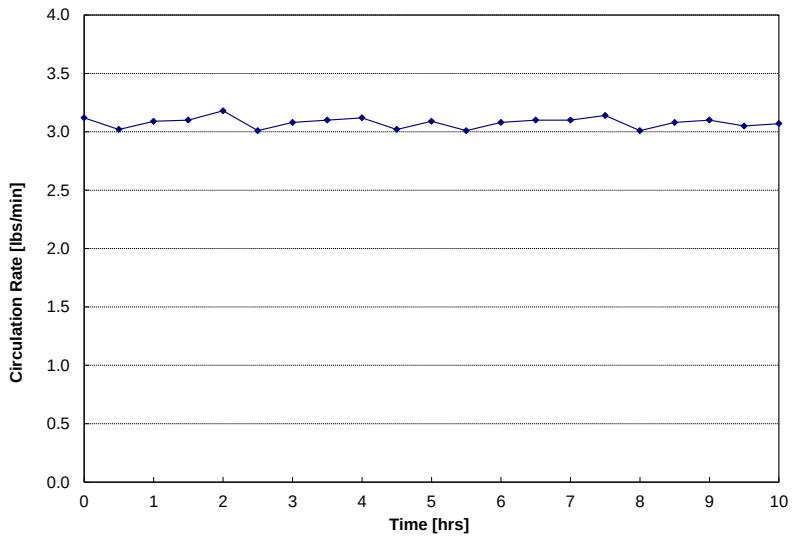

Figure 3-6. DCFBR solids circulation rate over extended operation.

3.2.2 Process Safety Review

To ensure the PSRS could be operated in a safe and reliable manner, a hazard and operability review (HOR) was conducted. The HOR was completed by a team consisting of PSRS design engineers and members from the organization fabricating the prototype unit. The team and the HOR were led by an outside engineer with expertise in the design and operation of fluidized-bed reactors and leading HOR studies. HOR objectives included identifying safety and operability issues and developing recommendations for any identified deviations that could significantly affect operability.

PSRS PIDs were reviewed to identify potential safety/operability issues and recommendations to address the issues were discussed. No major safety issues were identified. Recommendations to improve PSRS operability which were incorporated into the design include

- Obtaining material test reports for reactor materials and reviewing to ensure materials of construction met the required design criteria,
- Increasing vessel design rating from 300 psig to 500 psig at 550°C based upon materials of construction,

3.2.3 PSRS Fabrication and Installation

The PSRS unit was fabricated by an outside vendor selected through a competitive bid process. The PSRS design package was submitted to three fabrication organizations with experience fabricating fluidized-bed systems of similar size and complexity. Bid packages from the fabrication organizations were reviewed and the lowest cost vendor was selected. Activities associated with PSRS unit fabrication included

- Procurement of materials including steam boiler and super heater packages,
- Fabrication of DCFBR systems,
- Installation of electrical and data acquisition/control wiring,
- Development and installation of human-machine interface (HMI),
- ASME certification of the steam boiler package, and
- Hydrostatic pressure testing of the PSRS unit.

After completion of PSRS fabrication activities, RTI personnel traveled to the vendor's fabrication facility to complete a check-out of the PSRS unit before shipment to RTI. Figure 3-7 shows the PSRS unit at the vendor's fabrication facility during check out.

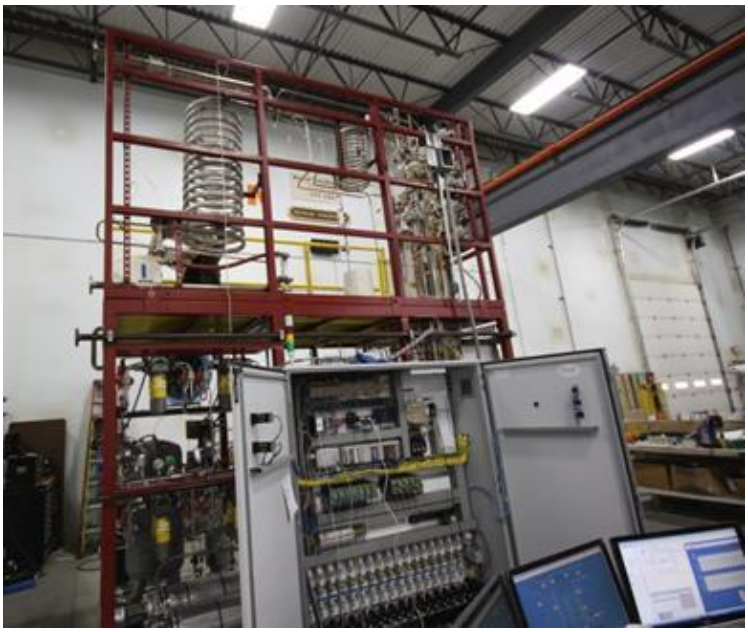

Figure 3-7. PSRS unit during check out activities at vendor's fabrication facility.

After checkout, the PSRS unit was prepared for shipment and delivered to RTI. RTI used industrial riggers to assist with installation of the unit in RTI's high-bay facility. Figure 3-8 presents images of the test unit installation activities.

(a)

(b)

Figure 3-8. PSRS unit installation. (a) Raising of the test unit's upper half. (b) Completion of test unit installation

Figure 3-8demonstrates that this bench-scale prototype unit was specifically designed for its intended location within RTI's high-bay facility. To facilitate installation, select sections of the unit were delivered disassembled. During installation, these sections were reassembled. Additional installation activities completed involved

- Utility connections (nitrogen, instrument air, chilled water, and power supply)
- Process gas manifolds
- Boiler system (boiler, feed water pump, and blow-down vessel)
- Heat tracing and insulating

When installation was complete, commissioning of the bench-scale prototype unit was started. Initial work involved demonstration of operability and functional control of different system components including heaters, mass flow controllers, and pressure control values. Figure 3-9 presents an image of the commissioned SIP bench-scale test unit.

Figure 3-9. Commissioned PSRS unit

The final commissioning activity was cold flow testing to demonstrate solids circulation at high pressure conditions, which was not possible in the cold flow system. The results from this cold flow solids circulation test demonstrated solids circulation was stable and controllable. The maximum solids circulation rate observed during this testing was greater than the design maximum at high pressure.

4. PSRS Testing Results

While commissioning of the PSRS was being completed, a test plan was developed which consisted of a set of parametric tests that would investigate the effects of temperature (400°C to 500°C), pressure (150 psig to 250 psig), syngas composition (GE, MHI, and Shell), and finally exposure to a syngas mixture containing 100 ppmv of H_2S. This parametric test plan was implemented during three weeks of intensive PSRS operation. The key to stable operation of the PSRS was maintaining a suitable pressure differential between the reducer and oxidizer reactors. This pressure differential was maintained by the loop seal. Stable operation required maintaining the pressure differential on this loop seal at less than 2 psi. Because of the typical flow rates and target operating pressures, special and slow start up procedures were required to maintain this small pressure differential. Unfortunately, implementing these startup procedures reduced the time available for operation. A total of between 20 and 30 hours of operating time was accumulated during the parametric testing.

The longest continuous period of testing occurred during parametric testing of the syngas composition. The five syngas compositions chosen for parametric testing were based on different gasifier designs and included a slurry-fed O_2-blown, (GE), a dry-fed O_2-blown (Shell), an air-blown (MHI) and a generic slurry-fed O_2-blown (Generic). The syngas compositions for the different syngas composition tests are provided in Table 4-1. Argon was included as an internal tracer to enable more accurate determination of the effluent gas flow rate from analytical results for the effluent product gases. The temperature and operating pressure for these tests were 500°C and 150 psig for the reducer and oxidizer. The concentration of the feed gas for the oxidizer was 62.5 mol% steam in nitrogen.

The effluent gas compositions for three reactive gases (H_2, CO, and CO_2) for the reducer and oxidizer are provided in Figures 4-1 and 4-2, respectively. The other reactive gas, which is steam, cannot be easily measured and must be estimated from other information like mass of condensate collected.

Table 4-1. Syngas Compositions used during Parametric Testing in PSRP

Component (vol%)	Generic	GE	MHI	Shell
CO	45.0	36.8	21.7	57.3
H_2	15.0	27.5	11.2	32.0
CO_2	8.0	11.0		
N_2	19.0	9.1	61.3	7.9
Ar	1.0	1.0	1.0	1.0
H_2O	12.0	14.6	4.8	1.9

Although full understanding of the results in Figures 4-1 and 4-2 requires solving the full mass balance for both the reducer and oxidizer, there are several key observations that can be made just from these results. The first is that CO is being consumed in the reducer based on the fact that the Shell and MHI syngas do not contain any CO_2, but the product gas for both these tests has a significant amount of CO_2. The two anticipated reactions that could result in CO decreasing and CO_2 increasing are the desired reduction of iron oxide and the water gas shift reaction. The next observation is that iron oxide is being reduced in the reducer as there is hydrogen production from the oxidation of reduced iron in the oxidizer for all four syngas compositions. The amount of hydrogen produced in the oxidizer for the generic, GE and MHI syngases is approximately the same. However, the amount of hydrogen produced by the Shell syngas is between 3 and 4 times the amount produced for the other syngases. This strongly suggests that a

significant portion of the CO consumed for the Shell gas results in the reduction of the iron oxide. The final observation is that the product hydrogen contains essentially no CO, but a significant amount of CO_2, this CO_2 is assumed to be carried from the reducer to the oxidizer in the inter-particle void spaces as the catalyst is transferred from the reducer to the oxidizer. Improvement the stripping of the gas from these inter-particle void spaces would eliminate this gas transfer.

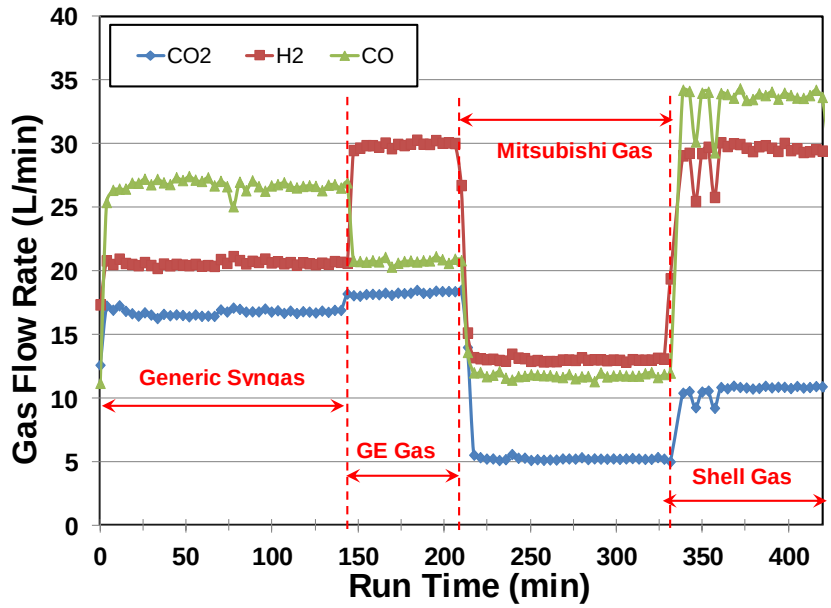

Figure 4-1. Results from parametric testing of syngas composition in the reducer reactor.

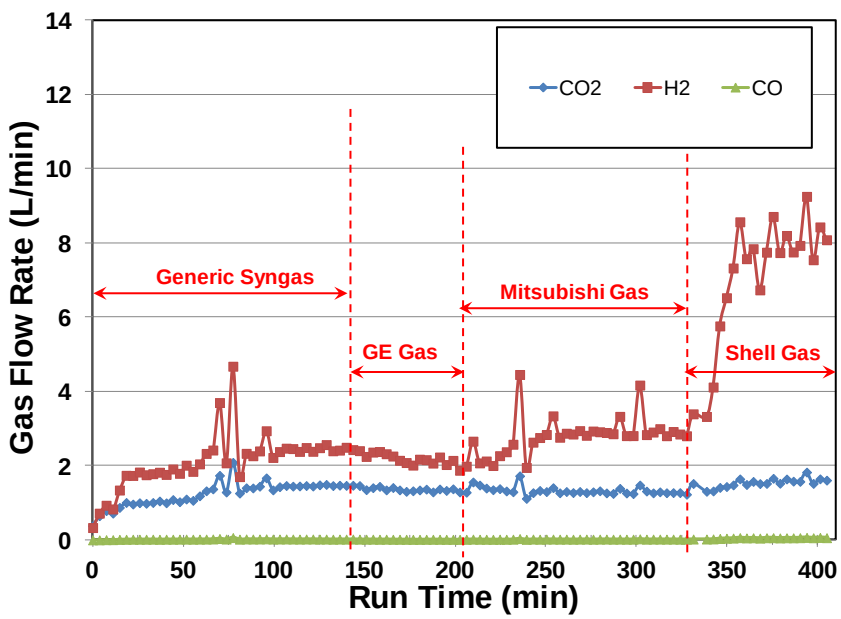

Figure 4-2. Results from parametric testing of syngas composition in the oxidizer reactor.

The next parametric test investigated the effects of reducer temperature on the performance of the reducer and oxidizer. The syngas composition used for these tests was the GE syngas composition. The parametric test was performed at 150 psig and 400°C, 450°C, and 500°C. The effluent gas compositions for three reactive gases (H_2, CO, and CO_2) for the reducer and oxidizer are provided in Figures 4-3 and 4-4, respectively.

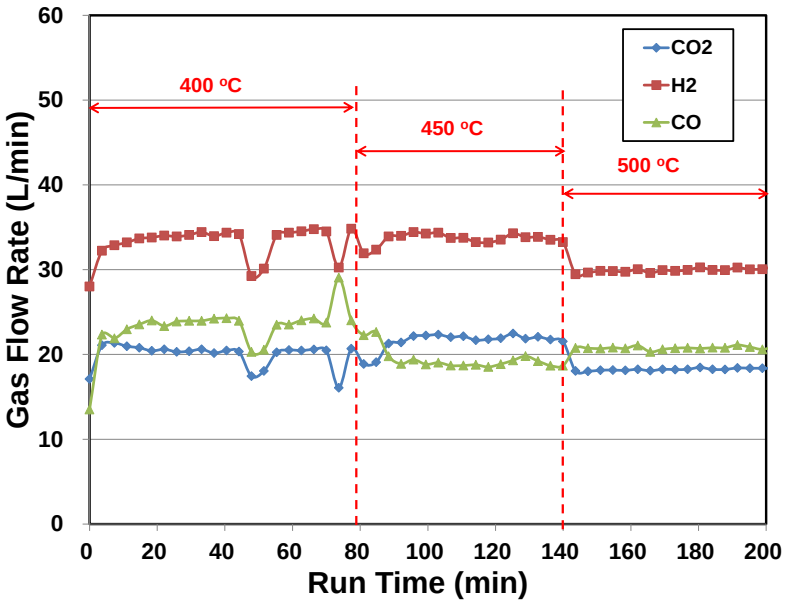

Figure 4-3. Results from parametric testing of temperature in the reducer reactor.

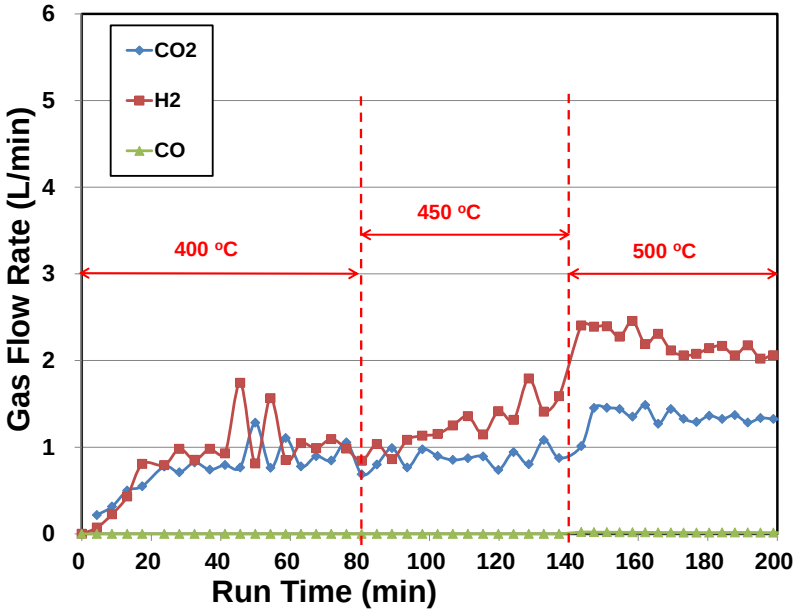

Figure 4-4. Results from parametric testing of temperature in the oxidizer reactor.

The effluent flow rates for H_2, CO and CO_2 from the reducer do not indicate any significant difference in concentration. The effluent concentrations from the oxidizer show that the hydrogen production remains constant at 400 °C and 450 °C, but increases by about a factor of two at 500°C. For a more detailed interpretation of the effects of temperature, mass balance analysis was completed and is described below.

In addition to parametric testing of temperature, testing was conducted at two different pressures. These tests were completed with the Shell syngas composition at 500ºC. The two different operating pressures were 150 and 265 psig. Figures 4-5 and 4-6 show the effluent concentrations for H_2, CO and CO_2 from both the reducer and oxidizer, respectively.

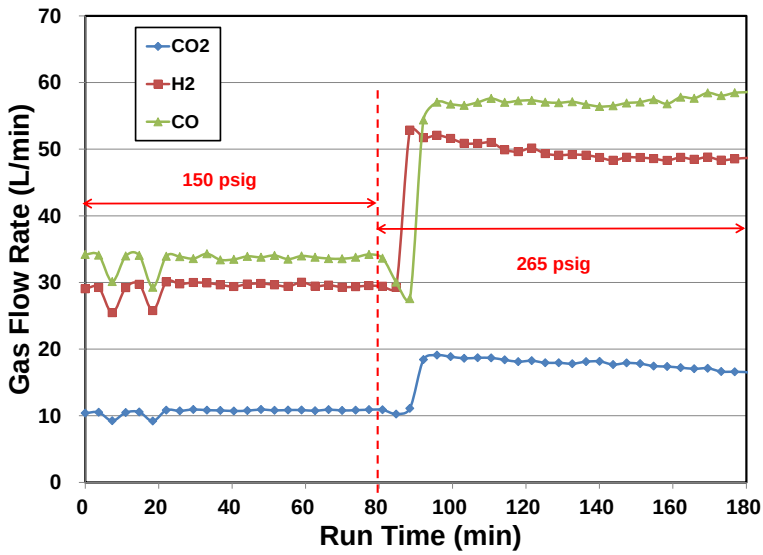

Figure 4-5. Results from parametric testing of pressure in the reducer reactor.

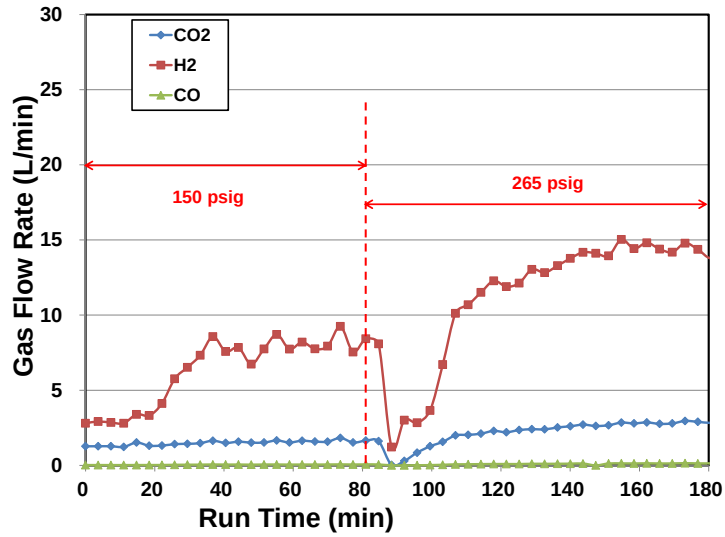

Figure 4-6. Results from parametric testing of pressure in the oxidizer reactor.

To maintain the same superficial velocity in the riser, the flow must be increased at higher pressure. Because of this flow increased at higher pressure, the flow for the 265 psig test is about 160% compared to the flows at 150 psig. In Figure 4.5, the effluent flow rates for H_2, CO and CO_2 at 265 psig are all roughly 160% of the flow rates at 150 psig. Therefore, no immediate effect of higher pressures is observed.

Although the flow rate is also increased in the oxidizer, this increase comes from an increase in nitrogen flow and not the steam. Thus, the increase in hydrogen production in the oxidizer indicates an increase in the oxidation rate of the reduced iron with steam at higher pressures.

The final parametric test involved the introduction of H_2S into the syngas to investigate the potential poisoning of the catalyst. Because this sulfur poisoning might be irreversible, this test was last parametric test completed. The syngas used for this test was the GE syngas with 100 ppmv of H_2S. The operating conditions were 450°C and 150 psig. The effluent concentrations for H_2 CO and CO_2 from both the reducer and oxidizer are shown in Figures 4.7 and 4.8, respectively

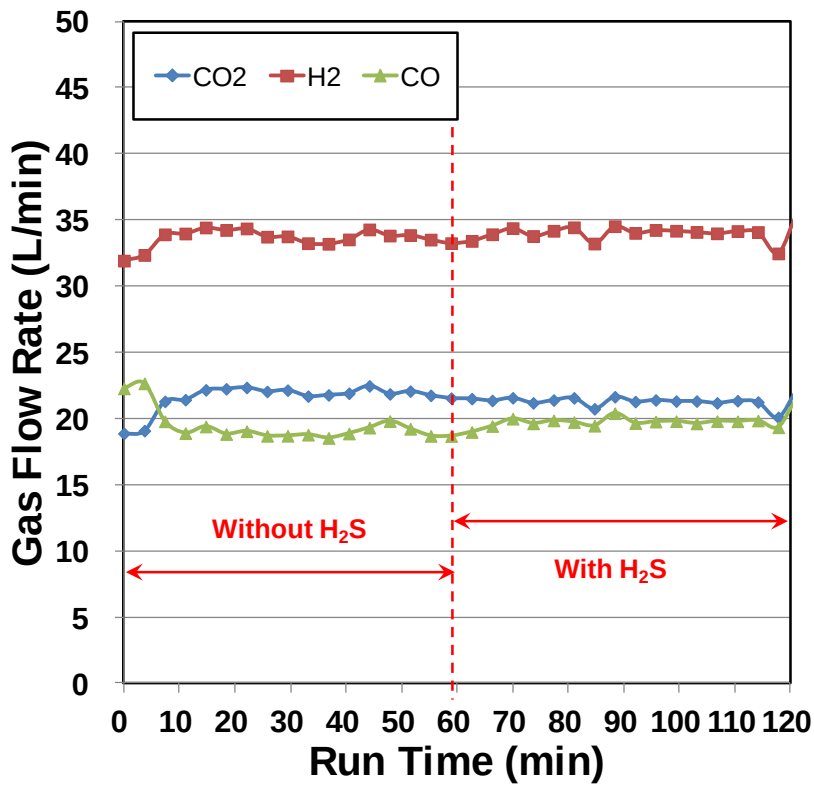

Figure 4-7. Results from testing with syngas containing H_2S in the reducer reactor.

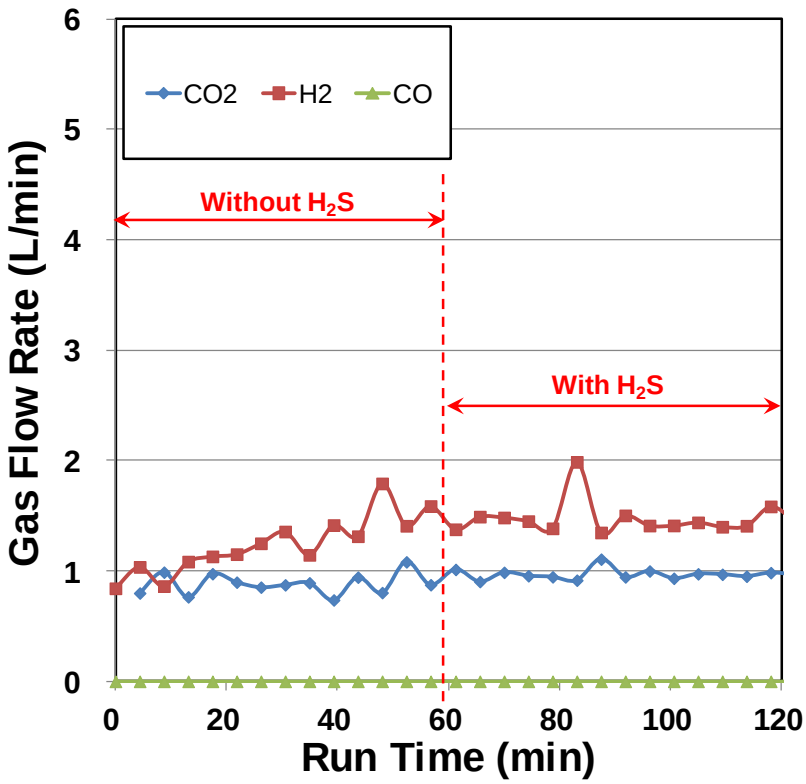

Figure 4-8. Results from testing with syngas containing H_2S in the oxidizer reactor.

The fact that there is no significant change in the effluent flow rates for the reactive gases in either the reducer or oxidizer for syngas with and without 100 ppmv of H_2S shows that the process can easily tolerate a syngas with 100 pmmv of H_2S without any adverse effect on reactivity of the iron material.

To complete the analysis of the results from the parametric tests, the results were used to complete species mass balances. These result enabled determination of the reaction rates for the water gas shift and reduction based on both the CO and CO_2 mass balances in the reducer and the oxidation or hydrogen production rate in the oxidizer. These results from the mass balance calculations for the different parametric tests are shown in Figure 4-9.

The most prominent feature of Figure 4.9 is that the Shell syngas results in the most reduction of the iron catalyst and also the highest hydrogen production rates. Increasing the operating pressure from 150 to 265 psig resulted in an increase in both the rate of iron reduction and steam oxidation. From the rates of the water-gas-shift and reduction reaction, there is not significant change in the reaction rates in the reducer between 400 and 500°C. However, there is a significant increase in the rate of steam oxidation at 500°C. The water-gas-shift reaction is the predominate reaction for the generic, GE and MHI syngases. It is worth noting that these three syngas all have 5 vol% or greater steam content. Another interesting observation to make is that MHI syngas is the only syngas for which the rate of reduction in the reducer and rate of steam oxidation in the oxidizer approximately the same magnitude. The results from testing with a GE syngas containing 100 ppmv of H_2S clearly show that the presence of H_2S had no adverse effect on the reaction rates in either the reducer or regenerator.

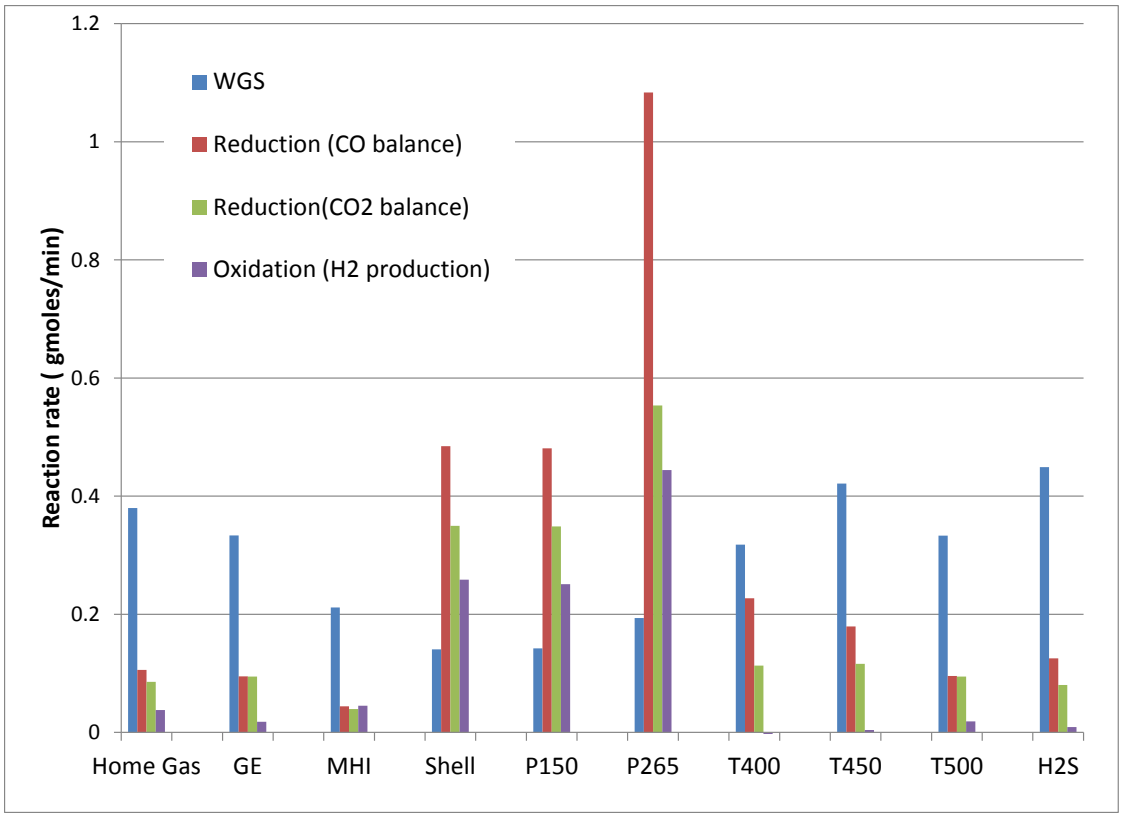

Figure 4-9. Reaction rates for the water-gas-shift and reduction reaction in the reducer and steam oxidation in the oxidizer.

In summary the results from parametric testing in the PSRS show that the iron catalyst is preferentially reduced with CO at temperatures from 400°C to 500°C. In this temperature range, the rate of the water-gas-shift reaction is also important. For syngas compositions with significant steam, the water-gas-shift reaction rate will exceed the reduction reaction rate. From 400 to 500°C, temperature has no effect on the reactions in the reducer. However, a large increase in steam oxidation was observed at 500°C. Increasing pressure from 150 to 265 psig resulted in increased rates of the reduction and steam oxidation reactions, but results in little or no change in the water-gas-shift reaction. No adverse effect on either the reactions in the reducer (water-gas-shift or reduction) or steam oxidation in the oxidizer were observed for a syngas with 100 ppmv of H_2S. Finally, all the parametric test results demonstrate that the dual circulating fluidized-bed reactor system is technically feasible.

5. Techno-economic Analysis

Since the one of the key goals of this project was to examine the economic feasibility of the SIP technology, a techno-economic analysis of the process was completed. The benchmark for comparison of economic feasibility was an integrated combined cycle (IGCC) system equipped with pressure swing adsorption unit enabling coproduction of hydrogen and electricity. Off-the-shelf coal gasification technologies were evaluated based on the amount of public information available about process modeling. In the end, a General Electric Energy (GEE) gasifier (formerly Texaco gasifier) was selected for the process model. Process specifics for the coal gasification model were gathered from U.S. Department of Energy (DOE) reports and example models built by Aspen Technology, Inc. For the SIP process, laboratory data from bench-scale and PSRS testing were used to develop models for the SIP process. AspenPlus was the simulator used for process modeling.

Once the process modeling was complete, these models were used to develop the economics for both the benchmark and SIP cases. For this comparison, the same unit size of gasifier and the same total hydrogen production capacity were used for both cases. The process models were used to develop heat and mass balances, which were used to size equipment. Aspen Process Economic Analyzer (formerly Aspen Icarus Process Evaluator) was used to develop capital cost estimates for each case. From the capital cost estimate, factorized estimates were used to derive operating expenses and fixed cost. Because the process was an integrated facility, producing electricity and hydrogen, operating expenses and fixed costs were allocated based on energy (electrical work produced and hydrogen higher heating value).

Details on the process model development and the techno-economic analysis are provided in the following sections.

5.1 Overall Process Description

5.1.1 Block Flow Diagram

Figures 5-1 and 5-2 represent the two processes modeled for this study. Major streams are labeled, with the properties and compositions of these streams listed below in Tables 5-1 and 5-2.

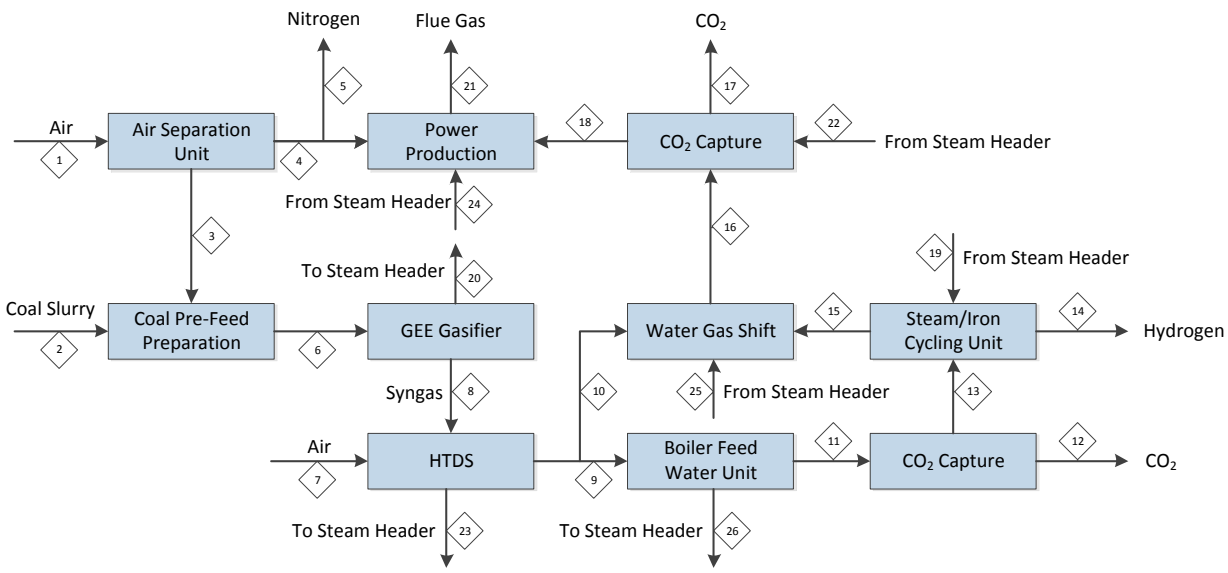

Figure 5-1. Block flow diagram of proposed process for production of hydrogen from the SIP technology.

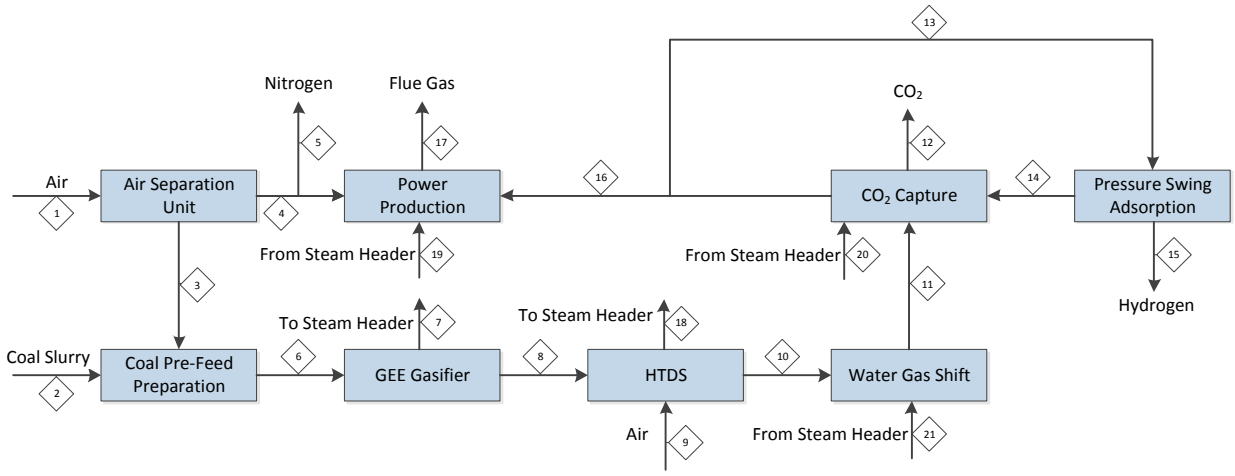

Figure 5-2. Block flow diagram of reference process for production of hydrogen from pressure swing adsorption of syngas produced from a gasifier unit.

Table 5-1. Major Streams Associated with the Proposed Process for the Production of Hydrogen from the SIP Technology

	1	2	3	4	5	6	7	8	9	10	11	12	13	14	15
Temperature F	81.6	82.7	206	104.9	383.5	87.4	350	830	533.3	533.3	208.4	120	113.1	100	376.2
Pressure psia	14.7	14.7	980.0	16.9	460.0	980.0	664.7	799.7	739.7	739.7	700.0	25.0	696.2	695.2	695.2
Vapor Frac	1	0	1	1	1	0.645	1	1	1	1	1	1	1	1	1
Mass Flow lb/hr															
OXYGEN	420,210	-	413,455	6,700	4,422	413,455	18,006	-	-	-	-	-	-	-	-
NITROGEN	1,566,830	-	8,196	1,558,640	1,028,780	8,196	70,736	14,125	64,495	20,367	64,494	21	64,473	-	64,473
ARGON	18,831	-	15,479	3,350	2,211	15,479	-	15,479	11,764	3,715	11,763	7	11,756	-	11,756
WATER	40,117	255,604	-	3	3	255,604	3	164,670	130,365	41,168	13,816	6,608	1,111	208	1,111
CO2	819	-	-	-	-	-	-	302,610	244,073	77,076	244,005	216,850	26,885	-	380,728
H2	-	-	-	-	-	-	-	29,737	22,003	6,948	22,002	12	21,990	16,207	21,990
CO	-	-	-	-	-	-	-	520,359	387,647	122,415	387,644	171	387,473	-	162,268
COAL	-	435,215	-	-	-	435,215	-	-	-	-	-	-	-	-	-
OTHER	3	-	-	-	-	-	-	14,705	241	76	224	211	4	-	2
Mass Fraction															
OXYGEN	20.5%	0.0%	94.6%	0.4%	0.4%	36.7%	20.3%	0.0%	0.0%	0.0%	0.0%	0.0%	0.0%	0.0%	0.0%
NITROGEN	76.5%	0.0%	1.9%	99.4%	99.4%	0.7%	79.7%	1.3%	7.5%	7.5%	8.7%	0.0%	12.6%	0.0%	10.0%
ARGON	0.9%	0.0%	3.5%	0.2%	0.2%	1.4%	0.0%	1.5%	1.4%	1.4%	1.6%	0.0%	2.3%	0.0%	1.8%
WATER	2.0%	37.0%	0.0%	0.0%	0.0%	22.7%	0.0%	15.5%	15.1%	15.1%	1.9%	3.0%	0.2%	1.3%	0.2%
CO2	0.0%	0.0%	0.0%	0.0%	0.0%	0.0%	0.0%	28.5%	28.4%	28.4%	32.8%	96.9%	5.2%	0.0%	59.3%
H2	0.0%	0.0%	0.0%	0.0%	0.0%	0.0%	0.0%	2.8%	2.6%	2.6%	3.0%	0.0%	4.3%	98.7%	3.4%
CO	0.0%	0.0%	0.0%	0.0%	0.0%	0.0%	0.0%	49.0%	45.0%	45.0%	52.1%	0.1%	75.4%	0.0%	25.3%
COAL	0.0%	63.0%	0.0%	0.0%	0.0%	38.6%	0.0%	0.0%	0.0%	0.0%	0.0%	0.0%	0.0%	0.0%	0.0%
OTHER	0.0%	0.0%	0.0%	0.0%	0.0%	0.0%	0.0%	1.4%	0.0%	0.0%	0.0%	0.1%	0.0%	0.0%	0.0%

Table 5-1. Major Streams Associated with the Proposed Process for the Production of Hydrogen from the SIP Technology (cont.)

	16	17	18	19	20a	20b	21	22	23a	23b	24a	24b	25	26a	26b
Temperature F	270	120	112.6	505.5	636.7	596	290.8	344.2	433.2	281	503.2	281	503.2	365.9	297.7
Pressure psia	695.2	25.0	696.2	714.7	2000.0	1514.7	14.7	124.7	355.0	50.0	700.0	50.0	700.0	164.7	64.7
Vapor Frac	1	1	1	1	1	1	1	1	1	1	1	1	1	1	1
Mass Flow lb/hr															
OXYGEN	-	-	-	-	-	-	672,451	-	-	-	-	-	-	-	-
NITROGEN	84,840	52	86,060	-	-	-	5,091,260	-	-	-	-	-	-	-	-
ARGON	15,471	16	15,687	-	-	-	15,687	-	-	-	-	-	-	-	-
WATER	35,905	25,650	1,071	321,058	1,354,966	216,318	445,120	1,110,517	185,002	40,217	250,186	40,215	172,947	13,964	8,109
CO2	895,868	843,769	64,684	-	-	-	74,041	-	-	-	-	-	-	-	-
H2	49,004	51	49,688	-	-	-	0	-	-	-	-	-	-	-	-
CO	5,872	5	5,956	-	-	-	1	-	-	-	-	-	-	-	-
COAL	-	-	-	-	32	32	24	-	16	16	-	-	-	16	16
OTHER	80	74	2	-	-	-	3	-	-	-	-	-	-	-	-
Mass Fraction															
OXYGEN	0.0%	0.0%	0.0%	0.0%	0.0%	0.0%	10.7%	0.0%	0.0%	0.0%	0.0%	0.0%	0.0%	0.0%	0.0%
NITROGEN	7.8%	0.0%	38.6%	0.0%	0.0%	0.0%	80.8%	0.0%	0.0%	0.0%	0.0%	0.0%	0.0%	0.0%	0.0%
ARGON	1.4%	0.0%	7.0%	0.0%	0.0%	0.0%	0.2%	0.0%	0.0%	0.0%	0.0%	0.0%	0.0%	0.0%	0.0%
WATER	3.3%	2.9%	0.5%	100.0%	100.0%	100.0%	7.1%	100.0%	100.0%	100.0%	100.0%	100.0%	100.0%	99.9%	99.8%
CO2	82.4%	97.0%	29.0%	0.0%	0.0%	0.0%	1.2%	0.0%	0.0%	0.0%	0.0%	0.0%	0.0%	0.0%	0.0%
H2	4.5%	0.0%	22.3%	0.0%	0.0%	0.0%	0.0%	0.0%	0.0%	0.0%	0.0%	0.0%	0.0%	0.0%	0.0%
CO	0.5%	0.0%	2.7%	0.0%	0.0%	0.0%	0.0%	0.0%	0.0%	0.0%	0.0%	0.0%	0.0%	0.0%	0.0%
COAL	0.0%	0.0%	0.0%	0.0%	0.0%	0.0%	0.0%	0.0%	0.0%	0.0%	0.0%	0.0%	0.0%	0.1%	0.2%
OTHER	0.0%	0.0%	0.0%	0.0%	0.0%	0.0%	0.0%	0.0%	0.0%	0.0%	0.0%	0.0%	0.0%	0.0%	0.0%

Table 5-2. Major Streams Associated with the Proposed Process to Produce Hydrogen Using Pressure Swing Adsorption

	1	2	3	4	5	6	7a	7b	8	9	10	11
Temperature F	81.6	82.7	206	104.9	104.9	87.4	636.7	596	830	350	529.1	270
Pressure psia	14.7	14.7	980.0	16.9	16.9	980.0	2000.0	1514.7	799.7	729.7	739.7	700.0
Vapor Frac	1	0	1	1	1	0	1	1	1	1	1	1
Mass Flow lb/hr												
OXYGEN	420,210	-	413,455	6,700	2,278	413,455	-	-	-	18,006	-	-
NITROGEN	1,566,830	-	8,196	1,558,640	529,859	8,196	-	-	14,125	70,736	84,861	84,861
ARGON	18,831	-	15,479	3,350	1,139	15,479	-	-	15,479	-	15,479	15,479
WATER	40,117	255,604	-	-	-	255,604	1,354,962	216,314	164,670	-	171,533	30,774
CO2	819	-	-	-	-	-	-	-	302,610	-	321,148	1,105,110
H2	-	-	-	-	-	-	-	-	29,737	-	28,951	64,860
CO	-	-	-	-	-	-	-	-	520,359	-	510,062	11,104
COAL	-	435,215	-	-	-	435,215	-	-	-	-	-	-
OTHER	3	-	-	-	-	-	-	-	14,705	-	316	311
Mass Fraction												
OXYGEN	20.5%	0.0%	94.6%	0.4%	0.4%	36.7%	0.0%	0.0%	0.0%	20.3%	0.0%	0.0%
NITROGEN	76.5%	0.0%	1.9%	99.4%	99.4%	0.7%	0.0%	0.0%	1.3%	79.7%	7.5%	6.5%
ARGON	0.9%	0.0%	3.5%	0.2%	0.2%	1.4%	0.0%	0.0%	1.5%	0.0%	1.4%	1.2%
WATER	2.0%	37.0%	0.0%	0.0%	0.0%	22.7%	100.0%	100.0%	15.5%	0.0%	15.1%	2.3%
CO2	0.0%	0.0%	0.0%	0.0%	0.0%	0.0%	0.0%	0.0%	28.5%	0.0%	28.4%	84.2%
H2	0.0%	0.0%	0.0%	0.0%	0.0%	0.0%	0.0%	0.0%	2.8%	0.0%	2.6%	4.9%
CO	0.0%	0.0%	0.0%	0.0%	0.0%	0.0%	0.0%	0.0%	49.0%	0.0%	45.0%	0.8%
COAL	0.0%	63.0%	0.0%	0.0%	0.0%	38.6%	0.0%	0.0%	0.0%	0.0%	0.0%	0.0%
OTHER	0.0%	0.0%	0.0%	0.0%	0.0%	0.0%	0.0%	0.0%	1.4%	0.0%	0.0%	0.0%

5.2 Process Modeling Details

5.2.1 Gasification

The following sections discuss the process specifics of the unit operations required for the General Electric Energy gasification model used as the basis of this work.

5.2.2 Coal Pre-Feed Treatment

Coal enters the process in the pre-feed treatment unit. The basis for the model was 5,200 dry-tons per day. This unit mixes coal with water to form a slurry containing a dry solids content of 63%. This unit also grinds the slurry to a particle size of 3 mm. The crushing unit operation is a multiple roll crusher with a Hardgrove grindability index of 45. Table 5.3 lists the properties of Illinois #6 coal used.

Table 5-3. Coal Properties[1]

Proximate Analysis (wt%)	
Moisture	11.12
Fixed Carbon	44.19
Volatile Material	34.99
Ash	9.70
Ultimate Analysis (wt%)	
Ash	10.91
Carbon	71.72
Hydrogen	5.06
Nitrogen	1.41
Chlorine	0.33
Sulfur	2.82
Oxygen	7.75
Sulfur Analysis (wt%)	
Pyritic	27.64
Sulfate	8.21
Organic	64.14

[1]Baxter

5.2.3 Air Separation Unit (ASU)

The air separation unit produces a concentrated 95 mass% oxygen stream that is used in the gasification units. The incoming saturated air is compressed to 95 psi in a multi-stage compressor with inter-stage cooling. Residual water not removed in the multi-stage compressor's knock out drums and carbon dioxide is removed before entering the cold box using an adsorber unit. This prevents solids formation in the cryogenic section of the unit. The cold box contains a large heat exchanger that crosses the hot air streams entering the cryogenic section with the cold liquid streams that either flow from the high pressure distillation column to the low pressure distillation column or leave the cryogenic section as enriched nitrogen or oxygen. After leaving the cold box, the incoming air is then split to a high pressure cryogenic distillation column running at 94 psi and a low pressure distillation column running 19 psi.

5.2.4 Gasifier Unit

The design basis for the gasification unit was Aspen Technologies solution ID 121246. This example was developed by Paul Talley of Aspen Technologies based on the Department of Energy report entitled "Tampa Electric Polk Power Station Integrated Gasification Combined Cycle Project, Final Report" dated August 2002. The gasifier modeled was a GEE (formerly Texaco) gasifier. The GEE gasifier is an entrained flow gasifier, where the feed and oxidizer are fed at the same point. Typical temperatures for

the GEE gasifier are 1200 to 1500 °C with pressures about 1150 psia. The GEE gasifier is slurry fed and typically oxygen blown. The GEE gasifier produces a H_2/CO ratio usually around 0.95 with a CO_2 concentration of 12-20 mol% for the standard Illinois coal used in this study.

In the modeled gasifier, the incoming coal slurry is sent to the gasifier along with the oxygen from the air separation unit. The coal to oxygen ratio used is 95%. The RGIBBS reactor block in Aspen was used to simulate the gasifier. The reactor was set to run at 815 psi and 2400 °F. The GEE gasifier has a radiative cooling unit which produces 2000 psig steam before going to the quench section. To simulate this process, heat exchangers take the syngas leaving the first RGIBBS reactor and cool it to 1100 °F. After cooling, the syngas enters a second RGIBBS reactor block to simulate the reactions taking place prior to the radiative cooling unit. The syngas leaves this reactor at 800 °F and 785 psig. The approach temperature for the second RGIBBS reactor was manipulated to influence the CO:H_2 molar ratio to match the syngas composition typically produced by a GEE gasifier. This parameter was set to 745 °F.

A typical GEE gasifier also contains a quench unit, where the hot syngas is cooled through a water-containing region at the bottom of the gasifier unit. The cooling prevents gasification reactions from occurring any further. The quench unit also allows for the removal of unreacted coal and separation of the slag from the syngas stream. It is assumed that the dry solids being removed in the quench unit is 30%. In addition to the syngas quench and solids separation, the quench unit produces a sour gas, which is typically sent to a Claus unit. However, in the modeled integrated system, a high temperature desulfurization cleanup unit is used for removal of sulfur, mercury, and chlorides. This unit runs at a high temperature, so the syngas is not quenched or used for boiler feed water production. Instead of a quench unit for removing particulate matter, it is assumed a cyclone would be used to remove slag and unreacted coal.

5.2.5 High Temperature Desulfurization Cleanup

In the High Temperature Desulfurization Process (HTDP), or Warm Gas Clean-Up (WGCU), sulfur is removed from the syngas before the syngas is quenched or cooled. Therefore, the operating costs of the process are lower compared to a typical IGCC unit that would normally use a Selexol based process to clean the syngas of sulfur. The HTDP unit was modeled in Aspen Plus using the RSTOIC reactor while using laboratory data to determine the extent of reaction. Zinc oxide, acting as a sorbent, is reacted with hydrogen sulfide in a transport reactor to form zinc sulfide and water. The zinc sulfide is then removed from the syngas and regenerated using oxygen in a separate reactor. The regeneration reaction of zinc sulfide and oxygen produces zinc oxide and sulfur dioxide. Elemental sulfur is removed from the system directly by reacting sulfur dioxide with carbon monoxide and hydrogen. This reaction also forms carbon dioxide and water. Any remaining sulfur dioxide is then converted back to hydrogen sulfide to get recycled back into the original transport reactor.

The lower sulfur syngas is sent to additional clean-up stages where mercury and chlorides are removed. In this warm clean-up process, the chlorides are removed using sodium biocarbonate. Sodium chloride, carbon dioxide, and water are formed in this reaction. The salt is separated from the syngas.

In the high temperature desulfurization model, Aspen's RSTOIC reactors are used to model the absorber and regenerator, in which only a fractional conversion is specified. The amount of hydrogen sulfide converted to zinc sulfide in the absorber is set at 98%. All zinc sulfide is regenerated back to zinc oxide with air (oxygen). The adsorber operates at a temperature of 896.4 °F and at a pressure of 739.7 psia. The regenerator operates at a temperature of 1914.9 °F and at a pressure of 664.7 psia. The direct sulfur recovery unit operates at a temperature of 2513.3 °F and a pressure of 664.7 psia.

5.2.6 Boiler Feed Water Unit

Cleaned syngas leaving the HTDS unit that is split for the hydrogen production train, can be cooled in a boiler feed water unit because the amine adsorption unit cannot accept hot syngas. The boiler feed water unit produces 150, 50, and 20 psig steam that can be used for power generation or process steam. Units requiring process steam include the water-gas-shift, SIP, and amine adsorption units. Water is knocked out from the syngas after heat is removed in the steam boilers. This water can either be sent to waste water treatment or recycled to the coal pre-feed unit as slurry water.

5.2.7 SIP Reaction

Reaction

The SIP technology uses iron particles in a circulating fluidized system with two reactors to produce hydrogen from steam. In the first reactor, an oxidation reaction takes places in which iron is oxidized using steam to produce hydrogen. These oxidation reactions are:

$$Fe(s) + H_2O(g) \rightarrow FeO(s) + H_2(g)$$

$$3FeO(s) + H_2O(g) \rightarrow Fe_3O_4(s) + H_2(g)$$

In the second reactor, a reduction reaction occurs where iron is reduced using syngas. The reduction reactions are:

$$Fe_3O_4(s) + 4H_2(g) \rightarrow 3Fe(s) + 4H_2O(g)$$

$$Fe_3O_4(s) + 4CO(g) \rightarrow 3Fe(s) + 4CO_2(g)$$

The solids are circulated through both units in consecutive oxidation-reduction cycles.

Reactor Model

The circulating fluidized system contains two reactors, the oxidation and reduction reactors. Each reactor required different models as these reactors are operated in different fluidization regimes. The SIP iron catalyst has a sauter mean diameter (SMD) of 40 micron and a particle density of 2.08 g/cm^3. Based on the particle properties, the catalyst falls under the Geldart A classification. Geldart A particles present smooth fluidization at low gas velocities and bubbling with stable bubble size for higher velocities; fast fluidization is typically observed at gas velocities twenty times the minimum fluidization velocity. Experiments were performed in a bench top fluidized bed to determine the minimum fluidization velocity and the minimum bubbling velocity and found to be 0.0238 ft/s and 0.025 ft/s correspondingly. The void fraction at the minimum fluidization condition can be estimated by the Ergun equation:

$$\frac{\Delta P}{L} = 150 \cdot \frac{(1-\varepsilon)^2}{\varepsilon^3} \cdot \frac{\mu_g u_s}{(\phi_s d_p)^2} + 1.75 \cdot \frac{(1-\varepsilon)}{\varepsilon^3} \cdot \frac{\rho_g u_s^{\,2}}{\phi_s d_p}, \tag{5.1}$$

where ΔP is the pressure drop, L is the bed length, ε is the bed void fraction, μ_g is the gas viscosity, u_s is the superficial gas velocity, ϕ_s is the particle sphericity, d_p is the sauter mean diameter, and ρ_g is the gas density. The solids fraction at minimum fluidization velocity is 0.57; the solids fraction at the minimum bubbling velocity was assumed to be 0.56.

The oxidation reactor runs under bubbling fluidization regime. Iron is a reactant and should be included as such; however, at the expected solid recirculation rate the iron particles will not be the limiting factor. The limiting factor will be the steam residence time in the bed and thus the reaction was modeled as first order catalytic reaction. The model includes the calculation of bubble properties to properly account for the gas distribution and particle inventory within the reactor. Particles in the bed are distributed among the emulation, within bubbles, in bubble clouds (bubble-emulsion interphase), and wake of bubbles. The overall rate constant, K_f, for a bubbling fluidized bed with mass transfer resistances is given by:

$$K_f = \left[\gamma_b K_r + \cfrac{1}{\cfrac{1}{K_{bc}} + \cfrac{1}{\gamma_c K_r + \cfrac{1}{\cfrac{1}{K_{ce}} + \cfrac{1}{\gamma_e K_r}}}} \right], \tag{5.2}$$

where γ_b is the volume of solids in bubbles divided by volume of bubbles, K_r is the reaction rate constant, K_{bc} is the coefficient of gas interchange between bubble and cloud-wake region, γ_c is the volume of solids in cloud-wake region by volume of bubbles, K_{ce} is the coefficient of gas interchange between cloud-wake region and emulsion phase, and γ_e is the volume of solids in emulsion divided by volume of bubbles. The distribution of solids within the bed and the interchange coefficient are a function of the bubble properties; correlations for these parameters can be found in Kunii and Levenspiel (1991). The overall conversion, X_A, is given by:

$$1 - X_A = \exp\left(-K_f \frac{L}{u_b} \right), \tag{5.3}$$

where u_b is the bubble rise velocity. Correlations for the bubble rise velocity are also available in the above reference.

The reducer reactor is a riser and presents a fast fluidization regime. In this type of system, particles are transported along with the gas and the bed density decreases with increasing height. As the reaction rate is a function of the concentration of the catalyst, the model needs to account for the decreasing particle concentration as the riser is short and the flow condition is not fully developed. In addition, gas-particle contact efficiency increases with increasing height. The overall conversion in the riser can be approximated using the model proposed by Kunii and Levenspiel (1990):

$$\ln\left(\frac{1}{1 - X_A} \right) \cong \frac{(1 - \varepsilon_i) K_r}{u_s a} \left[\left(1 - e^{-aH} \right) - \frac{1 - \eta_i}{1 + a'/a} \cdot \left(1 - e^{-(a+a')H} \right) \right] \tag{5.4}$$

where ε_i is the void fraction at the inlet of the riser, a is the decay constant of solids, H is the height of the riser, a' is the corrected decay constant for reduced gas-solids contact, and η_i is the contact efficiency at the inlet of the riser.

The reaction rate constant was determined from experimental data generated in a bench scale fluidi5ed bed reactor. Figure 5-3 presents data from an experiment at 300 psig with 15 cc of catalyst with 34.1% iron content. The left axis shows the dry mole composition of the syngas as percentage and the right axis the gas flow rate in slpm as a function of time. Argon is used as a carrier gas. The plot shows one full

cycle with injection of syngas (reduction step) and then steam (oxidation step). In the reducing cycle (denoted in Figure 5-3 as Syngas On), carbon monoxide reacts with the catalyst to form carbon dioxide. An increase in hydrogen concentration is due to the water gas shift reaction. The kinetic model assumes hydrogen does not reduce the catalyst as the concentration of hydrogen increases. The consumption of CO due to the water gas shift reaction was accounted for to calculate the conversion of CO due to the catalyst. The calculated first order reaction rate constant for the oxidation reaction is 0.1813 s^{-1}. In the oxidation cycle, hydrogen is generated as the steam oxides the catalyst. The calculated first order reaction rate constant for the oxidation reaction is 0.0753 s^{-1}.

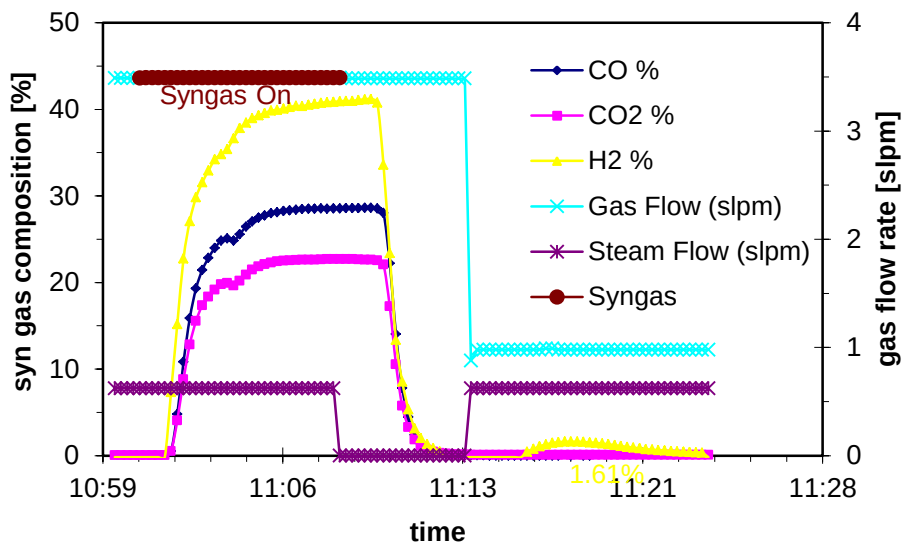

Figure 5-3. Experimental run in bench top fluidized bed reactor at 300 psig with 15 cc of catalyst with 34.1% iron content; syngas composition and gas flow rate as a function of time.

5.2.8 Power Generation

Gas Turbine

The clean syngas stream enters the power and steam production section of the process. There are two gas turbine and heat recovery steam generators (HRSG) working in tandem, with one steam turbine system. In developing the model, the physical property method used for the gas turbine and HRSG was the Peng–Robinson equation of state with Boston-Mathias modifications (PR-BM). The syngas enters the combustion chamber of the gas turbine and is combined with compressed air. The combustor was modeled as an R-YIELD reactor that is adiabatic and isobaric. The hot gas is then sent to an expander where the temperature is reduced and electricity is produced. The gas then enters the HRSG system, in which steam is produced through a series of heat exchange units. There are two systems within the HRSG, a high pressure and intermediate pressure. The high pressure section operates at 1800 psi, while the intermediate section operates at 420 psi. Fresh water enters the intermediate pressure section first, while the hot flue enters the high pressure section first, resulting in a countercurrent flow. Approximately half of the water input to the system, including the recycle from the steam turbine, is sent to each section. The cooled flue gas is sent to the stacks.

Steam Turbine

In the steam turbine, steam is used to produce electricity as it passes through a series of turbines operating at different pressures. The steam turbine section was modeled as three turbines, with each stepping down to a lower pressure. The steam produced in each of the HRSGs are combined and sent to the steam turbine system. The physical property method used for all steam turbine unit operations was the ASME 1967 steam table correlations (STEAM-TA). The first turbine reduces the pressure of the steam to 420 psi. Most of the steam is recycled back to the HRSG after this first turbine. In the second turbine, the remaining steam, from the high pressure turbine and the steam produced in the intermediate pressure section of the HRSG are expanded to 65 psi. Most of the steam that exits the intermediate pressure turbine is sent to the low pressure turbine. The low pressure turbine is a condensing turbine, which enhances the electrical production at the expense of a cooling medium.

5.2.9 CO_2 Capture

The design basis for the amine adsorption unit was Aspen Technologies solution ID 122272. This example solution includes kinetic and equilibrium parameters used in the modeling of amine adsorption of CO_2, which were used in this work's model. Chemical reaction based adsorption was selected for this process, with methyl diethanolamine (MDEA) as the specific amine chosen for adsorption. The adsorption and desorption was modeled using the rate-based module. Rate based simulations are based on mass and heat transfer correlations, and thus can be scaled to differing flow rates without losing accuracy. Specifically in CO_2 capture, a rate-based distillation model ensures accurate reaction kinetics. Since kinetic reactions are based on time, the liquid holdups are used to determine the rate of reaction. These times must be specified in an equilibrium-based distillation model.

The process that produces hydrogen using the SIP unit requires two sets of amine adsorption units to ensure that 90% of the produced CO_2 is captured. Each unit has multiple trains of adsorption and stripping columns. The adsorber unit runs at a pressure of 48 bar and the stripper runs at a pressure of 1.7 bar. The stripper reboiler was modeled to run at a temperature of 250 °F. One train was prior to the SIP hydrogen production unit, and one was after the water-gas-shift unit. In the capture model, a 50 wt% MDEA solution is used for the lean stream. Additionally, heat integration between within the amine adsorption unit was modeled to reduce the duty of the stripper reboiler. The stripper reboiler duty was shown to be approximately 1,040 Btu/lb-CO_2 captured.

5.2.10 Pressure Swing Adsorption

A standard pressure swing adsorption (PSA) unit was modeled for the benchmark case. Prior to the PSA, the syngas is treated in a conventional water-gas shift unit. The shift reactors were modeled in Aspen Plus using the REquil block. The high temperature shift operates at a temperature of 905 °F and a pressure of 350 psia. The low temperature shift operates at a temperature of 519.8 °F and a pressure of 350 psia. The PSA unit was first modeled using Aspen Adsorption, with the results of this model being used in the full benchmark case Aspen Plus model using SEP blocks within Aspen Plus. The adsorption bed was modeled as three layers: alumina, followed by activated carbon, and finally a zeolite layer.

5.3 Performance and Economic Comparison

These process models were used to develop full heat and mass balances for the reference PSA case (Figure 5-2) and the SIP comparison case (Figure 5-1). The information in these heat and mass balances was subsequently used to calculate equipment size and materials of construction for all major equipment. With this sized equipment, equipment costs were estimated using Aspen Process Economic Analyzer. From the equipment cost factored estimates for total installed cost were developed. The results from this estimation process are summarized for the SIP comparison and reference PSA cases in

Tables 5.4 and 5.5, respectively. These results show that the SIP case reduces of the total installed cost by $69 million or approximately 7 % for the total installed cost for entire plant. Considering that the cost of the gasifier, ASU, gas turbine, HSRG and steam turbine, which are identical for each case, represent roughly 60% of the total installed cost, the SIP process represents a reduction in cost of about 17% for gas cleanup and processing.

Table 5-4. Capital Cost Summary for the Proposed Process to Produce Hydrogen from the SIP Technology

Equipment Cost	$491,466,600
Direct Cost	$574,982,900.00
Equipment Setting	$3,287,448.50
Piping	$43,493,900.00
Civil	$10,843,862.00
Steel	$1,069,043.60
Instrumentation	$12,917,568.00
Electrical	$13,677,868.00
Insulation	$7,373,804.00
Paint	$1,076,515.20
Other	$100,223,704.00
G and A Overheads	$16,658,121.00
Contract Fee	$14,281,830.00
Contingencies	$110,059,696.00
Total	**$909,946,260**

Table 5-5. Capital Cost Summary for the Base Case Scenario to Produce Hydrogen Using Pressure Swing Adsorption

Equipment Cost	$513,325,600
Direct Cost	$617,973,500
Equipment Setting	$3,378,706
Piping	$56,617,742
Civil	$11,515,835
Steel	$1,129,050
Instrumentation	$13,602,929
Electrical	$12,877,452
Insulation	$8,362,312
Paint	$1,211,036
Other	$105,471,713
G and A Overheads	$17,352,053
Contract Fee	$15,081,410
Contingencies	$114,335,371
Total	**$978,909,110**

5.3.1 Operating Costs

Operating costs for the SIP and benchmark processes were calculated based on the Aspen Plus simulation results and the assumed unit costs summarized in Table 5-6. Table 5-7 summarizes these results for the SIP process and Table 5-8 summarizes these results for the base case process. A 10 year straight line depreciation was assumed in this study for both scenarios. Because no specific information is available on the SIP catalyst cost, this catalyst cost was assumed to be equal to cost of zinc oxide.

Table 5-6. Summary of the Unit Costs Used in this Study

Material	Unit Price	
Coal	42.75	$/ton
ZnO	0.64	$/lb
MDEA	1.21	$/lb
Alumina	350	$/ton
Activated Carbon	0.75	$/lb
Zeolite	1.50	$/lb

Table 5-7. Operating Cost Summary for the Proposed Process to Produce Hydrogen from the SIP Technology

Costs	$/lb H_2	$/MW
Materials		
Coal	0.23	15.09
ZnO	0.0001	0.0037
MDEA	0.0001	0.0020
SIP Catalyst	0.0001	0.0037
Utilities		
Cooling Water	0.03	1.93
Depreciation		
Capital Depreciation	0.25	16.57
Total	**0.508**	**33.60**

Table 5-8. Operating Cost Summary for the Base Case Process to Produce Hydrogen Pressure Swing Adsorption

Costs	$/lb H_2	$/MW
Materials		
Coal	0.22	14.84
ZnO	0.0001	0.0036
MDEA	0.0001	0.0018
PSA Adsorbent	0.000004	0.0003
Utilities		
Cooling Water	0.04	1.78
Depreciation		
Capital Depreciation	0.27	17.52
Total	**0.53**	**34.14**

Comparison of the results in Table 5-7 and 5-8 indicate the SIP case reduces the cost of hydrogen by about 2 ₵/lb of hydrogen and 54 ₵/MW of electricity. Closer examination of the information in Tables 5-7 and 5-8 indicates that the most significant contributions to operating cost come from the capital depreciation and coal costs. These costs represent close to 92% of the operating cost for hydrogen and 94 % of the cost for electricity production. The difference in the operating costs for the SIP and PSA processes are extremely small and represent less than 0.5% of the total operating cost. Thus, the fact that the SIP process results in a reduction in operating cost for both hydrogen production and electricity demonstrates the significant reduction in total installed cost for the SIP case versus the PSA case.

6. Biomass Transportation Model

The techno-economic analysis in the previous chapter was completed based on the conventional approach that would be used for any fossil fuel especially coal. However, the use of biomass as the fuel driving the process would require more detailed analysis of the costs associated with biomass collection, transportation, and storage, because the growth of biomass is distributed over large areas and availability is seasonal. There are many reasons to seriously consider biomass for coproduction of hydrogen and electricity. Biomass is a domestic renewable fuel source and the CO_2 generated from the biomass does not result in any net increase in GHG emissions. Processing of agricultural product consumes energy and produces a byproduct stream of biomass waste. Hydrogenation of vegetable oils is done with large amounts of hydrogen that are generally obtained from steam methane reforming of natural gas. Experimental testing has shown that SIP can effectively recover high purity hydrogen from air blown gasification processes, which is the most prevalent gasifier design for biomass. This chapter expands the techno-economic analysis completed in the last chapter focusing on biomass and a fuel source.

6.1 Biomass Selection

Agricultural residues are abundant in the Midwest and thus are potential feedstocks for the production of hydrogen. An estimated 110 million tons per year of corn stover could be harvested (Graham et al., 2007) and is the feedstock of choice for the present study. The SIP process yields 52 lb of hydrogen per ton of corn stover and 1.2 MW·h per ton of corn stover. The potential hydrogen production from the available corn stover in the Midwest is 2.9 million tons per year. Corn stover was selected as the feedstock for the SIP process due its abundance.

6.2 Biomass Production, Transportation, and Storage Costs

The scale of biomass processing plant is limited by the logistic of feedstock collection and transportation. As the plant size of a biomass processing plant increases, economies of scale leads to a reduction in production cost; however, the greater mass of feedstock needed to satisfy plant demand requires it to be transported greater distances, thus increasing the transportation cost. As a result of these competing factors, an optimum plant size exist which minimizes the total production cost. Transportation of feedstock requires an in-depth analysis as it plays an important role in the economics of biomass-based processes. A detailed model based on work by Leboreiro and Hilaly (2011) was used to perform an economic analysis of corn stover collection, transportation, and storage for the SIP process. For the sake of brevity a brief description of the model is presented here; the reader is referred to Leboreiro and Hilaly (2011) for an in-depth description of the complete model.

The two main components of the model are the production cost and transportation cost. The model was developed so both components scale with capacity to determine the optimum plant size. The transportation portion was developed in a two-step manner. First, a detailed model referred to as the "Farm Model", in which individual farms are modeled, is used to calculate a non-dimensional transportation factor for a single plant size. In the second step, the dimensionless factor is used in a simplified transportation model to scale the transportation cost with plant capacity. The simplified transportation model and the production cost model are used to perform the plant optimization analysis; the combined model is referred to as the "Optimization Model". The production cost is based on the present work.

The transportation model accounts for costs associated with harvesting the corn stover at the farm, farm–to–plant transportation, farm–to–storage transportation, storage operations, and capital depreciation for storage depots. The elements of the model cover all the steps in the supply chain. At the farm level, the total payment for corn stover bales is estimated at $48.88 per ton; this includes $28.68 per ton for baling, $9.38 per ton for fertilizer value, and a $10.86 per ton profit for the farmer. All mass related quantities are on a dry basis. The biomass collected on the farm is loaded on truck to be transported to the plant or the storage depots. Transportation cost from the farm to the plant is calculated from the collection radius. The model assumes a circular collection area with the plant at the center as shown by the schematic diagram in Figure 6-1. The collection radius is calculated by the following expression:

$$R_c = \sqrt{\frac{1}{\pi} \cdot \frac{P \cdot O}{Y_s \cdot F_f \cdot F_c \cdot F_p \cdot F_a \cdot (1 - F_l)}}, \tag{6.1}$$

where P is the daily plant capacity, O is the plant operating days per year, Y_s is the corn stover yield per area, F_f is the farmland fraction, F_c is the fraction of total farmland planted with corn or crop rotation factor, F_p is the fraction of farmers selling corn stover or farmer participation, F_a is the accessibility factor, and F_l is the loss factor.

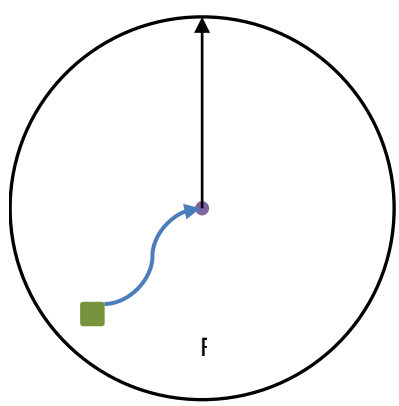

Figure 6-1. Schematic diagram of transportation model; where Rc is the collection radius, Ac is the collection area, and dt,i is the road distance from farm i to the plant.

The model assumes the plant operates 350 days per year. The corn stover yield estimated by Leboreiro and Hilaly (2011) was 1.52 tons/acre. The factors associated with corn acreage were calculated from 2007 USDA crop data; the data indicates that F_f is 0.78 and F_c is 0.65. The farmers participation was assumed to be 0.5 due to the findings by Leboreiro and Hilaly (2011); the previous authors recommend that at a bio-fuel producers intending to use agricultural residues as feedstock should work towards a farmer participation of fifty percent as the cost of the delivered corn stover is proportional to the square root of the inverse of the farmer participation. The accessibility factor, F_a, accounts for the corn stover that is not collected and was set at 0.9. Finally, the loss factor, F_l, accounts for all the losses through the supply chain and is set to 0.1. Note that the collection area, A_c, is given by the second term on the right side of Equation 6-1.

The collection radius as function of the hydrogen production for the SIP process is presented in Figure 6-2. As the plant capacity increases the transportation distance increase as corns stover needs to be collected from a larger area. As a consequence, farm–to–plant transportation cost increases with plant

capacity. The collection radius presents a parabolic behavior since it is proportional to the square root of the plant capacity; this observation can be derived from inspection of Equation 6-2.

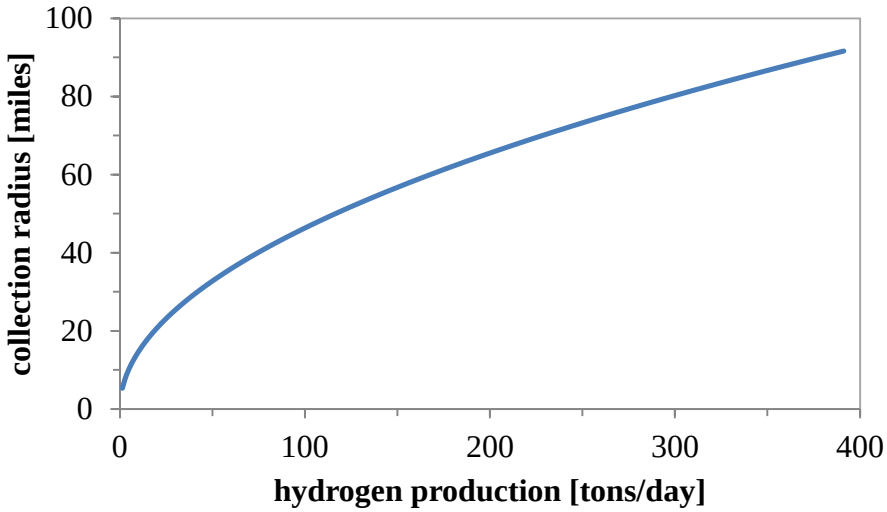

Figure 6-2. Collection radius as a function of hydrogen production for the SIP process using corn stover as a feedstock.

The average farm–to–plant transportation cost is based on the collection radius calculated from the following expression:

$$d_{t,avg} = d_t^* \cdot R_c, \tag{6.2}$$

where d_t^* is the non-dimensional transportation parameter calculated from the Farm Model. The expression for d_t^* is:

$$d_t^* = \frac{\sum_{i=0}^{i=n_f} r_i \cdot (1+f_w)}{n_f} \cdot \frac{1}{R_{c,\text{farm}}}, \tag{6.3}$$

where r_i is the straight–line, farm–to–plant distance from the farm i to the plant, f_w is the winding factor, and n_f is the number of farms. A plant size with a capacity to process 5876 tons/day was used in the Farm Model; the hydrogen production is 153 tons/d with an electricity output of 299 MW. A total of 2000 farms and a winding factor of 0.28 were used for the analysis. The straight–line, farm–to–plant distance is converted to road transportation distance by means of the winding factor, $d_t = r \cdot (1+f_w)$. Once the average transportation distance is known, the transportation cost can be calculated as a function of plant capacity. The collection radius for the 5876 ton/d plant in the Farm Model is 48.7 miles and the corresponding farm–to–plant transportation cost is $28.87 per ton.

Corn stover can only be harvested between grain harvest and the snow fall season leading to the need for storing the feedstock for year-round operation of the plant. The bales can be left on the field during harvest season corresponding to 3 months per year. Storage is necessary for 9 months of feedstock to allow year round operations. Farm–to–storage transportation cost is $14.79 per ton. The total cost of delivered corn stover bales at the plant gate for the Farm Model is $92.54 per ton.

6.3 Evaluation of Biomass Cost on Plant Size

The three main components of the total production cost for hydrogen are plotted as a function of hydrogen production in Figure 6-3; specifically, cost of delivered corn stover, capital depreciation for the plant and the storage depots, and other costs. The last item includes maintenance, taxes and insurance, and labor. A cost allocation factor based on the energy split between the hydrogen and the electricity is used; the energy split for a plant running only on corn stover is 0.39 for the hydrogen. Depreciation includes capital for the plant and the storage depots. The capital depreciation was obtained using a straight-line 10 yr depreciation. The capital needed for a 5876 ton/d is 909.9 million dollars. A scaling exponential factor of 0.6 was used to scale the capital investment. The total production cost for the 5876 ton/d plant is $1.06 per lb. The cost of delivered corn stover increases as the plant capacity increases due to larger collection radius (see Figure 6-2). The other costs drop sharply with increasing hydrogen production. Labor cost will scale exponentially with a scaling exponent of 0.25 (Peters and Timmerhaus, 1991). Maintenance as well as taxes and insurance are a function of capital investment and thus decrease with increasing plant capacity.

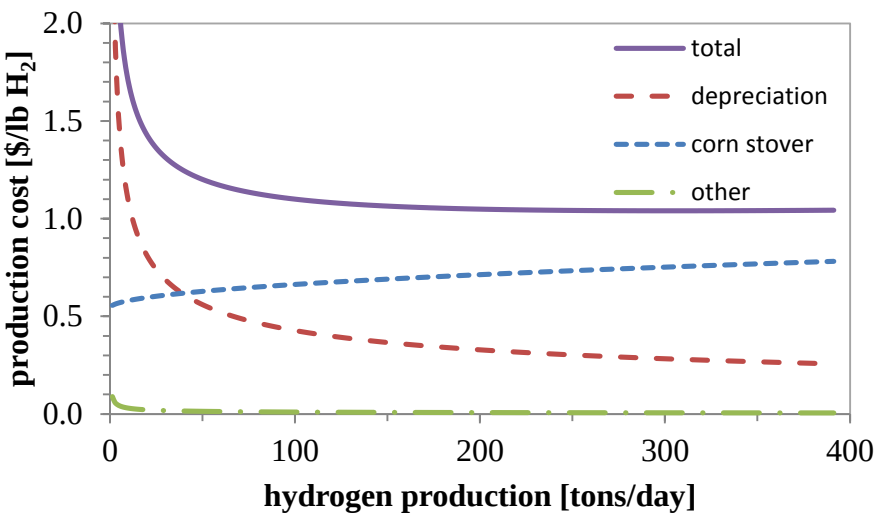

Figure 6-3. Breakdown of production cost per lb of hydrogen as a function of plant capacity for the SIP process using corn stover as a feedstock; total production cost, cost of delivered corn stover, capital depreciation, and other costs (which include maintenance, taxes and insurance, and labor).

For plant sizes below 1350 ton/d corresponding to a hydrogen production of 35.2 ton/d (plant capacities left of the intersection between the depreciation and cost of the delivered corn stover lines in Figure 6-3), the total cost is dominated by depreciation. For plant sizes above 1350 ton/d, the cost of the delivered corn stover is greater than depreciation. The total production cost declines rapidly as plant capacity increases due to the steep drop in depreciation. As the fixed cost rate of change decreases with plant capacity, the increase in transportation cost leads to an increase in the total production cost. The nature of the tradeoff between the economies of scale and transportation cost leads to minimum total production cost. The optimum plant size for the SIP process is 11500 ton/d producing 300 ton/d of hydrogen; the corresponding minimum production cost is $1.02 per lb.

6.4 Practicality Analysis

In general, the process economics for implementing new facilities using coal to produce electricity, hydrogen or even a combination of electricity and hydrogen cannot compete with natural gas-based

facilities at the current price of natural gas and available conversion technologies. By contrast with biomass, there are potential niche applications were biomass gasification being used to cogenerate electricity and hydrogen could be viable.

To assist in evaluation of this potential, RTI and Archer Daniel Midland (ADM) have teamed up to perform the techno-economic analyses of the technology and application for biomass. From their involvement with these analyses, ADM has identified two products where this type of hydrogen production might be attractive. These products are sorbitol and propylene glycol (PG).

ADM is one of the largest producers of sorbitol in USA. Sorbitol is produced by hydrogenation at high pressure. ADM has also begun to offer bio-based chemicals in the chemicals market. It produces bio-based propylene glycol (PG) using glycerol as the starting material. ADM is one of the largest producers of biodiesel and glycerol is a byproduct of biodiesel production. Currently, ADM has 3 biodiesel plants in USA. The glycerol from biodiesel plant is first purified and then hydrogenolysis is conducted to produce PG from glycerol. PG is mainly used in deicing (airports) applications, detergents and unsaturated polyester resin (UPR) manufacturing.

For both these products ADM is currently using steam methane reforming (SMR) to generate the hydrogen necessary for production of these products. It is possible to utilize the SIP process for supplying the necessary hydrogen for future expansions of these products. The decision to use SIP process will be dictated by economics, environmental impacts, raw materials supply and continued development of SIP for commercial deployment.

7. Life Cycle Analysis

7.1 Introduction

In our resource constrained world, life cycle assessment (LCA) is a useful tool for environment impact analysis of various products and services. Use of LCA started as a decision making tool in early 1970s to compare sustainability of various products (Baumann and Tillman 2004). Since then LCA has been widely used in product development, public policy, marketing; and LCA methodology has been standardized under ISO 14040 (2006) and 14044 (2006) standards.

The worldwide hydrogen production is 96% fossil fuel based, with most of it (>75%) using natural gas as feedstock and steam methane reforming (SMR) based hydrogen production the most common production route (Dufour et al. 2009). In comparison, 67 % of worldwide electricity generation in 2006 was fossil fuel based (IEA 2008).

Given this reliance on fossil fuels, the hydrogen and electricity production processes are far from sustainable, especially with respect to global warming emissions. Spath et al. (2001) reported life cycle greenhouse gas (GHG) emissions of 11.89 kg CO_2-equivalents per kg of hydrogen produced using natural gas fed SMR process; whereas Dufour et al. (2009) reported emissions of 10.55 kg CO_2-equivalents per kg of hydrogen. World Energy Outlook (IEA 2008) reports 2006 average worldwide coal, oil, and natural gas based electricity generation CO_2 emissions of 1.08, 0.81, 0.58 kg CO_2-equivalents per kWh of electricity, respectively.

7.2 Goal of the LCA Study

As discussed above, several LCA studies have investigated sustainability of stand-alone hydrogen and electricity generation processes. The current study, however, examines life-cycle CO_2 emissions for co-production of hydrogen and electricity using coal gasification coupled with SIP unit (Coal SIP process) and coal gasification coupled with pressure swing adsorption (Coal PSA process).

Since coal is gasified in a 95wt% oxygen stream, the resulting syngas has a high concentration of CO_2 (13.4 mole % in current study), which enables cost effective CO_2 capture. In the current study, CO_2 is captured using amine adsorption unit, with methyl-diethanolamine (MDEA) selected as the specific amine. After the capture step, CO_2 can be either compressed/dehydrated and subsequently sequestered in an underground reservoir or sold commercially. Some of the current markets for CO_2 are carbonated beverage industry, inert agent for food packaging, refrigeration systems, fire extinguishers, and oil industry where extended oil recovery (EOR) using CO_2 injection has been successfully used for 35 years (IPCC 2005). The multiple end uses of CO_2 (sequestered or sold) are considered as alternative scenarios in this LCA study.

A comparison is also made with conventional steam methane reforming based co-production of hydrogen and electricity (NG PSA process). Carbon dioxide produced in the reforming process has low partial pressure (Damen et al. 2006) and capturing it will require large steam consumption. Since no commercial SMR plants employ such capture, it is excluded from the NG PSA process in our study.

7.3 Scope of the LCA Study

7.3.1 System Boundary

This LCA study examines life cycle CO_2 emissions for co-production of hydrogen and electricity using a novel Coal SIP process and compares it to conventional Coal PSA and NG PSA process. The detailed description of Coal PSA and SIP processes is presented in Chapter 5 of this report; and NG PSA process details can be obtained from 2001 NREL study (Spath and Mann 2001) and SRI report (1994). Figures 7-1 through 7-3 show the block flow diagram and system boundary of examined processes. A cradle-to-factory-gate system boundary was selected for this LCA study, which implies energy use and GHG emissions* were tracked until the production of gaseous hydrogen and excludes compression, transmission and distribution steps; and similarly it excludes electricity transmission and distribution losses. Energy use and emissions associated with plant construction and decommissioning were excluded, since previous LCA studies have shown such emissions to be minor. For example, 2001 NREL study (Spath and Mann 2001) presented that 0.41% of life cycle GHG emissions are due to hydrogen plant construction and decommissioning.

7.3.2 Functional Unit

It is important to select an appropriate functional unit, in order to provide a clear understanding of LCA results. For example, previous hydrogen LCA studies (Spath and Mann 2001, Dufuor et al. 2009, Damen et al. 2006) use kg H_2, Nm^3 H_2, GJ H_2 as a functional unit, respectively, and kWh electricity as a functional unit for electricity LCA (Damen et al. 2006). In our study, we choose energy units of 1,000 million-BTU/hr (MMBTU/hr) of hydrogen and electricity co-production as a functional unit. Lower heating value is used to convert hydrogen production volumes to energy units.

In our study, we make an important assumption about energy equivalence of electricity and hydrogen. In real world operations, energy equivalence will depend on end use of electricity and hydrogen. For example, electricity has very high exergy† efficiency, i.e. electricity can be converted to physical or chemical work with minimal losses (Williams et al. 2008, Dewulf et al. 2008)). However, hydrogen exergy efficiency will be very high, while performing chemical work, and will be lower when it is converted to physical work such as fuel for internal combustion engine or fuel cell vehicle. Since, the current study does not consider use phase, energy equivalence is a reasonable assumption.

7.3.3 Data Sources, Quality Requirements, and Key Assumptions

The geographical focus of this study is production in the United States and therefore, all background data is for U.S. production, unless specified otherwise. The LCA data for coal mining and transport, natural gas extraction, transmission and distribution, electricity production was obtained from GREET model (version 1.8d_1) developed by Argonne National Laboratory (2010). LCA data for MDEA production was unavailable, and therefore it was substituted with U.S. diethanolamine (DEA) production data obtained from GaBi U.S. extension database (2006). The plant level input and output data for Coal PSA and Coal SIP process is based on the AspenPlus techno-economic model developed in this study. The input-output data for NG PSA process was obtained from GREET model and utility data (specifically cooling water use) was obtained from 1994 SRI report (1994).

---

* Emissions of major greenhouse gases: CO_2, CH_4, and N_2O were tracked. The study also included emissions of volatile organic compounds (VOC), carbon monoxide (CO), carbonyl sulfide (COS), because these emissions have a short atmospheric lifetime of days, after which they are converted to CO_2 and therefore these emissions are added to direct CO_2 emissions.

† Exergy as defined by Dewulf et al. is, "the maximum amount of useful work that can be obtained from this system or resource when it is brought to equilibrium with the surroundings through reversible processes in which the system is allowed to interact only with the environment."

The input-output data from these sources does not include electricity use for running cooling tower pumps and fans. Therefore, it was calculated by considering a typical 10,000 gallon/minute counterflow induced-draft cooling tower operation, with a cooling range of 15F (hot water temp = 105 F, cold water temp = 90 F), and approach of 10 F (i.e. wet bulb temp = 80 F). The pump horsepower was calculated based on rated power of pump designed to deliver 10,000 gallons/minute of water. The fan horsepower was calculated using sizing and horsepower charts available in Perry's Chemical Engineers' Handbook (Green et al. 2008).

The energy and utility use for CO_2 compression, dehydration, and sequestration was obtained from an AspenPlus techno-economic model of a typical carbon capture and sequestration (CCS) facility.

As mentioned in the goal of this study, we consider two scenarios for end use of CO_2. The base case LCA study considers carbon sequestration and Table 7-1 presents the input and output data for this case. The input and output data shows a significant amount of electricity consumption by cooling tower operations and CCS process. For example in Coal SIP process, cooling tower and CCS processes accounted for 1.6% and 5.9% of gross electricity production respectively. The techno-economic analysis presents high carbon capture efficiency of 93.5% and 89.3% for Coal SIP and Coal PSA processes respectively. These efficiency results compare well with previously reported Coal SIP process carbon capture efficiency of 100% (based on data collected from a bench unit and subpilot unit) and conventional Coal PSA process carbon capture efficiency of 90% by Fan and Li (2010).

In the alternative LCA case, it is assumed that captured CO_2 is sold to beverage industry and in this case, saleable CO_2 is a co-product, and therefore total energy use and emissions needs to be allocated between hydrogen/electricity and saleable CO_2. ISO 14044 standard recommends avoiding allocation if possible by using system expansion, which is also known as substitution or displacement. However, in this case avoiding allocation is not possible, because of the lack of information about marginal CO_2 production process in United States[‡]. And, therefore, market allocation approach was used, by assuming a beverage CO_2 cost of $7/metric-ton, hydrogen cost of $0.55/lb, and electricity cost of $36/MWh. Table 7-2 shows the input and output data for this case.

7.4 Life Cycle Inventory Analysis

Table 7-3 presents the life cycle GHG emissions (presented as CO_2-equivalents) for the base case scenario with carbon sequestration. The non-combustion CO_2 emissions during hydrogen and electricity production account for the largest share of gross GHG emissions for all process types; whereas coal mining or natural gas extraction steps are the second largest source of gross GHG emissions. For Coal SIP and Coal PSA processes, non-combustion CO_2 emissions refer to CO_2 produced during water gas shift reaction, but not captured in the amine adsorption unit. Since, the Coal SIP process produces much cleaner CO_2 stream, it has higher carbon capture efficiency (see Tables 7.1 and 7.2) compared to Coal PSA process and therefore, it has lower non-combustion CO_2 emissions (6.5% of total non-combustion CO_2 emissions) than Coal PSA process (10.7% of total non-combustion CO_2 emissions). Process energy use is a significant source of GHG emissions for NG PSA process, since 17% of natural gas input is used in utility boilers to produce steam required for steam methane reforming process.

Finally, the carbon sequestration process is able to capture majority of non-combustion emissions, which results in a net negative CO_2 emissions for hydrogen and electricity coproduction using Coal SIP and Coal PSA processes. The LCA results are summarized in Figure 7-4 as grams-CO_2e/MMBTU fuel produced and present a GHG emission reduction of 307% and 280% for Coal SIP and Coal PSA processes respectively in comparison to NG PSA process.

[‡] Some of the commercial CO_2 production processes are as a byproduct of ethanol fermentation process, and a byproduct of ammonia production (also known as Haber-Bosch process).

The alternative LCA case in our study considers captured CO_2 being sold to the beverage industry and uses market value of products for allocating emissions to saleable CO_2. Table 7-4 shows the individual product revenue in the alternative LCA case and we can see that saleable CO_2 accounts for slightly larger share of total revenue in Coal SIP process when compared to Coal PSA process. The larger revenue share is due to the higher carbon capture efficiency of Coal SIP process.

Table 7-5 presents the detailed life cycle GHG emissions for the alternative LCA case. The contributions from individual life cycle steps follow the same trends as that for the base case, with the exception of sequestered CO_2 credits. Since captured CO_2 is sold to the beverage industry, Coal SIP and Coal PSA processes are credited 12% and 11% of gross CO_2 emissions based on the market value of saleable CO_2 in Table 7-4. The alternative LCA case results are also summarized in Figure 7-5, which presents a GHG emission reduction of 78% and 70% for Coal SIP and Coal PSA processes respectively in comparison to NG PSA process.

Table 7-1. Input and Output Data for the Base Case LCA of Hydrogen and Electricity Co-production

Process Type	Coal SIP Process	Coal PSA Process	Natural Gas PSA Process	
Inputs	Flow rate	Flow rate	Flow rate	Units
Coal use	116	112	-	Short tons/hr (as-is)
NG use	-	-	1,403,078	Nft3/hr
Process Electricity use	240	233	-	MWh
Cooling Water (CW) - process	255,716	217,749	1,225	gpm
Cooling Water (CW) - CCS	12,685	11,728	-	gpm
Total CW	268,401	229,478	1,225	gpm
Number of Cooling Towers	27	23	1	
CW - Pumping Electricity use	5.0	4.2	0.2	MWh
CW - Fan Electricity use	2.3	1.9	0.1	MWh
Total CW - Electricity use	7.2	6.2	0.3	MWh
CCS - Electricity use	26.7	24.7	0.0	MWh
CCS - Natural Gas use	0.9	0.9	0.0	MMBTU/hr
MDEA use	1.0	0.9	-	lb/hr
Outputs	Flow rate	Flow rate	Flow rate	Units
Hydrogen	39,216	38,111	93,598	Nm3/hr
Total Electricity-produced	449.8	442.5	12.4	MWh
Net-Electricity	175.4	178.7	12.1	MWh
Hydrogen	402	390	959	MMBTU/hr
Net-Electricity	598	610	41	MMBTU/hr
Sequestered CO2	-225.6	-208.5	-	metric tons/hr
Saleable CO2	0.0	0.0	-	metric tons/hr
Carbon capture efficiency (%)	93.5%	89.3%	-	
Total Energy out:	1,000.0	1,000.0	1,000.0	MMBTU/hr
Energy efficiency (%)	44.0%	45.5%	72.5%	

Table 7-2. Input and Output Data for the Alternative Case LCA of Hydrogen and Electricity Co-production

Process Type	Coal SIP Process	Coal PSA Process	Natural Gas PSA Process	
Inputs	Flow rate	Flow rate	Flow rate	Units
Coal use	106	104	-	Short tons/hr (as-is)
NG use	-	-	1,403,078	Nft3/hr
Process Electricity use	220	215	0	MWh
Cooling Water (CW) - process	234,112	200,699	1,225	gpm
Cooling Water (CW) - CCS	0	0	-	gpm
Total CW	234,112	200,699	1,225	gpm
Number of Cooling Towers	24	21	1	
CW - Pumping Electricity use	4.4	3.9	0.2	MWh
CW - Fan Electricity use	2.0	1.8	0.1	MWh
Total CW - Electricity use	6.4	5.6	0.3	MWh
CCS - Electricity use	0.0	0.0	0.0	MWh
CCS - Natural Gas use	0.0	0.0	0.0	MMBTU/hr
MDEA use	0.9	0.9	-	lb/hr
Outputs	Flow rate	Flow rate	Flow rate	Units
Hydrogen	35,902	35,127	93,598	Nm3/hr
Total Electricity-produced	411.8	407.8	12.4	MWh
Net-Electricity	185.2	187.5	12.1	MWh
Hydrogen	368	360	959	MMBTU/hr
Net-Electricity	632	640	41	MMBTU/hr
Sequestered CO_2	0.0	0.0	-	metric tons/hr
Saleable CO_2	206.5	192.2	-	metric tons/hr
Carbon capture efficiency (%)	93.5%	89.3%	-	
Total Energy out:	1,000.0	1,000.0	1,000.0	MMBTU/hr
Energy efficiency (%)	48.1%	49.4%	72.5%	

Table 7-3. Life Cycle GHG Emissions for the Base Case LCA of Hydrogen and Electricity Co-production

Process Type	Coal SIP Process	Coal PSA Process	Natural Gas PSA Process	Units
Life cycle CO_2 emissions	Flow rate	Flow rate	Flow rate	
Coal mining	10.53	10.20	0.00	metric tons CO2/hr
Natural Gas production	0.01	0.01	14.09	metric tons CO2/hr
MDEA production	0.002	0.002	0.000	metric tons CO2/hr
H2+Electricity production - non combustion emissions	15.70	25.09	68.01	metric tons CO2/hr
H2+Electricity production - process energy emissions	0.06	0.05	14.01	metric tons CO2/hr
Gross CO_2 emissions	26.30	35.35	96.11	metric tons CO2/hr
Sequestered CO_2	-225.56	-208.54	0.00	metric tons CO2/hr
CO_2 allocated to Saleable CO_2	0.00	0.00	0.00	metric tons CO2/hr
Net CO2 emissions	-199.26	-173.19	96.11	metric tons CO2/hr
Hydrogen	402	390	959	MMBTU/hr
Net-Electricity	598	610	41	MMBTU/hr
Total Energy out:	1,000.0	1,000.0	1,000.0	MMBTU/hr

Table 7-4. Individual Product Revenue for the Alternative LCA Case

Process Type	Coal SIP Process	Coal PSA Process	Natural Gas PSA Process	Units
Hydrogen revenue	$3,920 (33%)	$3,836 (32%)	$10,220 (96%)	$/hr (%)
Electricity revenue	$6,666 (55%)	$6,749 (57%)	$437 (4%)	$/hr (%)
Saleable CO2 revenue	$1,446 (12%)	$1,345 (11%)	$0 (0%)	$/hr (%)
Total revenue	$12,032	$11,930	$10,657	$/hr

Table 7-5. Life Cycle GHG Emissions for the Alternative Case LCA of Hydrogen and Electricity Co-production

Process Type	Coal SIP Process	Coal PSA Process	Natural Gas PSA Process	Units
Life cycle CO_2 emissions	Flow rate	Flow rate	Flow rate	
Coal mining	9.64	9.40	0.00	metric tons CO2/hr
Natural Gas production	0.00	0.00	14.09	metric tons CO2/hr
MDEA production	0.001	0.001	0.000	metric tons CO2/hr
H2+Electricity production - non combustion emissions	14.37	23.13	68.01	metric tons CO2/hr
H2+Electricity production - process energy emissions	0.00	0.00	14.01	metric tons CO2/hr
Gross CO_2 emissions	24.02	32.53	96.11	metric tons CO2/hr
Sequestered CO_2	0.00	0.00	0.00	metric tons CO2/hr
CO_2 allocated to Saleable CO_2	-2.89	-3.67	0.00	metric tons CO2/hr
Net CO2 emissions	21.13	28.86	96.11	metric tons CO2/hr
Hydrogen	368	360	959	MMBTU/hr
Net-Electricity	632	640	41	MMBTU/hr
Saleable CO_2	206.5	192.2	-	metric tons/hr
Total Energy out:	1,000.0	1,000.0	1,000.0	MMBTU/hr

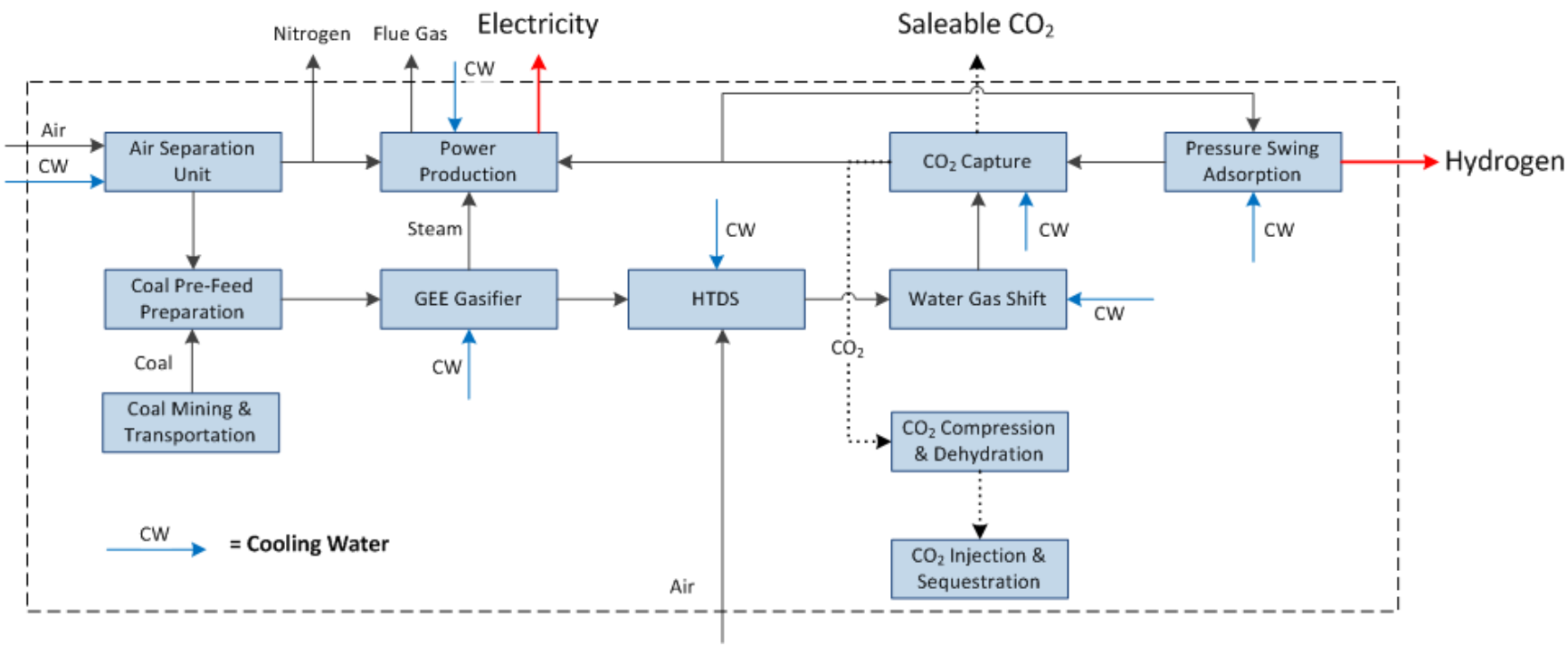

Figure 7-1. Block flow diagram and system boundary for hydrogen and electricity co-production using Coal PSA process.

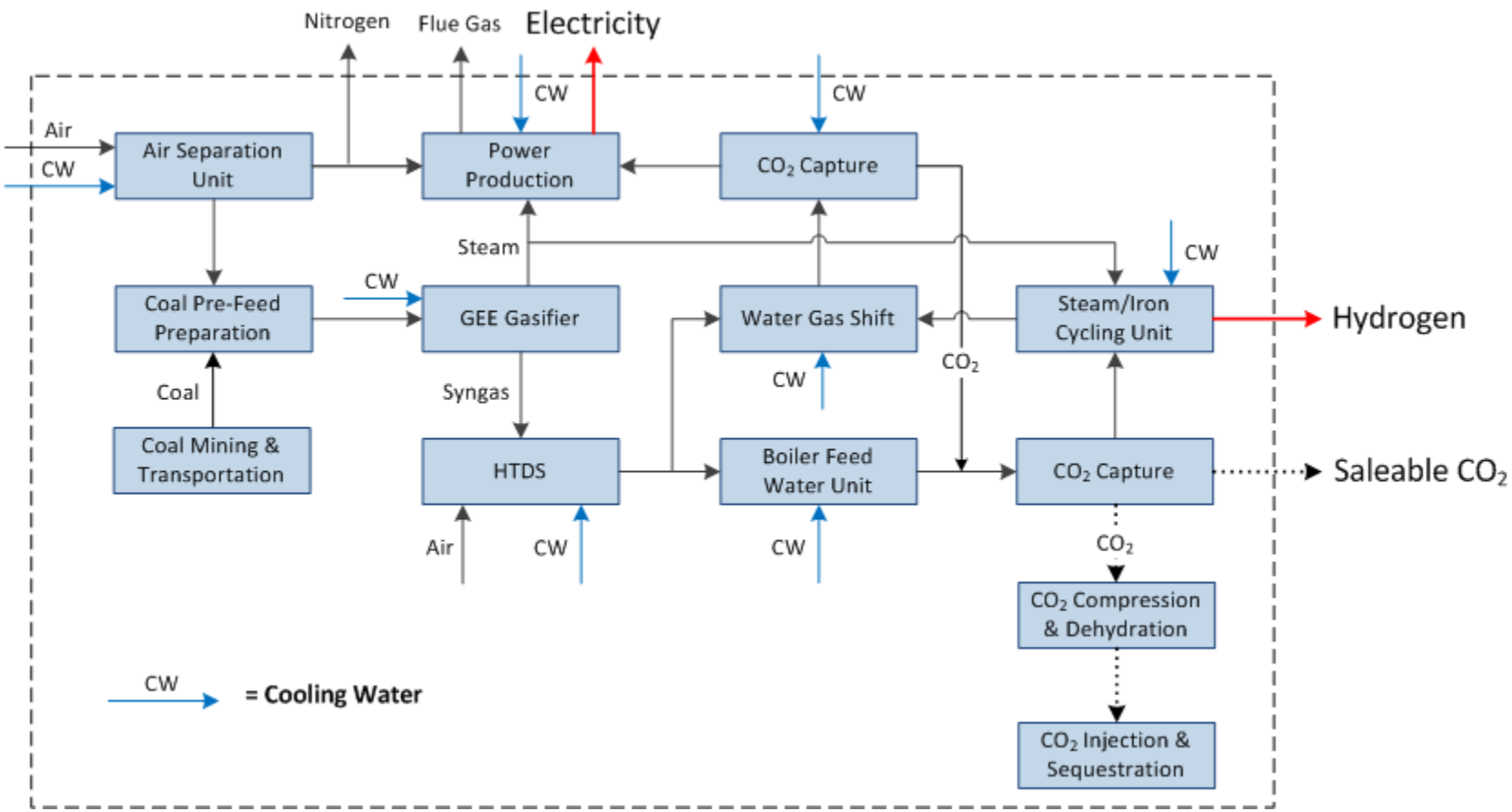

Figure 7-2. Block flow diagram and system boundary for hydrogen and electricity co-production using Coal SIP process.

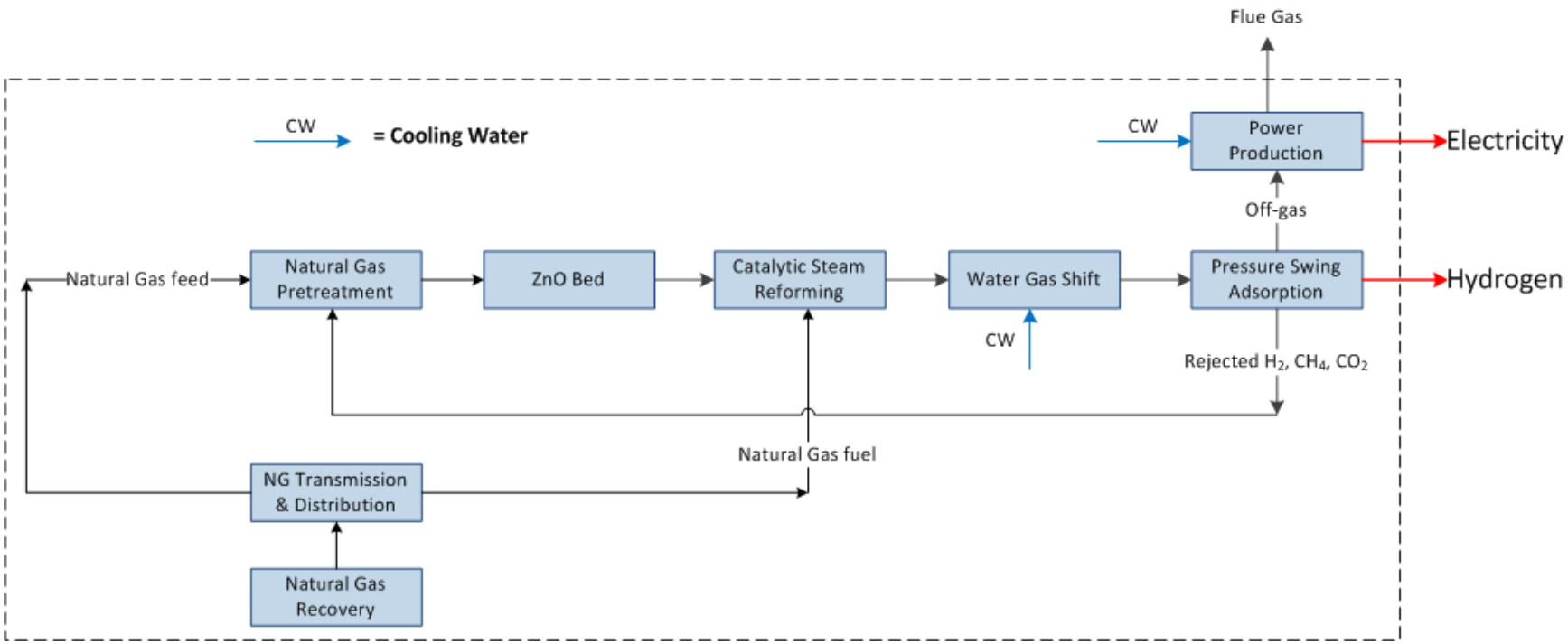

Figure 7-3. Block flow diagram and system boundary for hydrogen and electricity co-production using natural gas PSA process.

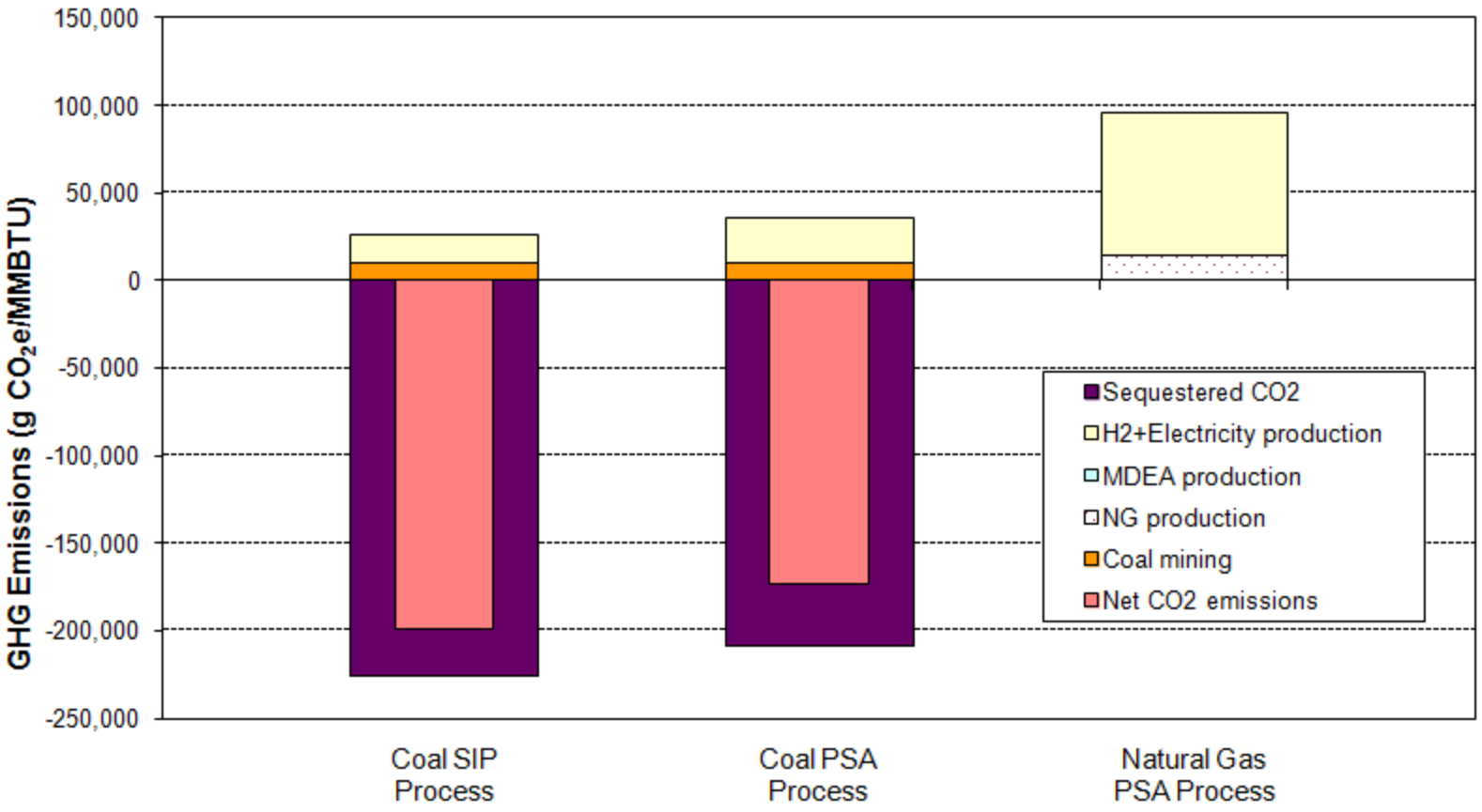

Figure 7-4. Life cycle GHG emissions for the base case LCA of hydrogen and electricity co-production.

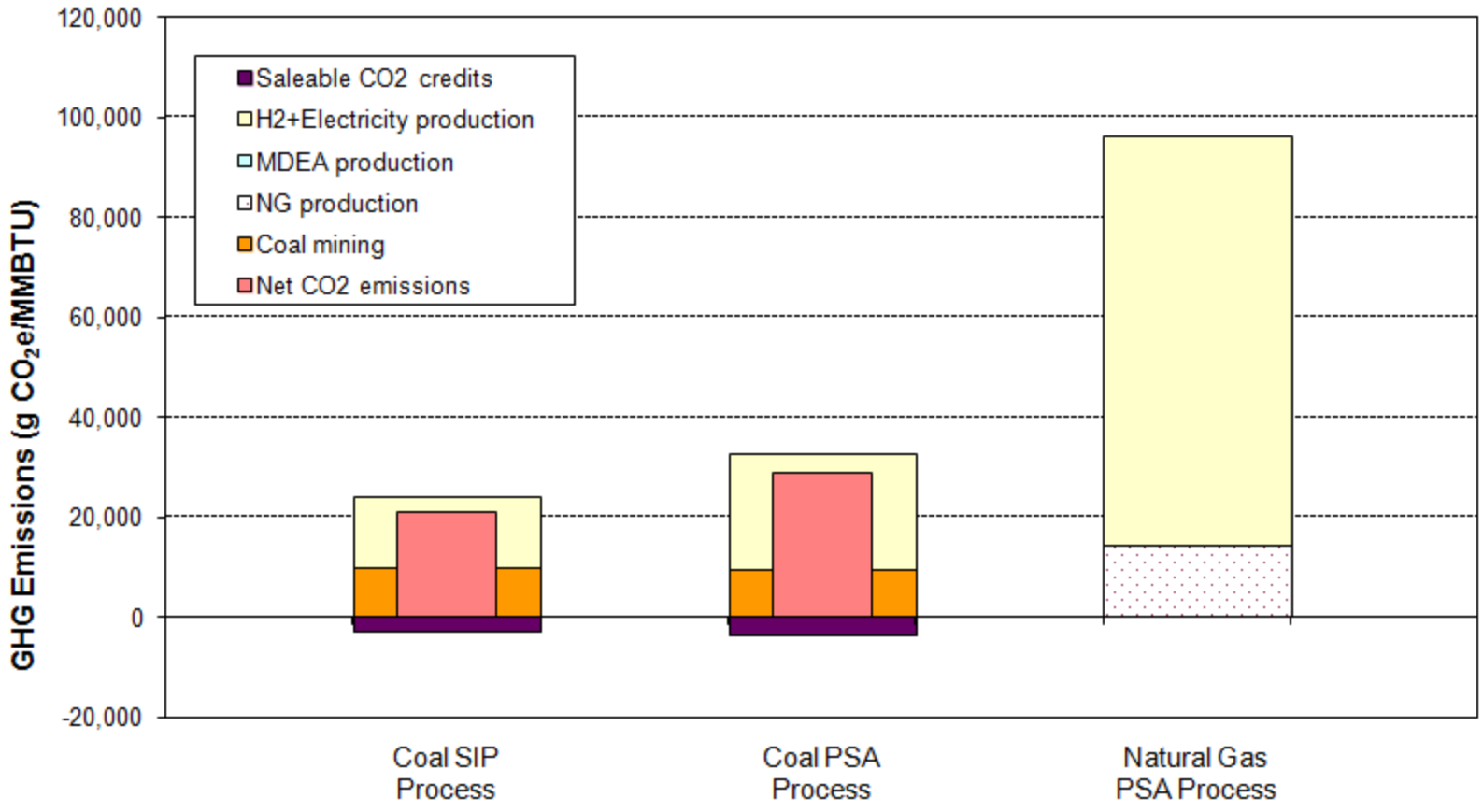

Figure 7-5. Life cycle GHG emissions for the alternative case LCA of hydrogen and electricity co-production.

8. Conclusions

This project focused on the development of a hydrogen production process that could be integrated within and integrated combined cycle (IGCC) plant to enable coproduction of hydrogen and electricity. Our hydrogen production process was based on reduction and oxidation of an iron-based catalyst in a circulating fluid-bed reactor system. Development of steam-iron process (SIP) in this project has focused on catalyst development, feasibility demonstration of circulating fluid-bed reactor system, techno-economic analysis of SIP and alternative conventional gasification-based technology and life cycle analysis.

Through the catalyst development activities on this project, we have been able to successful develop an attrition resistant iron-based catalyst that has stable cyclic reduction and oxidation performance at lower temperatures. Significant accomplishments include:

- Multiple promising iron catalyst formulations that operate at temperatures below 550°C using CO as the reduction agent.
- Addition of copper to the catalyst has lowered reduction temperature by 100-150°C and enhanced the hydrogen productivity.
- Addition of potassium enhanced the stability of the catalyst through reduction of coke and iron carbide formation.
- Stable activity was demonstrated for up to 100 reduction and oxidation cycles.
- Optimal reduction cycle length of $\leq$ 30 sec was demonstrated.
- Hydrogen production was demonstrated with syngas from all current commercial gasifier designs with the best performing catalyst formulations.
- Our SIP, with no modifications, was shown to be able to produce high purity hydrogen from air-blown syngas in spite of the high nitrogen in the syngas.

Catalyst development on this project continued until successful commercial preparation of a material with the same activity as the laboratory-based catalyst was demonstrated by a catalyst prepared by Clariant. The 100 lb batch of catalyst prepared by Clariant provided the technical feasibility information to confirm successful commercial production of this catalyst material.

To advance the technical readiness level of this technology, a special prototype-scale circulating fluid-bed reactor system was designed, built, and operated as part of this project. This prototype SIP reactor system (PSRS) consists of a transport reactor as the reducer and a bubbling fluidized-bed as the oxidizer. Parametric tests completed in the PSRS included syngas composition, temperature, pressure and syngas with 100 ppmv of H_2S. The results from this parametric testing show that the iron catalyst is preferentially reduced with CO at temperatures from 400°C to 500°C. From 400 to 500°C, temperature has no effect on the reactions in the reducer. However, a large increase in steam oxidation was observed at 500°C. Increasing pressure from 150 to 265 psig resulted in increased rates of the reduction and steam oxidation reactions. No adverse effect on either the reactions in the reducer or in the oxidizer were observed for a syngas with 100 ppmv of H_2S. The PSRS also demonstrated the technical feasibility of the circulating fluidized-bed reactor system for SIP.

A detailed techno-economical and life cycle assessment of SIP process was completed. ASPEN simulations were developed to analyze the material and energy balance of the entire plant producing hydrogen and electricity from coal. The estimated cost of hydrogen production is $0.508/LB. The production cost of electricity is $34.14/MWH. This economic analysis clearly indicates favorable

economics for SIP compared to standard process for making hydrogen by coal gasification using a pressure swing adsorption process. An expansion of this techno-economic analysis for coal to evaluate the potential for biomass demonstrated that a plant processing 11500 ton/d biomass could produce 300 ton/d of hydrogen with production cost of $1.02 per lb of hydrogen.

The life cycle GHG emissions of Coal SIP process are 15% lower than Coal PSA process in the base case scenario of carbon capture and sequestration. In the alternative scenario of carbon capture and selling CO_2 to beverage industry, Coal SIP process has 27% lower emissions than Coal PSA process. In addition, the LCA results for the base case as well as alternative case present a significant GHG emission reduction for Coal SIP and Coal PSA processes in comparison to conventional NG PSA process for hydrogen and electricity co-production. This is very promising news based on the fact the most promising means of sequestering CO_2 at this time is through enhanced oil recovery which has estimated ultimate storage capacity between 675 – 900 billion metric tons of CO_2 (IPCC 2005). Unfortunately, because of the stringent requirements for carbon capture and storage in underground reservoirs, this technology is still at experimental stage, with very few sites worldwide injecting CO_2 at a demonstration/commercial scale. Alternative use of the CO_2 is limited as demonstrated by the fact that the food industry (including carbonated beverage use) consumed 8 million metric tons of CO_2 (IPCC 2005) in 2000; whereas global fossil CO_2 emissions in that year stood at 23.5 billion metric tons

Both the technical and economic feasibility of our SIP process have been demonstrated in this project. Continued development of our SIP technology for commercial will require pilot plant testing of the process to gather the key technical information that will be required to successful design and operate a commercial SIP plant. The key data needed is demonstration of long term catalyst activity under representative if not actual, commercial operating conditions. The PSRS was able to demonstrate the technical feasibility of the circulating fluid-bed reactor concept, but a pilot plant unit is also required to address remaining scale up risks of the circulating fluid-bed reactor design before successful commercial deployment is possible. These include evaluation of the reactor design for both the reducer and oxidizer to optimize the reduction and steam oxidation reaction rates and duration, minimizing gas transfer in the inter-particles spaces between reactors, minimizing attrition losses through design selection based on knowledge developed with commercial circulating fluid-bed unit.

References

Akiyama, T. Miyazaki, A. Nakanishi, H. Hisa, M. and Tsutsumi, A., "Thermal and gas analyses of the reaction between iron carbide and steam with hydrogen generation at 573K," International Journal of Hydrogen Energy, 29, 721-724 (2004).

Ariadna Study 04/2302, "Sponge Iron Process for Manned Space Exploration," www.esa.int/gsp/ACT/ariadna/ongoing_studies_04_2302.htm, June 17 (2005).

Baxter, L., "Brigham Young University," [online] http://www.et.byu.edu/~larryb/index.html

Buchanan, T.L. et al, "Capital and operating cost of hydrogen production from coal gasification," NETL Report, April 2003.

Baumann, H. and Tillman, A.-M., "The hitch hiker's guide to LCA: an orientation in life cycle assessment methodology and application." Lund, Sweden: Studentlitteratur AB, 2004, p. 543.

Bop, J. (2006).

Casper, M.S., (ed.), "Hydrogen Manufacture by Electrolysis, Thermal Decomposition and Unusual Techniques," Noyes Data Corporation, pp 56-62 (1978).

Damen, K., Troost, M., Faaij, A., and Turkenburg, W., "A comparison of electricity and hydrogen production systems with CO_2 capture and storage. Part A: Review and selection of promising conversion and capture technologies," Progress in energy and combustion science, vol. 32, no. 2, pp. 215–246, 2006.

Doctor, R.D., Molburg, J.C., Brockmeier, G.J. Stiegel, "Designing for hydrogen, electricity and CO2 recovery from a Shell gasification-based system. In: Eighteenth Annual International Pittsburgh Coal Conference, paper 20-4, CD-Rom (2001).

Dewulf, J. et al, "Exergy: Its Potential and Limitations in Environmental Sciences and Technology," Environmental Science & Technology, vol.42, no. 7 pp 2221-2232, February 2008

Dufour, J., Serrano, D., Gálvez, J. Moreno, J., and Garcia, C., "Life cycle assessment of processes for hydrogen production. Environmental feasibility and reduction of greenhouse gases emissions," International Journal of Hydrogen Energy, vol. 34, no. 3, pp. 1370–1376, 2009.

Elliot, M.A., ed, "Chemistry of Coal Utilization," Second Supplementary Volume, Wiley Interscience Publication, pp 1686-1688 (1981).

Fan, L.-S. and Li, F., "Chemical Looping Technology and Its Fossil Energy Conversion Applications," Industrial & Engineering Chemistry Research, vol. 49, no. 21, pp. 10200-10211, Jul. 2010.

"GaBi Databases 2006" – Documentation. Extension database XVII: US extension database, available at: http://documentation.gabi-software.com/XVIIUSextensiondatabase.html

Gangwal et al., “Warm-Gas Desulfurization Process for ChevronTexaco Quench Gasifier Syngas,” 21st Annual International Pittsburgh Coal Conference, (2004).

Gasior, S.J., A.J. Forney, J.H. Field, Daniel Bienstock, and H.E. Benson, “Production of Synthesis Gas and Hydrogen by the SIP,” U.S. Bureau for Mines, Report of Investigations 5911 (1961).

Gray, D. and G. Tomlinson, Hydrogen from Coal. Report to the U.S. DOE, DE-AM26-99FT40465, 22pp (July 2002).

Hacker, V., Robert Fankhauser, G. Faleschini, H. Fuchs, K. Friedrich, M. Muhr, and K. Kordesch., “Hydrogen Production by SIP,” J. Power Sources, 86, 531 (2000).

Hacker, V., “A Novel Process for Stationary Hydrogen Production: the Reformer Sponge Iron Cycle (RESC),” J. Power Sources, 118,311 (2003).

International Energy Agency (IEA), World Energy Outlook 2008 Edition. Paris, France: International Energy Agency (IEA), 2008, p. 578.

IPCC, IPCC Special Report on Carbon Dioxide Capture and Storage. Cambridge, United Kingdom and New York, NY, USA: Cambridge University Press, 2005, p. 442.

ISO (International Standardization Organization) (2006). ISO 14040. Environmental management — Life cycle assessment — Principles and framework

ISO (International Standardization Organization) (2006). ISO 14044. Environmental management – Life cycle assessment – Requirements and guidelines.

Kang, Z. and Z. Wang, “Novel Oxides for Cycled H2 Production from Methane and Water Using a Temperature Swing,” Adv. Mater., 15, 6 (2003).

Kindig, J.K., B.R. Davis, R.R. Odle, T.E. Weyand, “Method for the Production of Hydrogen and Applications Thereof,” U.S. Patent 6,663,681 (2003).

Kindig, J.K., R.R. Odle, T.E. Weyand, and B.R. Davis, “Method for the Production of Hydrogen Gas,” U.S. Patent 6,682,714 (2004).

Kindig, J.K., and T.E. Weyand, “Method for the Production of Hydrogen-Containing Gaseous Mixtures,” U.S. Patent 6,685,754 (2004).

Kunii,D., and Levenspiel, O. “Fluidization Engineering Second Edition”, 1991

Longanbach, J., R. Rutkowski, M.D. Klett, J.S. White, R.L. Schoff, T.L. Buchanan, “Hydrogen production facilities- Plant performance and cost comparison,” Contract No. DE-AM26-99FT40465, Final Report to DOE (March 2002).

Messerchmidt, (German Patent) DE 266863, Germany (1911).

Roine, A., Chemical Reaction and Equilibrium Software with Extensive Thermochemical Database, Outokumpu HSC Chemistry for Windows, August 12, (2002).

Otsuka, K., S. Murakoshi, and A. Morikawa, "Potential Metal Oxides for the Production of Hydrogen From Water by a Reduction Oxidation Cycle Using Carbon as Reductant," Fuel Processing Technology, 7, 203 (1983).

Otsuka, K., T. Kaburagi, C. Yamada, and S. Takenaka, "Chemical Storage of Hydrogen by Modified Iron Oxides," J. Power Sources, 122, 111 (2003).

Pena, J.A. Lorente, E. Romero, E. and Herguido, J., "Kinetic study of the redox process for storing hydrogen: Reduction stage," Catalysis Today, 116, 439-444 (2006).

Perry, R.H. and Green, D.E. (eds.), Chemical Engineers' Handbook, 7th ed., McGraw-Hill, 1997, pp. 17.27-17-31.

Pizak, V., M. Weinberger, A. Eiler & J. Garche, "Investigation of the Kinetics and Catalysis of the iron/steam-magnetite/hydrogen system in a low temperature regime with regard to its use to produce and store hydrogen," Proc. Hydrogen Energy Progress XI, 11th World Hydrogen Energy Conf., Stuttgart, Germany, June, 1996, 1175–1183.

Shimokawabe, M. Furuichi, F. and Ishii, T., "Influence of the preparation history of α-Fe2O3 on its reactivity for hydrogen reduction," Thermochimica Acta, 28, 287 (1979).

Spath, P. L. and Mann, M. K., Life Cycle Assessment of Hydrogen Production via Natural Gas Steam Reforming, no. February. Golden, CO , 2001, p. 24.

SRI International. (1994). Options for Refinery Hydrogen. Report No. 212. Menlo Park, CA.

Takenaka, S., T. Kabwagi, C. Yamada, K. Nomura, and K. Otsuka, "Storage and Supply of Hydrogen by Means of the Redox of the Iron Oxides Modified with Mo and Rh Species," J. Catalysis, 228,66 (2004).

Takenaka, S., K. Nomura, N. Hanaizumi, and K. Otsuka, "Storage and Formation of Pure Hydrogen mediated by the Redox of Modified Iron Oxides," Applied Catalysis A: General, 282,333 (2005).

Thaler, M. Hacker, V. Anilkumar, M. Alberig, Besenhard, J.O., Schrottner, H. Schmied, M. "Investigations of cycle behavior of the contact mass in the RESC process for hydrogen production," International Journal of Hydrogen Energy, 31, 2025 (2006).

"The Greenhouse Gases, Regulated Emissions, and Energy Use in Transportation Model (GREET)." Argonne National Laboratory, Argonne, Illinois, 2010.

Williams, E., Warr, B., and Ayres, R. U., "Efficiency Dilution: Long-Term Exergy Conversion Trends in Japan," Environmental Science & Technology, vol. 42, no. 13, pp. 4964-4970, May 2008.